A two-dimensional numerical model for the investigation of the effects of dams on the Zambezi River Delta

by
Robyn Kime

Thesis presented in partial fulfilment of the requirements for the degree of Master of Engineering (Research) in the Department of Civil Engineering at Stellenbosch University

Supervisor: Prof. Gerrit Basson

April 2014

DECLARATION

By submitting this thesis electronically, I declare that the entirety of the work contained therein is my own, original work, that I am the authorship owner thereof (unless to the extent explicitly otherwise stated) and that I have not previously in its entirety or in part submitted it for obtaining any qualification.

Date: 17 February 2014

ABSTRACT

The Zambezi River is the largest east-draining river in Africa. It captures runoff from 8 different countries before draining into the Indian Ocean in Mozambique through the Zambezi Delta which is recognised as a (Ramsar) Wetland of international importance. The Zambezi River flows are currently regulated by four large hydropower dams within its catchment. Much attention has been given in recent literature to the detrimental effects of the altered flow regime as a result of dams on the Zambezi River and the Delta in particular. Existing research relating to these negative effects includes many detailed ecological, hydrological and qualitative morphological studies but to date no detailed morphological modelling studies have been conducted in this regard.

In this thesis a two-dimensional coupled hydrodynamic and morphological numerical model of the Zambezi Delta is created using topographical information obtained from a navigational study (Rio Tinto, 2011). The model hydrodynamics are calibrated using recorded water levels and flows at two gauging stations within the model domain. The bed load sediment transport is calibrated using field measurements (ASP, 2012b).

The effects of dams on the Zambezi Delta are investigated by performing two 10 year simulations, one representing the current (post-dam) scenario and the other representing a pre-dam scenario. These simulation results show a significant decrease in flooded areas and sediment movement on the floodplains as a result of dams. Additional effects on channel widths and depth, on bed gradings, and on tidal water level variations are analysed.

The model is then used to simulate a proposed environmental flood release scenario. Such releases have been recommended as a means to partially mitigate the negative impacts of dams on the Zambezi River. In this case an annual flood release supplying a peak flow of 8500 m^3/s (slightly less than the pre-dam mean annual flood of 10 000 m^3/s) was found to

cause slightly more flooding of the close floodplains and to have small effects on the river channel width.

The model predicts hydrodynamics and bed sediment transport of non-cohesive sediments with suitable accuracy but an issue with the suspended transport of cohesive sediments was identified. Recommendations are made for addressing the suspended sediment transport inaccuracy. The model, in its current form, can provide quantitative information regarding the hydrodynamics and course sediment transport of the general delta region on a coarse scale. With additional computational resources and accurate topographical information the model can be refined to give accurate predictions for localised areas within the delta. Such information would be valuable to specialist studies addressing the environmental effects of various proposed flooding scenarios or future dams.

OPSOMMING

Die Zambezirivier is die grootste oos-dreineerende rivier in Afrika. Dit ontvang afloop van ag verskillende lande voor dit in die Indiese Oseaan in Mozambiek uitmond. Die Zambezidelta work erken as 'n RAMSAR vleiland van internasionale belang. Die vloei in die rivier word tans gereguleer deur vier groot hidro-elektriese damme binne sy opvangsgebied. Baie aandag is in die onlangse literatuur gegee aan die nadelige gevolge van die veranderde vloei as gevolg van damme op die Zambezi Rivier en spesifiek op die Delta. Bestaande navorsing met betrekking tot hierdie negatiewe effekte sluit in detail ekologiese, hidrologiese en kwalitatiewe morfologiese studies, maar tot op datum is geen gedetailleerde morfologiese modelleringstudies gedoen nie.

In hierdie tesis is 'n twee-dimensionele gekoppelde hidrodinamiese en morfologiese numeriese model van die Zambezi Delta geskep met behulp van topografiese inligting wat verkry is uit 'n navigasiestudie (Rio Tinto, 2011). Die model hidrodinamika is gekalibreer deur teen watervlakke en vloei by twee meetstasies in die model domein. Die bedvrag sedimentvervoer is gekalibreer met behulp van veldmetings (ASP, 2012b).

Die ïnvloed van die damme op die Zambezi Delta is ondersoek deur twee 10-jarige simulasies, een wat die huidige (na-dam) scenario en die ander wat 'n voor-dam scenario ondersoek. Hierdie simulasie resultate toon 'n beduidende afname in die oorstroomde gebiede en sedimentbeweging op die vloedvlaktes as gevolg van damme. Bykomende effekte op kanaalbreedtes en -diepte, op die bedgraderings , en op getywatervlak variasies is ontleed.

Die model is vervolgens gebruik om 'n voorgestelde omgewingings vloedloslaating te ondersoek. Sodanige loslaatings is aanbeveel om die negatiewe impak van damme op die rivier gedeeltelik te verminder. In hierdie geval gee 'n jaarlikse vloedloslaating met 'n piekvloei van 8500 m^3/s (effens minder as die voor-dam gemiddelde jaarlikse vloed van 10

000 m^3/s) effens meer oorstromings van die vloedvlaktes en het 'n klein uitwerking op die rivierkanaalbreedte.

Die model voorspel die hidrodinamika en bedsedimentvervoer van nie-kohesiewe sedimente met betroubaarheid, maar 'n probleem met die vervoer van kohesiewe sedimente is geïdentifiseer. Aanbevelings word gemaak vir die aanspreek van die kohesiewe sedimentvervoer onakkuraatheid. Die model, in sy huidige vorm, kan kwantitatiewe inligting oor die hidrodinamika en natuurlik sedimentvervoer van die algemene delta streek by benadering verskaf. Met bykomende rekenaar hulpbronne en akkurate topografiese inligting kan die model verfyn word om akkurate voorspellings vir plaaslike gebiede binne die delta te gee. Sulke inligting kan waardevol wees vir spesialis-studies van die omgewingsimpakte van verskillende voorgestelde vloedloslaatings of toekomstige damme.

ACKNOWLEDGEMENTS

The financial assistance of the National Research Foundation (NRF) towards this research is hereby acknowledged. Opinions expressed and conclusions arrived at, are those of the author and are not necessarily to be attributed to the NRF.

In addition, the following people deserve acknowledgement for their assistance in making this thesis project possible:

- Prof GR Basson, my supervisor, for guidance throughout my Masters study program;
- Christiaan Visser and Ousmane Sawadago, for assistance with *Mike21C* modelling;
- Patrick Kime, my father, and Michael Owen, my boyfriend, for endless support as well as assistance with language and proof reading this thesis.

TABLE OF CONTENTS

LIST OF FIGURES

LIST OF TABLES

LIST OF SYMBOLS AND ABBREVIATIONS

α	helical flow calibration constant
Δs	spatial step
Δt	time step
ζ	integration parameter
η	dimensionless logarithmic vertical coordinate
θ	Shields parameter
θ_c	critical Shields parameter
κ	Von Karman's constant
v	kinematic viscosity of water
a	calibration factor for slope effect on bed load
a	reference level
AD	advection-diffusion
ADCP	acoustic Doppler current profiler
BF	bed load factor
c	concentration
C	Chezy roughness coefficient
ca	concentration at reference level a
cb	concentration close to the bed
Cr	Courant number
d	sediment diameter
D^*	non-dimensional particle parameter
d_{50}	median sediment diameter
DEM	digital elevation model
E	turbulent / eddy viscosity
EFR	environmental flood release

EFZ	Engelund, Fredsoe & Zyserman sediment transport theory
Fr	Froude number
FSL	full supply level
g	gravitational acceleration
G	calibration factor for slope effect on bed load
h	water depth
H	water level / surface elevation
HD	hydrodynamic
ICOLD	International Commission on Large Dams
M	Manning roughness coefficient
MSL	mean sea level
n	curvilinear coordinate
p	probability
p	water flux
q	water flux
Q	water discharge
Qs	sediment load
Qw	water discharge
R	radius of curvature
s	curvilinear coordinate
s	relative density of sediment
Sbl	bed sediment load
Sn	transformed bed load component in n-direction
SRTM	shuttle radar topography mission (source of elevation data)
Ss	transformed bed load component in s-direction
Ssl	suspended sediment load

u	mean flow velocity
uf	friction velocity
UTM	Universal Transverse Mercator (projected global coordinate system)
vR	van Rijn sediment transport theory
Vss	settling velocity
ws	settling velocity
x	horizontal cartesian coordinate
y	horizontal cartesian coordinate
z	vertical coordinate
Z	Rouse suspension parameter

1 INTRODUCTION

1.1 Dams and the Zambezi River

Dams have been constructed for more than 5000 years to provide water security and/or hydropower essential for human economic and social development. However, since the 1950's there has been increasing attention in the literature to the negative environmental and social impacts of large dams and they have been increasingly perceived as destructive (Petts & Gumell, 2005). In developed parts of the world very few dams have been developed over the past 20 years but in developing regions large dams are still being constructed (ICOLD, 2013). With increasing knowledge there is increasing responsibility on future developers to fully consider the overall benefits as well as negative impacts of proposed dams in order to make informed decisions and to minimise trade-offs.

Hydropower is a renewable and emission-free source of potentially huge amounts of energy in Africa; indeed according to the International Commission on Large Dams (ICOLD) only 8% of the hydropower potential in Africa has been exploited to date. The Zambezi River (the largest east-draining river in Africa with a catchment area of approximately 1 350 000 km^2 falling into eight different countries) currently has four large hydropower dams within its catchment (Kariba and Cahora Bassa on the Zambezi River, and Kafue Gorge and Itezhitezhi on the Kafue River) and several potential future dams have been identified (Mhlangwa & Sakala, 2013). The literature contains a multitude of papers on the environmental and social effects of the altered flow regime as a result of the existing reservoirs on various sections of the Zambezi River (eg. Acreman, 1996; Beilfuss & dos Santos, 2001; Davies et al. 2000; Pritchard et al., 2009). One of the areas of particular environmental concern, especially since the construction of Cahora Bassa in the 1970's, is the Zambezi Delta: an extensive network of

distributaries in a large triangular wetland which extends about 120 km inland from the coast where the Zambezi drains into the Indian Ocean (Beilfuss & Brown, 2006). Major changes to river morphology and floodplain vegetation of the delta region since the construction of Cahora Bassa have been noted as well as severe declines in bird and mammal numbers, in fish and prawn catches, and in the productivity of floodplain agricultural lands (Davies, et al., 2000). Many authors have suggested that prescribed environmental flood releases from Cahora Bassa could mitigate many of the adverse environmental effects of the dams (eg. Beilfuss & Brown, 2006; Acreman, 1996; Brown & King, 2012).

Existing research on the lower Zambezi includes many specialist ecological studies; detailed hydrological studies of the region (eg. Beilfuss & dos Santos, 2001); water-balance-type hydropower modelling studies; qualitative reviews of morphological changes based on aerial photographs and maps (Davies, et al., 2000); and one quantitative one-dimensional simplified long-term hydro-morphological modelling study (Ronco, et al., 2010). To the author's knowledge no morphological modelling studies have been undertaken in more than one-dimension or using less than a monthly time step.

1.2 Available information

A general lack of information as well as difficulties in accessing what information does exist has been a major challenge for all studies on the Zambezi River (eg. Ronco, et al, 2006). A considerable amount of data on the Lower Zambezi was made available for this research project through a navigation study undertaken in 2011 (Rio Tinto, 2011), including:

- Daily water levels and flows at most gauging stations on the Lower Zambezi for a 10 year period (2000-2010);
- A digital elevation model of the Lower Zambezi including results from bathymetric surveys;

- Tidal water levels at the Zambezi Mouth; and
- Physical field measurements of flow parameters and sediment loads at various cross-sections on the Lower Zambezi (for model calibration).

1.3 Motivation and Objectives

Dams alter the natural flow regime and sediment loads in the river downstream resulting in morphological changes which in turn affect the riverine ecology. As the channel response to altered flow patterns and sediment loads is complex and varies from river to river as well as spatially and temporally along the same river (Brandt, 2000), the best way to accurately predict the morphological effects downstream of a proposed dam is through the use of state-of-the-art mathematical models (Basson, 2004).

As mentioned previously, such models are hampered by a lack of field data necessary for calibration and for use in generating suitable model boundary conditions. With the data made available by the 2011 navigation study on the Lower Zambezi an opportunity to develop a calibrated numerical model of this section of the river has arisen.

This thesis aims to develop a suitably calibrated two-dimensional hydraulic and sediment transport model of the Lower Zambezi that can be used to analyse and quantify the effects of dams on the river and floodplain morphology of the Zambezi Delta. Once these differences are quantified the model can be used to determine the effectiveness of prescribed environmental flooding scenarios.

1.4 Methodology

The methodology employed in this study was as follows:

- A review of the relevant literature relating to the Zambezi Delta and the modelling of flow and sediment transport in rivers was conducted.

- Based on available literature assumptions and calculations allowed for the generation of suitable best-approximation pre-dam and post-dam boundary conditions for use in a numerical model.
- Preliminary simulations were used to determine suitable grid resolution, modelling parameters, sediment transport equations and calibration parameters.
- The resulting final numerical model was used to simulate full ten-year flow series' for a pre-dam and a post-dam flow scenario.
- The results of the simulations were processed and analysed.
- And finally, an additional simulation was performed of an example flood release scenario.

1.5 Scope and limitations

This study focuses on the fluvial morphology of the delta region of the Lower Zambezi. The two-dimensional modelling domain extends from the gauging station at Caia, just downstream of the Shire River confluence, to the Ocean (approximately 160 km). The width of the model domain, approximately 84 km at the coastal end, was determined by the range of supplied elevation data.

All numerical modelling analyses are subject to certain limitations and uncertainties. The uncertainty and possible sources of error associated with each of the inputs and model components are discussed under each relevant section while the two most critical limitations deserve mention here:

(a) The bathymetry for the model was developed from surveys performed between 2000 and 2010 (as no earlier survey information was available). The starting morphology has therefore already undergone decades of unnatural flows as a result of dams. The

"pre-dam" condition therefore does not truly represent the situation before dams but rather the situation if dams were suddenly removed in 2000, which may be a very different scenario.

(b) The resolution of the model grid is limited by fairly large cell sizes. The coupled fully hydrodynamic and sediment transport simulations are computationally expensive and the simulation times increase exponentially with the number of grid cells. A trade-off therefore has to be made between model resolution and simulation time. In this study the grid size was chosen to maximise resolution while keeping individual simulation times to less than one week. With a higher-powered license (the Mike by DHI academic license currently allows simulations to run on a maximum of 4 parallel CPU's but licenses are available for up to 24) and greater computational resources more detailed simulations would be possible.

2 LITERATURE REVIEW

2.1 General information on the Zambezi River

2.1.1 Political location

From its source in north western Zambia the Zambezi River flows southwest into eastern Angola before turning south to re-enter Zambia at the Chavuma Falls. It then cuts south to southeast through western Zambia to Katima where it turns east to form the border between Zambia and Namibia until Kazungula. Downstream of Kazungula the Zambezi forms the border between Zambia and Zimbabwe for about 900 km before it enters Mozambique where it reaches the ocean near the town of Chinde. Its catchment area (approximately 1 350 000 km^2) falls into eight countries: Angola (18.2%), Botswana (2.8%), Malawi (7.7%), Mozambique (11.4%), Namibia (1.2%), Tanzania (2.0%), Zambia (40.7%) and Zimbabwe (16.0%) (Tumbare, 1999).

2.1.2 The Zambezi Delta

About 120 km inland of the Indian Ocean, the Zambezi River anabranches to form the Zambezi Delta: a vast alluvial pan comprised of an assortment of freshwater swamps, grassland, coastal dunes, woodland, mangroves and sea grass beds. The southern part of the delta, including the Marromeu Buffalo Reserve and surrounding hunting concession areas, was listed as a wetland of international importance (in accordance with the Ramsar Convention on Wetlands) in 2004 and is Mozambique's only Ramsar Site.

The delta provides a breeding ground for dense populations of water birds including White- and Pinkbacked pelicans, Yellowbilled and African Openbill Storks, Black Storks, Pel's Fishing Owls, African Skimmers and at times up to 30 % of the global population of Wattled Cranes. Mammals of the delta include numerous antelope, elephant, hippopotamus, buffalo,

lion, leopard, wild dog, and hyena. The delta is also home to thousands of rural people who make a living from subsistence fishing and agriculture (Pritchard, et al., 2009).

2.1.3 Runoff patterns

The Zambezi River is often referred to in three segments: the *Upper Zambezi* from the source to Victoria Falls, the *Middle Zambezi* from Victoria Falls to Cahora Bassa, and the *Lower Zambezi* from Cahora Bassa to the Indian Ocean (Davies, 1986). Beilfuss and Dos Santos (2001) give a detailed description and explanation of the hydrological patterns of the Zambezi River which are summarised below.

For approximately the first 500 km the upper Zambezi River and its tributaries drain the steep wooded slopes of the Northern Highlands of Zambia and Angola in fast flowing distinct channels with rapids. It then meanders through the Barotse Plain for about 200 km before dropping over the Sioma Falls to form a narrow channel for roughly 150 km and then widening out again into the Chobe Swamp. Downstream of the Chobe Swamp the Zambezi flows over a series of small rapids before dropping over the Victoria Falls. The Barotse Plain, Chobe swamp and other smaller wetlands significantly attenuate the runoff in the Upper Zambezi resulting in peak flows at Victoria Falls in April following peak rains (and peak floods in the northern highlands) in February (Beilfuss & dos Santos, 2001).

Below Victoria Falls the Zambezi naturally rushes through a series of deep gorges including the Batoka Gorge, Devil's Gorge, the gorges of the Gwembe Rift Valley and Kariba Gorge. The Kariba Gorge was closed by a 131 m high concrete arch dam in 1958 and the reservoir now extends 280 km upstream to Devil's Gorge. The outflows from Kariba Reservoir are dictated by hydropower demands and a flood rule curve (Kariba Reservoir cannot pass the 10 000 year flood and thus reservoir levels are drawn down prior to the wet season to create extra storage capacity in case of a flood event) and are significantly altered from the natural

flows. Figure 2-1 shows how the dam severely reduces the mean annual flood peak and increases the dry season low flows. Downstream of Kariba Gorge the Zambezi River has a section of floodplains (now narrow and rarely inundated) followed by more deep gorges ending at the Cahora Bassa Gorge. Significant tributaries joining over this section include the Kafue River (which delivers attenuated run-off due to its numerous vast floodplains and two large dams) and the Luangwa River (which drains the steep Luangwa Rift Valley and is much more variable and flashy). Figure 2-2 shows the natural (pre-dam) mean annual hydrograph at Cahora Bassa Gorge with the contributions from each of the sub-catchments.

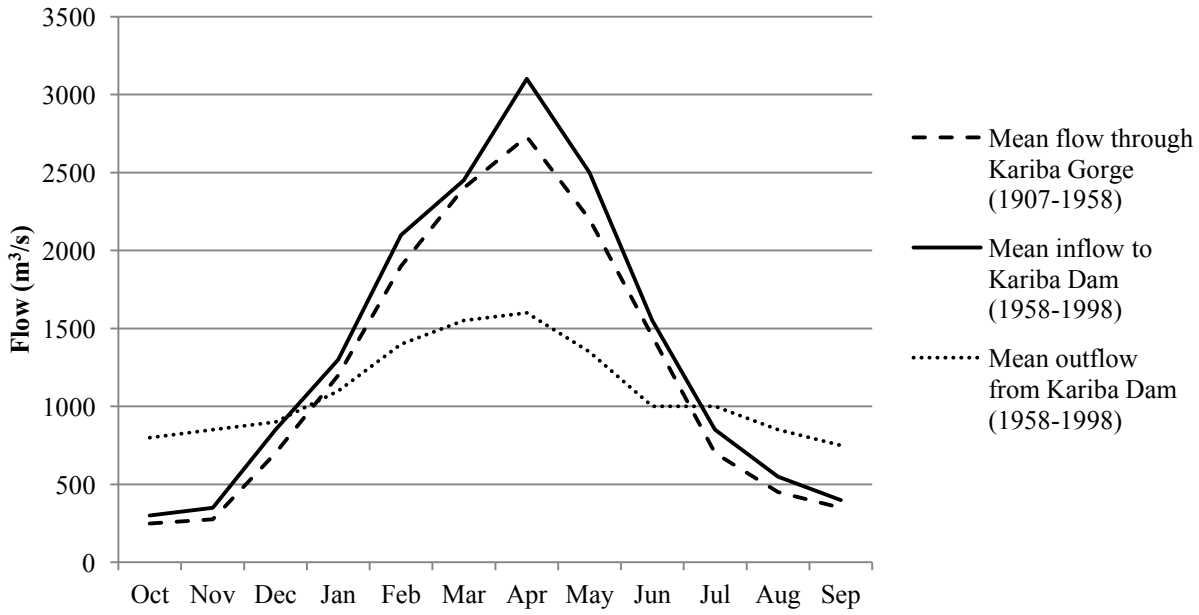

Figure 2-1 **Mean monthly distribution of Kariba Dam inflows, outflows and pre-dam flows (Beilfuss & dos Santos, 2001)**

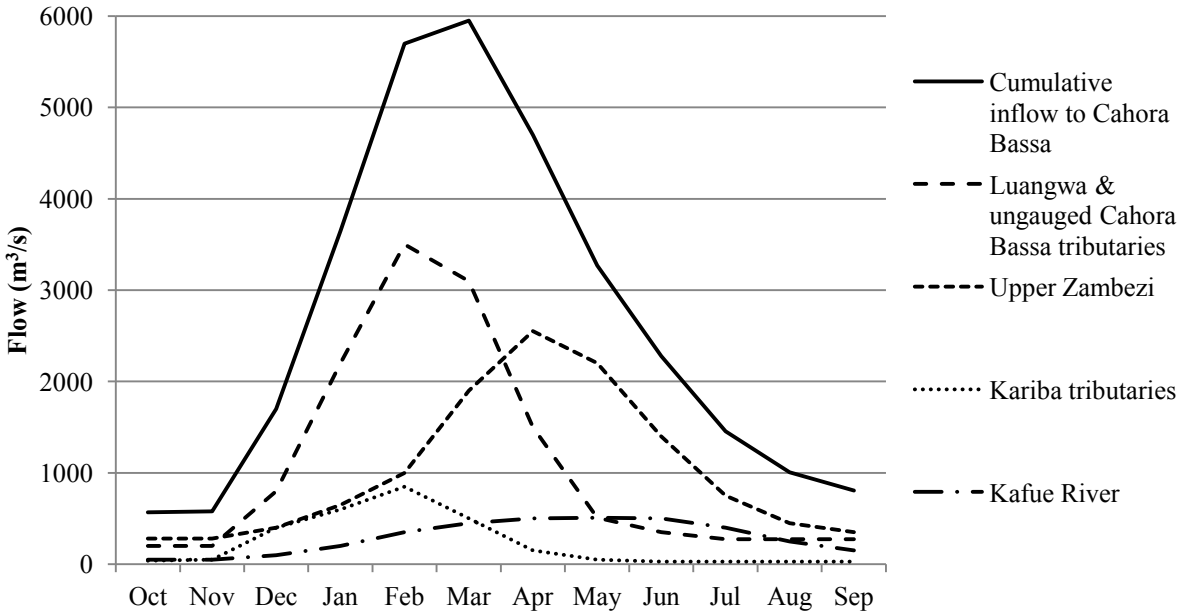

Figure 2-2 **Mean monthly flows at Cahora Bassa Gorge before the construction of dams (1907-1958) showing the contributions from sub-catchments (Beilfuss & dos Santos, 2001)**

The Cahora Bassa Dam, a 163 m high concrete arch dam across the Cahora Bassa Gorge, was completed in 1974. Like Kariba Dam, Cahora Bassa Dam is operated to maximise hydropower output and it imposes a further degree of consistency on the already altered flow regime. Figure 2-3 shows how Cahora Bassa further reduces the annual flood peak and increases the dry season low flow.

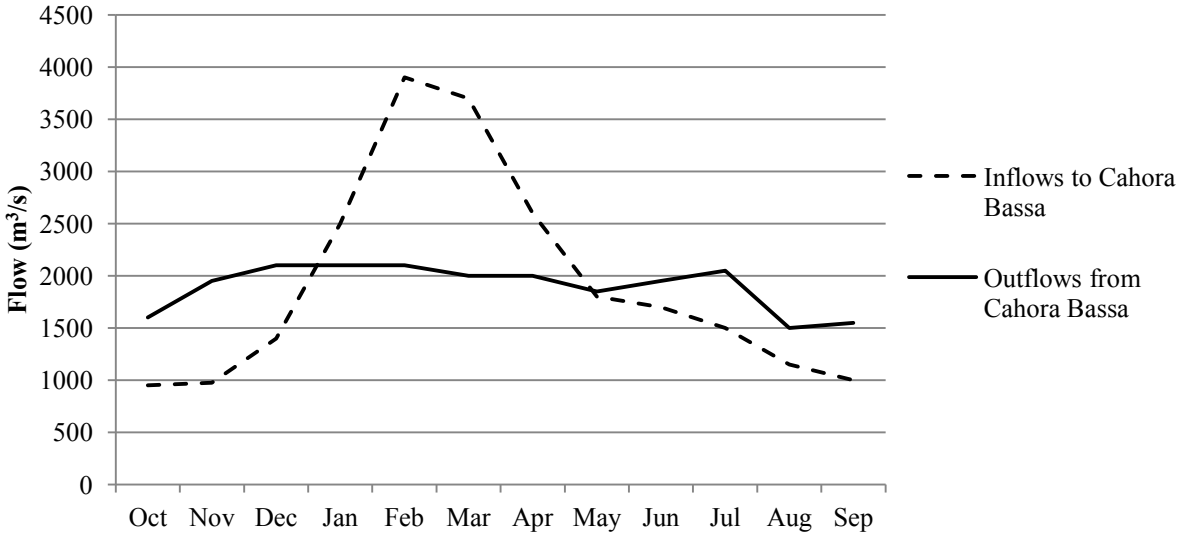

Figure 2-3 Mean monthly inflows and outflows from Cahora Bassa Dam (1976-2000)

Downstream of Cahora Bassa Dam the Zambezi River receives runoff from the Luia and Revubwe tributaries which drain the Moravia-Angonian Plateau to the north and the Luenha River to the south. The final and largest tributary of the Lower Zambezi is the Shire River which drains Lake Nyasa (Lake Malawi) and the southern parts of Malawi. The runoff from the majority of the Shire River catchment is heavily attenuated by the extensive Elephant Marsh; however, the Ruo River which drains the Mulange Mountains joins the Shire further downstream and can contribute considerable short-term floods to the Zambezi. The Shire River flows into the Zambezi River just upstream of the town of Caia and over the remaining 165 km to the ocean the Zambezi does not receive inflow from any significant tributaries.

2.1.4 Dams and hydropower in the Zambezi River catchment

There are currently four large dams in the Zambezi River catchment and an additional eight have been proposed in order to maximise the available head for hydropower (Mhlangwa & Sakala, 2013). Table 2-1 gives the characteristics of the four existing large dams and Figure 2-4 shows a schematic diagram of existing and proposed hydropower developments. .

Table 2-1 Characteristics of the existing four large dams in the Zambezi Catchment

		Kariba	Kafue Gorge	Itezhitezhi	Cahora Bassa	*Source*
Year of completion		1958	1972	1977	1974	
River		Zambezi	Kafue	Kafue	Zambezi	
Catchment area	(km^2)	663 800	151 400	105 620	1 050 000	*C '11*
Installed power	(MW)	1 320	900	120	2 075	*SMM'13*
Wall height	(m)	131	50	65	163	*B&dS'01*
Full supply level	(masl)	489	977	1 030	326	*C '11*
Total storage volume	(10^6 m^3)	180 600	785	5 624	65 000	*C '11*
Flooded area (at FSL)	(km^2)	5 577	805	374	2 670	*C '11*
Net annual evaporation	(mm)	955	780	1 045	1 523	*B&dS'01*
Mean annual flow	(m^3/s)	1 350	295	279	2 382	*C '11*

C'11 = (COBA, 2011)*; SMM'13* = (Schleiss, et al., 2013)*; B&dS'01* = (Beilfuss & dos Santos, 2001)

Kariba Dam, completed in December 1958 on the border between Zimbabwe and Zambia, was the first major hydropower project in Africa (Acreman, 1996). Two hydropower stations, 615 MW on the north bank and 705 MW on the south bank supply electricity to Zambia and Zimbabwe (WCD, 2000). The development of an additional 300 MW at the north bank station is currently nearing completion and a similar extension to the south bank station is planned in the near future (Mhlangwa & Sakala, 2013). Kafue Gorge Dam (900 MW) on the Kafue River in Zambia was completed in 1972. Soon thereafter the Itezhitezhi Dam was constructed further upstream, primarily to control the flow through the Kafue Flats wetland (between Itezhitezhi and Kafue Gorge) to reduce evaporation. Cahora Bassa (1974) is the most recent large dam constructed on the Zambezi River and has the largest hydropower capacity (currently 2075 MW with potential for a further 1200 MW on the north bank). Being the furthest downstream, Cahora Bassa Dam plays the biggest role in the regulation of flows to the delta region.

Additional existing hydropower installations within the Zambezi catchment include a run-of-the-river plant at Victoria Falls (108 MW) on the Zambezi River and small plants at the

Nkula Falls (104 MW), Tedzani Falls (40 MW) on the Shire River (Beilfuss & dos Santos, 2001).

Proposed future developments include those shown in Figure 2-4 as well as two additional dams, Boroma (444 MW) and Lupata (654 MW), further downstream of Cahora Bassa Dam. Currently, the Batoka Gorge (1600 MW, 55 km downstream of Victoria Falls) and the Mpanda Nkuwa (1600 MW, 70 km downstream of Cahora Bassa) projects are underway in the feasibility and environmental and social impact assessment (ESIA) stage (Mhlangwa & Sakala, 2013).

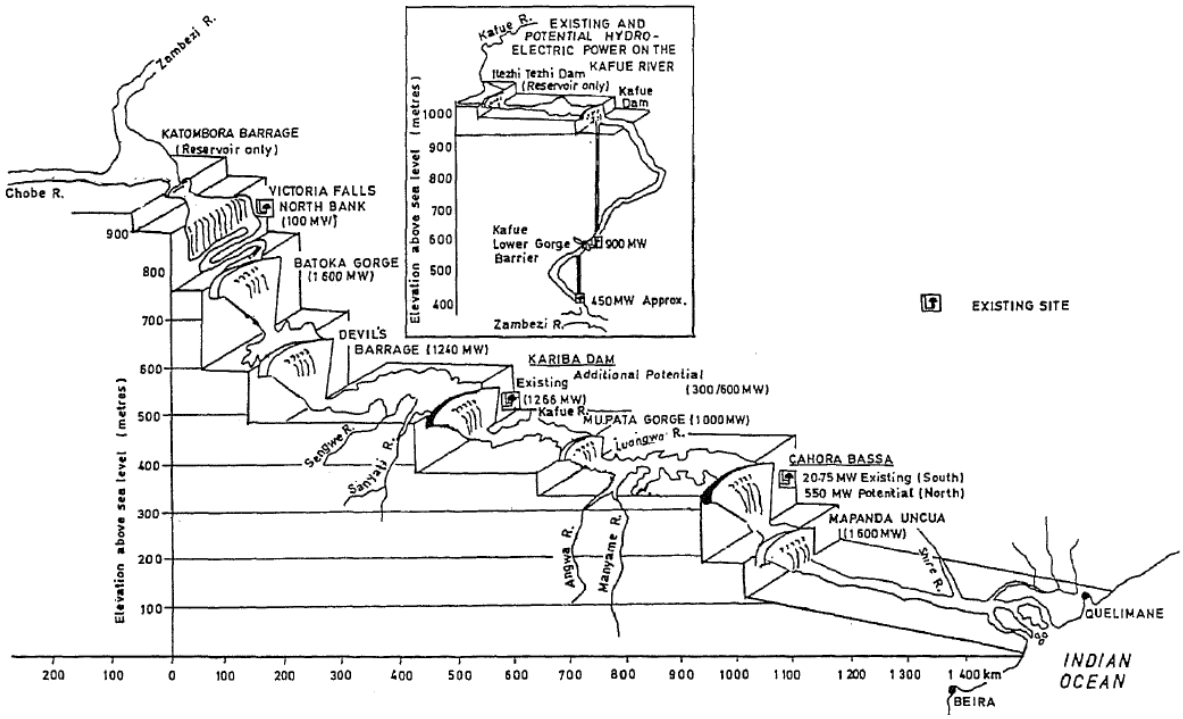

Figure 2-4 Existing and proposed large hydropower developments in the Zambezi Catchment (from Acreman, 2006)

2.2 Dams and the downstream river

2.2.1 Effects of dams on the downstream river morphology

Many studies have looked at the effects of dams on the downstream rivers. Comprehensive reviews are given by (for example) Brandt (2000), Petts & Gurnell (2005) and Beck & Basson (2003). Dams alter the geomorphology and ecology of the rivers downstream through the reduction of total flows (due to evaporation and abstraction), through the altering of natural flow patterns (almost always reducing the magnitude of frequent floods, and often increasing the dry-season low flows), and through the trapping of sediments and nutrients. The downstream impacts are highly dependent on dam operation as well as the dam capacity-to-inflow ratio. Alterations to the downstream river include changes in channel width, channel depth, bed material composition, sediment concentrations, channel slope, bed form (eg. ripples or dunes), plan form (i.e. channel patterns: straight, meandering or braided), and riparian vegetation. These changes in turn affect the riverine ecology.

Initial attempts at predicting the effects downstream of dams followed a regime-type analysis. Natural rivers are continuously subjected to varying influences but they are assumed to strive towards a quasi-equilibrium (or *regime* state) with a long-term stable configuration. A multitude of empirical *regime equations* have been derived to predict channel widths, depths and slopes as a function of discharge, sediment load and bed materials. These equations have been extended to predict channel response to changes in discharge and sediment load downstream of dams (eg. Beck & Basson, 2003).

Regime equations predict “final” altered channel widths, depths and slopes based on a single *dominant discharge*. A more sophisticated approach for predicting river changes with temporal and spatial information is available through numerical modelling. One-dimensional models can be used to run long-term simulations relatively quickly and can predict changes in

channel depth (Beck & Basson, 2003) suggested initially specifying channel widths determined from regime equations in order to predict the final channel widths and depths through the use of a one-dimensional model). For more detailed results two-dimensional or three-dimensional models are recommended but the high computational requirements of these models means long-term simulations are very time consuming (Beck & Basson, 2003). Morphological processes can take a long time and therefore time scales of at least 10 to 30 years should be considered (Petts & Gumell, 2005).

2.2.2 Observed effects of dams on the Lower Zambezi channel and floodplains

Davies et al. (2000) provides a detailed review of observed changes to the Lower Zambezi since the construction of Cahora Bassa including detailed descriptions of changes to the channel bed form and plan form for various river sections (see Figure 2-5 which was based on an aerial survey conducted in July 1996).

In addition to changes to the river channel configuration, the altered flow patterns and reduced sediment and nutrient loads due to dams cause significant disruptions to the natural ecological floodplain systems and local subsistence farming and fishing practices which depend on the annual cycles of flooding and low flow periods. An extensive review of the observed effects of the altered flows on the floodplain ecology and economy (which includes subsistence farming/fishing as well as commercial fishing, hunting, tourism, etc.) of the Zambezi delta is given in Beilfuss & dos Santos (2001). Some observed environmental effects since the construction of Cahora Bassa include (Davies, et al. 2000):

- a decline in coastal fisheries, shrimp industries (60%) and floodplain river fish catches (due to reduced silt and nutrient concentrations and reduced wetland flooding)
- coastal erosion and a 40% loss of mangrove (1974-1997);

- encroachment of woody species and invasive alien plants onto the herbaceous floodplains; and
- a severe decline in bird and mammal life (although this could partly be attributed to the civil war in Mozambique).

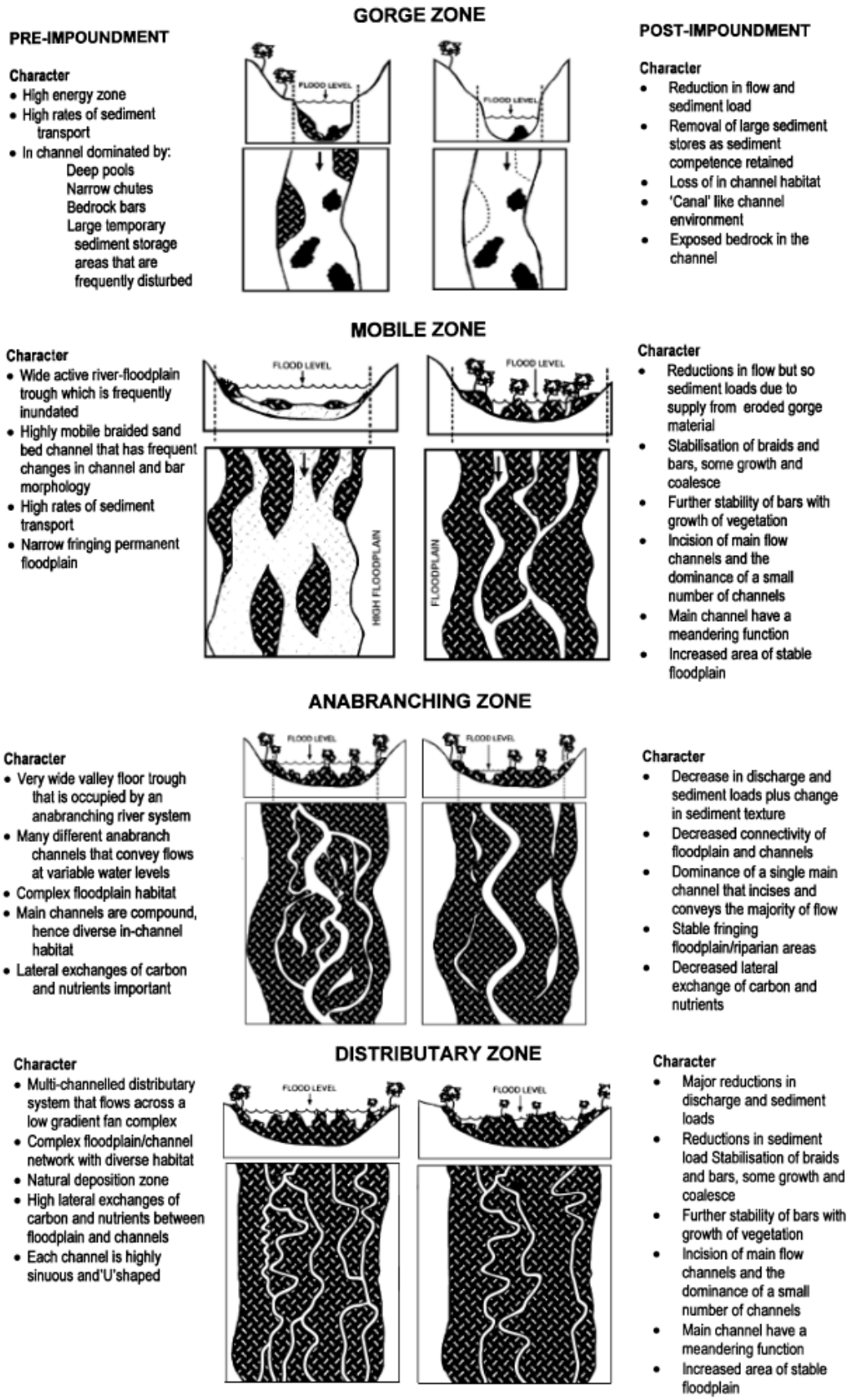

Figure 2-5 Morphological changes to the Lower Zambezi as a result of dams (Davies, et al., 2000)

2.2.3 Environmental flood releases

Since the 1980s many studies have suggested environmental flood releases from Cahora Bassa Dam to restore some degree of annual flooding to the Zambezi Delta (eg. Beilfuss, 2001; Acreman, 1996; Beilfuss & Brown, 2006; Beilfuss, 2010; and Brown & King, 2012). Worldwide, increasing attention is being given to environmental flow requirements downstream of dams and prescribed flood releases from a number of dams have been shown to benefit downstream river users and environments. Examples include Glen Canyon Dam in Colorado, Pongolapoort Dam in South Africa, Manatali Dam in Senegal, and Waza Logone and Maga Dams in Cameroon (Beilfuss, 2010).

Prescribed environmental flood releases (EFR's) are structurally feasible from Cahora Bassa Dam which is controlled by eight sluice gates situated well below the average operating level of the reservoir (Beilfuss, 2010). Beilfuss (2001, 2010) and Beilfuss & Brown (2006) used hydrological/hydropower modelling to investigate the effect of EFR's on hydropower. They found that releases which match the pre-dam hydrograph for 2 to 4 months each year are not possible without significant reductions in hydropower output, but a number of shorter period floods are feasible: An annual flood to the delta of 10 000 m^3/s (the pre-dam mean annual flood) for 2 weeks in February is possible with only 6 % reduction in hydropower; while smaller annual floods of 4 500 m^3/s (which will just over-top the banks at Marromeu) can be produced with less than 1% reduction.

Using a number of specialist studies Beilfuss and Brown (2006) found that EFR's are "perceived to be beneficial" for agriculture, estuarine ecology, coastal fisheries, freshwater fisheries, livestock, large mammals, water birds, floodplain vegetation, natural resource utilization, water quality, groundwater and navigation in the Zambezi Delta region. Furthermore, for most aspects and provided the floods occur between December and

February (in the natural flood season), benefits increase with increasing flood volumes and durations.

2.3 Mathematical modelling of flows and sediment transport

Mike 21C, DHI's mathematical modelling platform for two-dimensional river morphological simulations, is based on a curvilinear grid and incorporates an algorithm which takes account of the (three-dimensional) helical flow at river bends and the result thereof on the local sediment transport. The model can simulate the bed and suspended sediment loads of both cohesive and non-cohesive sediment fractions; and hydrodynamic and sediment transport calculations are coupled to provide accurate morphological evolution (DHI, 2011). This section covers selected aspects of the model theory and required inputs.

2.3.1 Hydrodynamic governing equations

2.3.1.1. Hydrodynamic equations

Mike21C solves vertically integrated two-dimensional forms of the Saint Venant equations for continuity (conservation of mass) and conservation of momentum over an orthogonal curvilinear grid, which is created through the solution of elliptic partial differential equations. (DHI, 2011)

The Saint Venant flow equations are defined for the curvilinear co-ordinate system with simplifying assumptions including the shallow water approximation, a hydrostatic vertical pressure distribution, and a "rigid lid" water surface with no shear stresses. The model is thus only valid for river flows with low Froude numbers which curve gently and have gradually changing beds. Figure 2-6 shows the locations of the defined water depth, h, and fluxes p and q along the s and n axes respectively in the curvilinear coordinate system.

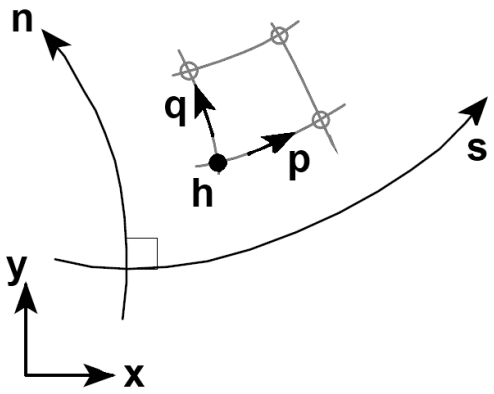

Figure 2-6 Definition sketch for curvilinear coordinate system

The continuity (2-1) and the s- and n-direction momentum (2-2 and 2-3 respectively) partial differential equations for the curvilinear coordinate system are as follows:

$$\frac{\partial H}{\partial t}+\frac{\partial p}{\partial s}+\frac{\partial q}{\partial n}-\frac{q}{R_s}+\frac{p}{R_n}=0 \qquad \textbf{2-1}$$

$$\frac{\partial p}{\partial t}+\frac{\partial}{\partial s}\left(\frac{p^2}{h}\right)+\frac{\partial}{\partial n}\left(\frac{pq}{h}\right)+2\frac{pq}{hR_n}+\frac{p^2-q^2}{hR_s}+gh\frac{\partial H}{\partial s}+\frac{g}{C^2}\frac{p\sqrt{p^2+q^2}}{h^2}=RHS \qquad \textbf{2-2}$$

$$\frac{\partial q}{\partial t}+\frac{\partial}{\partial s}\left(\frac{pq}{h}\right)+\frac{\partial}{\partial n}\left(\frac{q^2}{h}\right)+2\frac{pq}{hR_s}+\frac{q^2-p^2}{hR_n}+gh\frac{\partial H}{\partial n}+\frac{g}{C^2}\frac{p\sqrt{p^2+q^2}}{h^2}=RHS \qquad \textbf{2-3}$$

Where: H = water level / surface elevation [m]

h = water depth [m]

s, n = curvilinear coordinates

p, q = mass fluxes in the s, n directions [$m^3/s/m$]

R_s, R_n = radius of curvature of s, n gridlines [m]

C = Chezy roughness coefficient [$m^{1/2}/s$]

G = gravitational acceleration [m/s^2]

RHS = right hand side of the force balance equation including terms for Reynold's stresses, Coriolus force and atmospheric pressure

The momentum equations (2-2 and 2-3) show the terms for the time derivative, for convective and cross-momentum, for gravity and for resistance, while other terms that arise due to factors such as turbulence, Coriolus force and atmospheric pressure are grouped into the *RHS* term. Turbulence is accounted for using Reynold's stresses included in the *RHS* term with the following expressions for the *s* (2-4) and *n* (2-5) curvilinear directions:

$$\frac{\partial}{\partial s}\left(E\frac{\partial p}{\partial s}\right)+\frac{\partial}{\partial n}\left(E\frac{\partial p}{\partial n}\right)-\frac{2E}{R_s}\frac{\partial q}{\partial s}-\frac{\partial E}{\partial s}\frac{q}{R_s}-\frac{2E}{R_n}\frac{\partial q}{\partial n}-\frac{\partial E}{\partial n}\frac{q}{R_n} \qquad \textbf{2-4}$$

$$\frac{\partial}{\partial s}\left(E\frac{\partial q}{\partial s}\right)+\frac{\partial}{\partial n}\left(E\frac{\partial q}{\partial n}\right)+\frac{2E}{R_s}\frac{\partial p}{\partial s}+\frac{\partial E}{\partial s}\frac{p}{R_s}+\frac{2E}{R_n}\frac{\partial p}{\partial n}+\frac{\partial E}{\partial n}\frac{p}{R_n} \qquad \textbf{2-5}$$

Where E = turbulent/eddy viscosity [m^2/s]

2.3.1.2. Helical flow

The centripetal acceleration of flow particles around bends causes a secondary helical flow pattern as illustrated in Figure 2-7 and discussed in detail in the *Mike21C* Scientific Documentation (DHI, 2011). As a result of helical flow the direction of bed shear stress is:

$$\tan\delta_s=-\alpha\cdot\frac{2}{\kappa^2}\left(1-\frac{\sqrt{g}}{\kappa C}\right)\cdot\frac{h}{R_s} \qquad \textbf{2-6}$$

Where α = calibration constant

κ = Von Karman's constant, 0.4

C = Chezy number

h = flow depth

R_s = radius of curvature of stream lines

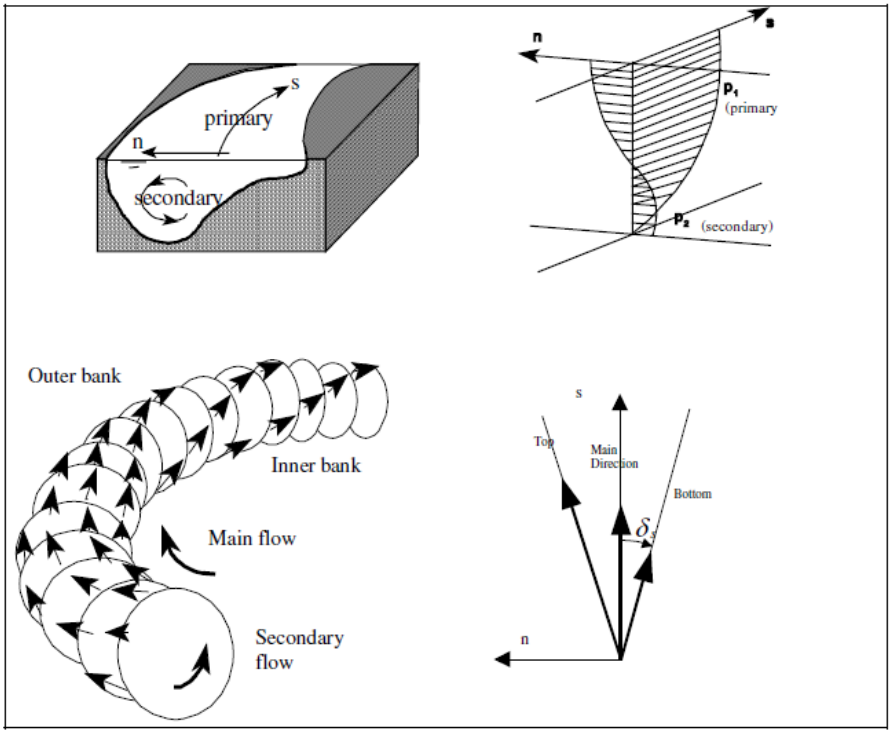

Figure 2-7 Helical flow patterns around bends (DHI, 2004)

2.3.2 Sediment transport

Sediment particles being transported by a river may roll, slide or saltate along the bottom as a *bed sediment load*, or they may be lifted off the bed and entrained in the flow as a *suspended sediment load*. The sum of the bed load and the suspended load make up the *total sediment load*[a]. The amount of sediment that is transported is influenced by many factors including size, grading and availability of sediment particles as well as flow characteristics such as slope, flow depth, and flow velocity.

Many researchers have investigated the transport capacity of uniform shear flows using a number of different approaches to arrive at many different formulae. They have all been verified for certain conditions but unfortunately there is no single formula that is considered

[a] A *wash load* of non-bed material that mostly floats down the river is also often listed as a type of sediment transport but it is generally neglected from morphological studies because it does not influence bed changes.

universally superior. Some of the approaches consider bed loads and suspended loads separately while others calculate the total load directly. Additionally, when incorporated into a mathematical model, some of the transport formulae require greater computational effort or are more prone to numerical instability than others. *Mike21C* offers a choice between 7 different transport equations (summarised in Table 2-2 using information from DHI (2011) and Gray & Simoes (2009)). When a total load transport theory is applied a differentiation between bed load and suspended load is made (if required) using a fixed ratio set by the user.

Table 2-2 Summary of sediment transport equations available in *Mike21C*

Transport theory	Type	Approach	Notes
Engelund & Hansen (1967)	total load	semi-empirical, based on energy concepts	widely used especially for sand dune beds, default theory for *Mike21C*, inaccurate very close to initiation of sediment motion
van Rijn (1984)	bed load & susp. load	semi-empirical, based on energy concepts	differentiation between bed and suspended loads based on ratio of bed shear velocity to particle falling velocity
Engelund, Fredsoe & Zyserman (1976)	bed load & susp. load	theoretical, probabilistic, semi-empirical	empirical concentration specification based on wide range of sediment sizes
Meyer-Peter & Muller (1948)	total load	theoretical, based on shear stress	total load based on magnitude of shear stress above critical shear stress, only valid for dominating bed load, $d > 1$ mm, $0.004 < S < 0.02$
Smart & Jaeggi (1983) and empirical	total load	semi-empirical, based on shear stress	extended from Meyer-Peter & Muller, eight user specified coefficients and exponents provide for custom transport theories
Yang (1983) – for sand	total load	theoretical, based on energy concepts	based on unit stream power, found to be most accurate formula for $0.063 < d < 2$ mm by many studies
Yang (1984) - for gravel	total load	theoretical, based on energy concepts	similar to Yang (1983) for sand but with modified coefficients

Mike21C predominantly models non-cohesive sediment transport but it does have the ability to include one cohesive fraction. When a cohesive fraction is included the suspended load follows a non-equilibrium description and therefore a total load formula which does not

differentiate between bed and suspended loads is not recommended (DHI, 2011). Additionally, a separation between bed load and suspended load is required for the effects of helical flow and bed slope to be accurately included (DHI, 2004). In this study a cohesive fraction was included so only two of the transport theories were applicable: the van Rijn, and the Engelund, Fredsoe & Zyserman methods. An overview of these two transport theories (DHI, 2011) is given in sections 2.3.2.3 and 2.3.2.4.

2.3.2.1. Bed load considerations

The bed load transport equations (detailed in sections 2.3.2.3 and 2.3.2.4) were derived for uniform shear flows in straight laboratory flumes. In natural rivers the magnitude and direction of bed load transport is also influenced by the local bed slope and by helical flow patterns around bends (which result in deviations of the bed shear stress from the main flow direction). *Mike21C* accounts for these effects with simplified transformations to the bed loads calculated from the transport theories. Equation 2-7 defines the transformation to account for the slope in the main flow direction, $\partial z/\partial s$, while equation 2-8 gives the transformation for the transverse direction:

$$S_s = \left(1 - \alpha \cdot \frac{\partial z}{\partial s}\right) S_{bl} \qquad \textbf{2-7}$$

$$S_n = \left(\tan\delta_s - G \cdot \theta^{-a} \cdot \frac{\partial z}{\partial n}\right) S_{bl} \qquad \textbf{2-8}$$

Where S_{bl} = bed load from transport theory

S_s = transformed bed load in main flow (s) direction

$\partial z/\partial s$ = bed slope in s-direction

α = calibration factor (varies from 0.2 to 1.5, default = 1)

S_n = transformed bed load in transverse (n) direction

$\tan\delta s$ = helical flow induced bed shear direction change

θ = Shields parameter

$\partial z/\partial n$ = bed slope in n-direction

G = calibration factor (1.25 recommended for rivers)

a = calibration factor (0.5 recommended for rivers)

In order to account for other differences that arise from extending theoretical equations derived in laboratory conditions to a natural river an additional bed load constant calibration factor may be set by the user to scale the sediment transport capacity by a constant value. Morphological changes due to bed load are determined by comparing the sediment transport capacity to the inflowing sediment transport volume at each cell in each time step: If the incoming sediment volume is greater than the transport capacity then the excess sediment is deposited; and if the incoming sediment volume is less than the transport capacity (and there is still sediment available in the bed layer) then erosion takes place.

2.3.2.2. Suspended load considerations

For the bed load morphological calculations, adjustments of the actual sediment loads to the sediment transport capacity are assumed to occur instantly in each cell in each time step. The same assumption cannot be made for suspended sediments, especially fine cohesive sediments. Suspended sediment concentrations do not react instantly to changes in river hydraulics therefore expressions for a *time lag* and *space lag* are incorporated into the model formulation. The suspended sediment loads are calculated by solving depth-averaged advection-dispersion partial differential equations (full expressions given in DHI, 2011), which require an expression for the equilibrium suspended sediment concentrations such as given by the van Rijn or Engelund, Fredsoe & Zyserman equations (described in sections 2.3.2.4 and 2.3.2.5). A constant factor which scales the equilibrium suspended sediment concentrations may also be specified by the user for calibration.

2.3.2.3. Van Rijn equations

Bed load

The van Rijn formula for bed load was derived by numerically solving the equations of motion for a single particle (in terms of defined dimensionless parameters) and applying an empirical expression for sediment concentration obtained from analysis of flume bed load measurements (with sediment sizes from 0.2 to 2 mm). The formula for bed load is:

$$S_{bl} = 0.053 \frac{T^{2.1}}{D_*^{0.3}} \sqrt{(s-1) g d_{50}^{\ 3}} \qquad \textbf{2-9}$$

Where S_{bl} = bed load per unit width [$m^3/s/m = m^2/s$]

T = non-dimensional transport stage parameter defined in equation 2-10

D_* = non-dimensional particle parameter defined in equation 2-11

s = relative density of sediment

$$T = \left(\frac{u_{f'}}{u_{fc}}\right)^2 - 1 = \left(\frac{u\sqrt{g}/C'}{\sqrt{\theta_c (s-1) g d_{50}}}\right)^2 - 1 \qquad \textbf{2-10}$$

$$D_* = d_{50} \left(\frac{(s-1)g}{\nu^2} \right)^{1/3} \qquad \textbf{2-11}$$

Where ν = kinematic viscosity of water

$u_{f'}$ = effective friction velocity [$= u\sqrt{g}/C'$]

u_{fc} = critical friction velocity [$= \sqrt{\theta_c (s-1) g d_{50}}$]

C' = resistance due to skin friction [$= 18\log(4h/d_{90})$]

h = water depth

u = mean flow velocity

θ_c = critical dimensionless shear stress (Shields parameter) defined in Table 2-3

Table 2-3 Critical Shields parameter for use in van Rijn's method

Range of D_*	θ_c
$D_* < 4$	$0.24/ D_*$
$4 < D_* < 10$	$0.14\ D_*^{-0.64}$
$10 < D_* < 20$	$0.04\ D_*^{-0.1}$
$20 < D_* < 150$	$0.013\ D_*^{0.29}$
$D_* > 150$	0.055

Suspended load

The van Rijn model includes suspended sediment transport if the bed shear velocity, u_f, is above a certain ratio of the sediment fall velocity, w_s:

- for $D_* < 10$, suspended transport occurs is $u_f > 4w_s / D_*$; *and*
- for $D_* > 10$, suspended transport occurs if $u_f > 0.4\ w_s$.

The suspended sediment concentration c_a (at a reference level $a = \max(0.01h, 2d_{50})$), is calculated from equation 2-12, and then the depth-integrated sediment load is calculated from equation 2-13 in which Z is a modified Rouse suspension parameter with empirically derived correction factors for the concentration profile and the diffusion coefficient for suspended sediment.

$$c_a = 0.015 \frac{d_{50} T^{1.5}}{a D_*^{0.3}} \qquad \textbf{2-12}$$

$$S_{sl} = f\ c_a\ u\ h = \frac{\left(\frac{a}{h}\right)^Z - \left(\frac{a}{h}\right)^{1.2}}{\left(1 - \frac{a}{h}\right)^Z (1.2 - Z)}\ c_a\ u\ h \qquad \textbf{2-13}$$

2.3.2.4. Engelund, Fredsoe and Zyserman equations

Bed load

The Engelund, Fredsoe and Zyserman (EFZ) formulae were derived based on a probabilistic approach first proposed by Einstein (1945). Engelund and Fredsoe (1976) found the probability of a sediment grain being moved by a flow to be a function of a non-dimensional skin shear stress, θ', acting on the particle and hence derived the following bed load transport formula:

$$S_{bl} = 5p(\sqrt{\theta}' - 0.7\sqrt{\theta_c})\sqrt{(s-1)gd_{50}^3} \qquad \textbf{2-14}$$

Where p = probability of movement defined in equation 2-15

θ' = non-dimensional skin shear stress defined in equation 2-16

θ_c = critical Shields parameter

$$p = \left[1 + \left(\frac{\frac{\pi}{6}\mu_d}{\theta' - \theta_c}\right)^4\right]^{-1/4}, \quad \theta' > \theta_c \qquad \textbf{2-15}$$

$$\theta' = \frac{u'_{*f}{}^2}{(s-1)gd_{50}} \qquad \textbf{2-16}$$

Where μ_d = dynamic friction coefficient [= tan27° = 0.51]

u_f = skin friction velocity

The skin friction velocity in equation 2-16 is calculated using equation 2-17 assuming a logarithmic vertical velocity profile.

$$u_f = \frac{u}{6 + 2.5\ln(h/2.5d_{50})} \qquad \textbf{2-17}$$

Suspended load

The Zyserman and Fredsoe (1994) empirical relation for the suspended sediment concentration near the bed (as a function of the difference between the actual and critical Shields stress parameters) is used to calculate the suspended sediment load.

$$c_b = \frac{0.331(\theta - \theta_c)^{1.75}}{1 + \frac{0.331}{0.46}(\theta - \theta_c)1.75} \quad \textbf{2-18}$$

A dimensionless logarithmic vertical coordinate, η, is then defined (equation 2-19), consisting of 99 grid points most densely stacked closest to bottom of the flow.

$$\eta_j = \eta_{j-1} + \frac{1}{\left(\frac{1-1.08^{99}}{1-1.08}\right)-1} \cdot 1.08^{j-1} \quad \textbf{2-19}$$

The velocity and concentration profiles are then defined in terms of η (equations 2-20 and 2-21) and the total suspended load is finally found through integration as shown in equation 2-22.

$$u(\eta) = \frac{\sqrt{g}}{0.4C} \ln\left(\frac{\eta}{\eta_0}\right) \quad \textbf{2-20}$$

$$c(\eta) = \left(\frac{1-\eta}{\eta} \cdot \frac{a}{1-a}\right)^Z \quad \textbf{2-21}$$

$$S_{sl} = c_b u h \int_{\eta_0}^{1} u(\eta) \cdot c(\eta) d\zeta \quad \textbf{2-22}$$

Where C = Chezy roughness

a = defined reference level [$=2d_{50}/h$]

Z = Rouse suspension parameter [$= w_s/\kappa u_f$]

η_o = no slip level (found by iterative solution)

ζ = integration parameter

2.3.3 Required inputs

A *Mike21C* river morphology model is first and foremost defined by the parameters which describe the physical river shape and boundary conditions. These parameters, listed and discussed in detail in section 2.3.3.1, have the largest impact on the model solutions.

- A curvilinear grid and associated bathymetry;
- hydraulic boundary conditions;
- sediment transport fractions and bed composition; and
- sediment transport boundary conditions.

Also of significant importance in determining the model results are the primary calibration factors. Resistance (or roughness) parameters are used to calibrate the hydrodynamic results; while the bed load factor and suspended load factor are used to calibrate sediment transport rates. Section 2.3.3.2 gives more information on the primary model calibration.

Additional parameters that must be specified include solver settings and secondary calibration factors including:

- hydrodynamic (HD) integration scheme;
- simulation time-steps;
- flooding and drying depths;
- eddy viscosity;
- helical flow constant;
- slope effect constants; and
- dispersion coefficients.

These parameters are described in more detail in section 2.3.3.3.

2.3.3.1. Primary physical model definition parameters

Grid and Bathymetry

The curvilinear grid required for a *Mike21C* simulation is created graphically and orthogonalised using the *Mike21C Grid Generator*. Once a satisfactory grid has been created an associated bathymetry file containing the elevations of each of the grid cells is created from a digital elevation model (DEM).

Hydraulic boundary conditions

For river applications, a flow hydrograph (or constant flow) is generally specified as the upstream (inlet) boundary while a water level series (or constant level) is specified at the downstream (outlet) boundary. Additional point sources or sinks may be specified anywhere within the model domain to represent tributary inflows or water abstraction points.

Sediment fractions and bed composition

The sediment size for the model may be specified as a number of fractions (each with a single grain size), and a number of layers may be specified for the bed each consisting of different ratios of the defined sediment fractions. A greater number of sediment fractions and layers increases the accuracy of the model but also increases the computational time required to complete a simulation.

Sediment transport boundary conditions

The amount of sediment entering and leaving the model domain needs to be specified as a load, a concentration or a bed level change for each fraction of the bed load and suspended load. A commonly used boundary condition is zero bed level change which sets the boundary sediment load equal to the equilibrium load (calculated by the chosen transport equation) so that no deposition or erosion occurs at the boundary.

2.3.3.2. Primary calibration parameters

Resistance specification

The mathematical equations solved by *Mike21C* incorporate Chézy roughness coefficients. However the model roughness may also be specified using Manning values which the model converts to Chézy coefficients using the water depth. Such a specification leads to a more stable numerical solution when the bed level varies significantly in the model. The calibration of the model resistance requires an iterative process: first an initial roughness is assumed[a], then a simulation is performed, the results are compared to field measurements (of flow velocities, water depths or water levels), and the guessed roughness is updated until the simulation results correspond suitably with field measurements.

Sediment transport calibration

A single bed load factor (for the entire model domain) and a single suspended load factor may be applied to the sediment transport formulae (for each fraction) to calibrate simulated loads to match selected field measured loads. Theoretically, and by default, the calibration factors are unity. For river applications, substantially more accurate results are often obtained by calibrating these parameters. The calibration process is the same as described above for the model resistance.

2.3.3.3. Additional parameters and solver settings

Hydrodynamic integration

The hydrodynamic (HD) integration for the model solution is *fully dynamic* by default but *quasi-steady* and *scaled-dynamic* options are also available for performing faster long-term simulations. However, when the model boundary conditions vary significantly (eg. rapidly

[a] Typical roughness values for various river types can be found in the literature (eg. Chow, 1959)

varying hydrographs or tidal water levels) the fully dynamic specification is required for accurate results.

Time steps

The hydrodynamic time step required for convergence of the numerical solutions is dependent on the size and shape of the curvilinear grid cells. A smaller time step is necessary for smaller grid cells and a less uniform grid. Generally, the hydrodynamic time-step, Δt, should be chosen so that the Courant number, Cr, is in the order of 1:

$$Cr = \frac{u\ \Delta t}{\Delta s} \qquad \textbf{2-23}$$

Where u = flow velocity

Δs = cell size in the flow direction

A separate, slightly longer, time step may be specified for the sediment transport calculations. When a simulation "crashes" or numerical convergence is not obtained the time steps often need to be decreased in order for accurate simulation to continue.

Flooding and drying depths

The flooding and drying depths are the maximum and minimum depths at which cells are included in the hydrodynamic calculations. The default flooding and drying depths are 0.3 m and 0.2 m respectively. Decreasing the flooding and drying depths increases the computation time of a simulation but may give more accurate results and improve numerical convergence in cases where significant flooding and drying are expected (DHI, 2003).

Eddy viscosity

The eddy viscosity can be specified as a constant or be calculated by the model using the Smagorinsky formula. In both cases a constant calibration parameter must be specified.

While the Smagorinsky formula is probably the most accurate formulation, it increases simulation time and may cause numerical instability in cases of significant flooding and drying. The Smagorinsky formula is therefore generally avoided in river applications (DHI, 2003). There is also an option between a flux based and a velocity based formulation. The flux based formulation is only valid for deep water or floodplain scenarios where there is either very little spatial variation in water depth or very high bed resistance. The velocity based formulation is thus preferred for river applications (DHI, 2011). The value of the velocity based constant eddy viscosity has been found to have very little effect on the solution in many river studies (eg. DHI, 2011; Dorfmann & Knoblauch, 2009).

Additional sediment transport calibration parameters

Like the eddy viscosity, which is a secondary calibration parameter for the hydrodynamic results, the *helical flow constant*, the *bed slope constants* and the *AD dispersion coefficients* provide extra calibration opportunities for the sediment transport calculations. However, a large amount of field information would be required to calibrate these constants and they normally have an insignificant effect on the overall solution in river applications (DHI, 2011).

3 MODEL SET-UP

To investigate the effects of dams on the Zambezi Delta a hydrodynamic-morphological model was created and two long-term simulations were performed: one to represent the current post-dam conditions and the other simulating the conditions before dams, or the *pre-dam* condition. For both scenarios the simulations were performed for a period of approximately 10 years (1 October 2000 to 25 August 2010 – the total period that flow records were provided for).

A hydrodynamic-morphological model is physically described by the shape and composition of the river-floodplain bed, and by boundary conditions of water flow rates or levels and sediment fluxes. Under ideal conditions these physical descriptions are all specified from accurately measured field data. When there is a shortage of accurate field information assumptions of the boundary conditions need to be made carefully and the limitations that they pose to the accuracy of the model results need to be understood. In sections 3.1 to 3.5 the sources of supplied boundary information, and the assumptions and calculation procedures performed to estimate the required boundaries where direct information was not available, are discussed.

The two-dimensional modelling computations are performed on a defined curvilinear grid over the model domain, the size and shape of which are important for model accuracy and resolution. The process used to determine the most suitable grid for this model study is discussed in section 3.6.

The hydrodynamic and sediment transport calculations performed by the model are influenced by a number of calibration factors. The dominant calibration factors are the hydraulic roughness and the sediment transport equation calibration factors and the

calibration of these factors in discussed in sections 3.7 and 3.8. A summary of the final model set-up is provided in section 3.9.

3.1 Bathymetry

The first step in the hydrodynamic/morphological modelling process is the set-up of a suitable grid and bathymetry. A mesh of curvilinear cells is created using the *Mike21C* elliptical grid generator (see section 3.6) and then a digital elevation model (DEM) is imported from which an elevation is assigned to each cell. The DEM used for the bathymetry of this study was obtained from the navigation study of the Lower Zambezi (Rio Tinto, 2011) and was prepared by Southern Waters (2011). The DEM of the river channel and floodplains (including all land to be flooded in the post-dam 100 year event) was derived from three data sets, namely:

- bathymetric surveys of the river bed (underwater) in the deepest channels of the river (2008 – 2010);
- mapped water edges derived from Landsat thematic images and recorded stage levels at gauging stations (2001 – 2008); and
- Shuttle Radar Topography Mission (SRTM) global digital elevation model (2000).

The data sources and methodology used by Southern Waters (2011) are discussed in the sections which follow.

3.1.1 Bathymetric surveys (Southern Waters, 2011)

From 2/12/2008 to 7/01/2009 a bathymetric survey of a proposed navigation channel from Tete to Chinde was performed using depth-sounding equipment. Transects were surveyed every 60 to 90 meters along the length of the river but did not always include the full width of

the river or all of the distributaries (as the focus of the study was on the region of a navigation channel). The collected data was used to develop a DEM with 5 x 5 m grid spacing.

In July to August 2010 another bathymetric survey of the major southern branch of the delta and a few of the other tributaries not included in the 2008/09 survey was performed, and the information was used to expand the DEM from the 2008/09 survey. The gauge plates at all the gauging stations on the Lower Zambezi were also surveyed.

Because the bathymetric surveys only included regions that were underwater at the time of survey (and in most cases not even the entire breadth), additional information was required to extend the bathymetry to the river banks and floodplains.

3.1.2 Mapped water edges from Landsat images (Southern Waters, 2011)

Satellite images from the Thematic Mapper – a multispectral Earth observation sensor onboard Landsat 4 and Landsat 5 which scans at seven different spectral bands to provide images with high resolution, sharp spectral separation and good geometric fidelity (NASA, 2013) – were obtained for the lower Zambezi region for selected dates between 2000 and 2010 (the period for which gauge plate levels were available at most of the lower Zambezi gauging stations). The cell size of the images is 30 m x 30 m.

Three reference frames covered the (Southern Waters) study area from Tete to the ocean and four to five scenes were selected for each frame to attain the widest possible range of water levels with images with no or minimal cloud cover (<10 %). The selected scenes are show in Table 3-1 and the minimum and maximum gauge plate levels recorded from 2000 to 2010 are shown in Table 3-2. Unfortunately the maximum water level for which an acceptable scene could be identified for the delta region (Reference frame 166073) was 5.26 m at Marromeu

which is significantly below the maximum recorded water level of 7.68 m, and therefore the mapped water edges in the delta region are limited to those active at the lower flood level.

Table 3-1 **Scene dates and corresponding daily average gauge plate readings for the three Landsat reference frames covering the study area (Southern Waters, 2011)**

Reference frame	Scene date	Average daily gauge plate reading (m MSL)				
		Tete	Tambara	Mutarara	Caia	Marromeu
168071	2005/05/17	2.57	2.16	3.33		
	2006/11/12	3.34	2.65	4.09		
	2001/05/06	4.48	3.90	5.14		
	2007/02/16	5.86	4.86	6.19		
167072	2007/08/04		2.15	3.50	3.58	3.17
	2007/09/05		2.53	3.92	3.91	3.78
	2007/01/24		3.26	4.75	5.64	5.07
	2007/02/09		4.93	5.85	6.83	6.25
	2001/03/12		5.31	6.37	8.02	7.68
166073	2005/09/24				3.04	2.75
	2007/06/26				3.80	3.29
	2008/05/11				4.85	4.43
	2001/07/11				5.27	5.26

Table 3-2 **Minimum and maximum gauge plate readings at stations on the lower Zambezi from 2000 to 2010**

	Average daily gauge plate reading (m MSL)				
	Tete	Tambara	Mutarara	Caia	Marromeu
Minimum	1.91	1.68	3.01	2.31	2.08
Maximum	7.45	5.68	7.17	8.23	7.68

The elevations of the edges of the flow area for each of the selected frames were determined by drawing the land/water boundaries (for the main Zambezi channel and all visible tributaries within 15 km of the banks) on the satellite images and then assigning them heights using the gauge plate readings and recently surveyed gauge plate heights. At the gauge plate locations the elevations were determined as the average level on the date of the image (gauge plate readings for most stations are recorded three times a day) and in between gauging

stations the elevations of the flow boundaries were estimated by linear interpolation along the flow course.

The accuracy of the elevation points derived from this method is limited by the resolution of the satellite images and by the uncertainty associated with interpolating between gauging stations. The cell size of the satellite images is 30 m by 30 m and the accuracy of the horizontal location of the mapped water edges can therefore not be greater than this. Further, any channels or distributaries that are less than 30 to 60 m wide may not be detected at all (or may not show a connection with the main channel) in the satellite images and therefore not be captured in the DEM. The accuracy of the interpolated heights of the water boundaries is most uncertain in the flood plain regions furthest from the main channel where two-dimensional flow patterns may exist.

The co-ordinates and elevations of the high flow boundary lines were used to extend the DEM from the bathymetric survey. In the final DEM the additional points created using the Landsat images are included as a grid with 30 m by 30 m spacing.

3.1.3 SRTM data (Southern Waters, 2011)

The Shuttle Radar Topography Mission collected elevation data for approximately 80% of the earth's surface using a radar system onboard the Space Shuttle Endeavour during an 11 day trip in February 2000. The data is freely available for internet download in the form of DEM tiles covering 1 degree latitude by 1 degree longitude. The resolution of the elevation sample points is 3 arc seconds (approximately 90 m) for areas outside of the USA. (NASA, 2009)

An objective of the SRTM was to provide at least 16 m absolute elevation accuracy at the 90% level (NASA, 2009). The radar wavelength used for the SRTM (5.6 cm) only partially

penetrates vegetation so the elevation recorded for areas with dense vegetation is somewhere in between the tree top height and the topography height and will vary depending on the density of the vegetation at each specific sample point (NASA, 2009). Therefore the accuracy of the DEM decreases in more densely vegetated areas. Southern Waters (2011) mentions studies in various regions which have found the average accuracy (defined either in terms of the mean absolute error or the root mean square error) of the SRTM data to range from 2.7 m in flat areas with 1 arc second sampling (USA) to 7.6 m in mountainous areas with 3 arc second sampling (outside of the USA). In some areas studies have revealed systematic shifts in the SRTM data which can be corrected for to significantly reduce the mean error. Karwel and Ewiak (2008) used such systematic shifts to reduce the root mean square error for flat and hilly areas in Poland from 2.9 m and 5.4 m to 1.0 m and 2.7 m respectively.

The SRTM data for the lower Zambezi was downloaded and the elevations were compared to those obtained using the Landsat images (Southern Waters, 2011). Substantial differences were observed in the steep areas through gorges and near the river mouth where dense forests occur. However, in the flatter regions the accuracy appeared “reasonable” and no clear systematic shifts were identifiable and hence the raw SRTM data without any correction factors was used to extend the DEM for the lower Zambezi model bathymetry (Southern Waters, 2011). Southern Waters (2011) do not mention mean or maximum differences between the SRTM and Landsat elevations for the whole extent of their domain except to observe that the differences are everywhere well within the SRTM quoted objective of 16 m and that for a selected length of floodplain (approximately 160 km between Tambara and Mutarara) the root mean square difference is approximately 1.8 m.

The SRTM elevation points were added to the DEM for the lower Zambezi on a 90 m by 90 m grid to supply elevations for the flood plains above the edge lines drawn from the Landsat images.

3.1.4 Summary and expected accuracies

The final grid format DEM prepared by Southern Waters (2011) consists of the following (Figure 3-1 shows the locations of elevation points at a selected river cross section):

- elevations within the main river channel, derived from bathymetric surveys (2008-2010), with 5 m x 5 m grid spacing;
- elevations of the main channel banks and frequently flooded floodplain areas, derived from Landsat Thematic Images (2001-2008), with 30 m x 30 m grid spacing; and
- elevations of the higher floodplain areas derived from the SRTM DEM (2000), with 90 m x 90 m grid spacing.

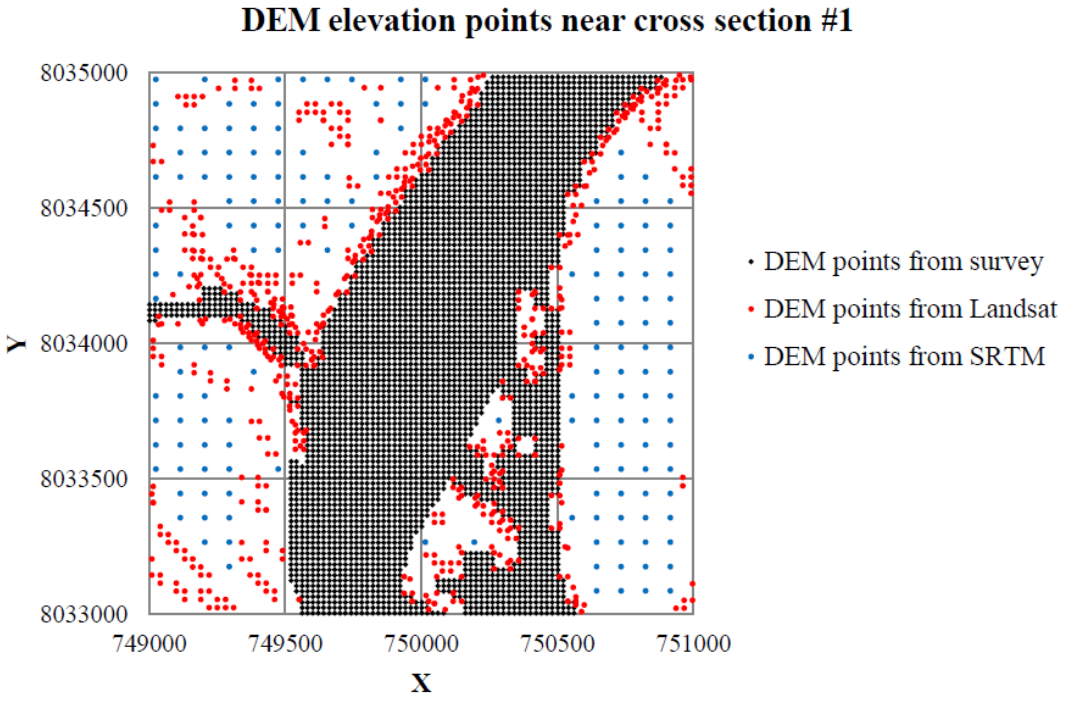

Figure 3-1 DEM elevation points at a selected river section (cross section #1 in Figure 3-20)

Southern Waters (2011) do not give values of accuracies associated with any of the bed elevations. The elevations determined through bathymetric surveys are generally very accurate at the locations where the cross-sections are measured (every 60 to 90 m) but become less accurate where elevations are interpolated between cross sections. Errors up to about 1 m could probably be expected (for the date of measurement) for the 5 m x 5 m data set. For the SRTM (90 m x 90 m) data set the errors may be as much as 5 to 10 m, while the accuracy of the Landsat derived data set is probably somewhere between the other two. A further source of inaccuracy is introduced by the time gaps between measurements. The sand bed of the Zambezi River is highly dynamic and bed level changes of several meters can occur within only a few months.

The bathymetry used is therefore an approximate representation of the bed of the Zambezi River and floodplains in the 2000's and therefore the model, while suitable for predicting general trends and wide-spread effects, cannot be relied upon to accurately predict changes at any specific site.

3.2 Water inflows

3.2.1 Post-dam scenario

The daily recorded water levels and flows for five gauging stations on the Lower Zambezi for a ten year period (October 2000 – September 2010) were supplied by Southern Waters (2011), and the flows for the Caia gauging station were used as the upstream boundary for the post-dam scenario (see Figure 3-2).

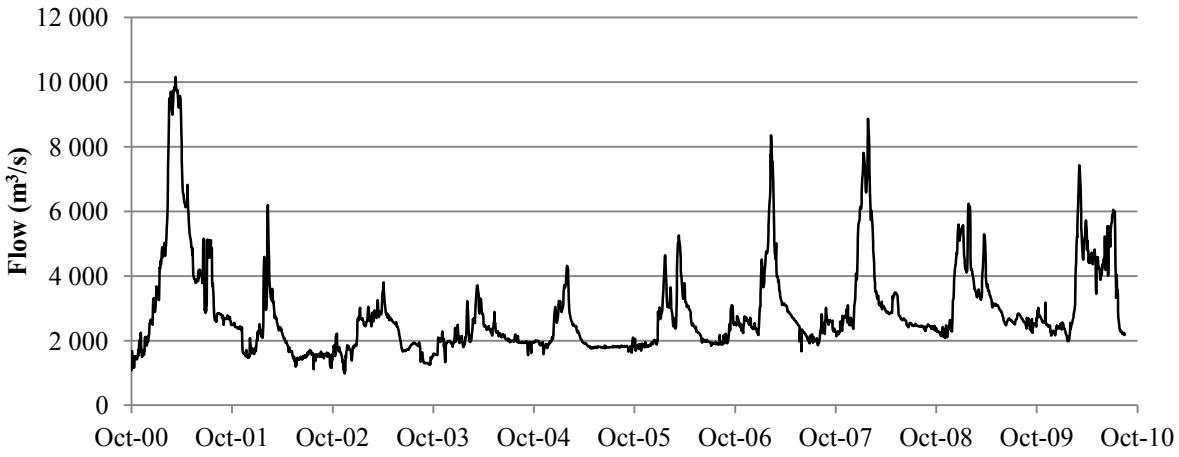

Figure 3-2 Inflow time series for post-dam scenario: observed flows at Caia

Gauge plate readings are generally recorded three times daily at the stations on the Lower Zambezi. The period from 2000 to 2010 contained the most complete stage records but there were still some gaps at all stations (Southern Waters, 2011). The original record for Caia had gaps for a total of 173 days in the 10 year record (approximately 5%). Additionally, the river has a dynamic sand bed at all stations and discharge measurements have rarely been made thus there are no reliable discharge rating curves. To obtain the flow series for Caia (Figure 3-2) Southern Waters (2011) patched the stage record (using data from the nearest stations if it was available, or otherwise averaging) and then applied a software-generated shifting rating curve based on the few available discharge measurements. The flow series can therefore not be expected to be highly accurate, but it is detailed and provides at the least a good approximation of the post-dam flow patterns to the delta region.

3.2.2 Pre-dam scenario

No daily flow records in the Lower Zambezi prior to dams were available for this study. The post-dam observed flows (Figure 3-2) were therefore adjusted to represent a pre-dam condition. The major dams in the Zambezi catchment result in decreased total flows downstream due to evaporation as well as drastically altered seasonal flow patterns. Beilfuss

and dos Santos (2001) provide average evaporation rates for each of the major reservoirs as well as the average monthly flows before and after the construction of dams at Mutarara, about 100 km upstream of Caia (see more in sections 3.2.2.1 to 3.2.2.3). Using this information monthly scaling factors were applied to increase the total flow to account for evaporative losses and to redistribute the flows to match pre-dam seasonal variations such that: The total flows for the pre-dam scenario equal the total observed post-dam flows plus evaporative losses[a];

$$\sum_{10yrs} Q_{pre-dams} = \sum_{10yrs} Q_{post-dams} + \sum_{10yrs} Q_{evaporation\ from\ dams} \qquad \textbf{3-1}$$

And, the mean monthly flow distribution (over the 10 year time series) is proportional to the mean monthly flow observed from 1930 to 1958;

$$\left[\frac{\overline{Q}_{January}}{\overline{Q}_{annual}}\right]_{pre-dams} = \left[\frac{\overline{Q}_{January}}{\overline{Q}_{annual}}\right]_{1930\text{-}1958}; \quad \left[\frac{\overline{Q}_{February}}{\overline{Q}_{annual}}\right]_{pre-dams} = \left[\frac{\overline{Q}_{February}}{\overline{Q}_{annual}}\right]_{1930\text{-}1958}; etc. \qquad \textbf{3-2}$$

Figure 3-3 shows the final scaled "pre-dam" flow series at Caia to be used as model input for the pre-dam scenario. The sections which follow give more details of the scaling process.

[a] Water abstractions from dams were not taken into account because net abstractions are small and river abstractions of the same volume would be possible without dams. It is therefore assumed that the "pre-dam" abstractions are equal to the post-dam abstractions.

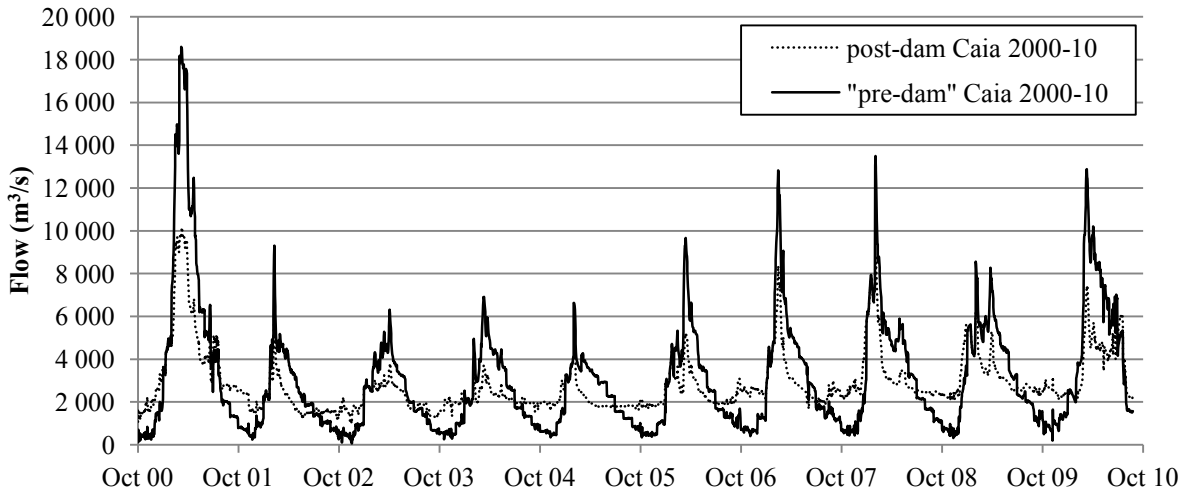

Figure 3-3 **Scaled inflow time-series at Caia for pre-dam scenario (solid line) with post-dam time-series (dotted line)**

3.2.2.1. Evaporation from dams

Table 3-3 shows the average annual evaporation rates (from Beilfuss & dos Santos, 2001) for the four major reservoirs in the Zambezi catchment. Cumulatively, evaporation from large dams decreases the Zambezi flows by an average of approximately 281 m^3/s.

Table 3-3 **Average annual evaporation from the major dams in the Zambezi River basin**

		Kariba	Kafue Gorge	Itezhitezhi	Cahora Bassa
Total annual evaporation	mm	1 694	1 620	1 784	2 200
Total annual rainfall	mm	739	840	739	677
Net annual evaporation	mm	955	780	1 045	1 523
Flooded area (at FSL)	km^2	5 577	805	374	2 670
85% FSL flooded area	km^2	4 740	684	318	2 270
*Net annual evaporation	10^6 m^3	4 527	534	332	3 456
Total evap. from all dams	10^6 m^3/yr	8 849			
Total evap. from all dams	m^3/s	281			

* Net annual evaporation volume calculated assuming the average flooded area = 85% of the flooded area at the full supply level (FSL)

The observed average flow rate at Mutarara between 2000 and 2010 (post-dams) was 2557 m^3/s and the average for the "pre-dam" scenario was therefore increased to 2838 m^3/s (11 %). At the model boundary at Caia (downstream of the Shire River confluence) the post-dam and "pre-dam" average flows for the 10 year period were 2841 and 3125 m^3/s respectively (an increase of 10%).

3.2.2.2. Changes in seasonal flow patterns

Beilfuss and dos Santos (2001) give the average monthly flows at Mutarara (100 km upstream of Caia) before and after the construction of dams showing a drastic reduction in the average annual peak (see darker lines in Figure 3-4). The average monthly flows observed at Mutarara from 2000 to 2010 (supplied record) and the scaled "pre-dam" flows have also been included in Figure 3-4. The average monthly distribution of flow (as a percentage of the total annual flow) for the pre-dam and post-dam periods is shown in Table 3-5.

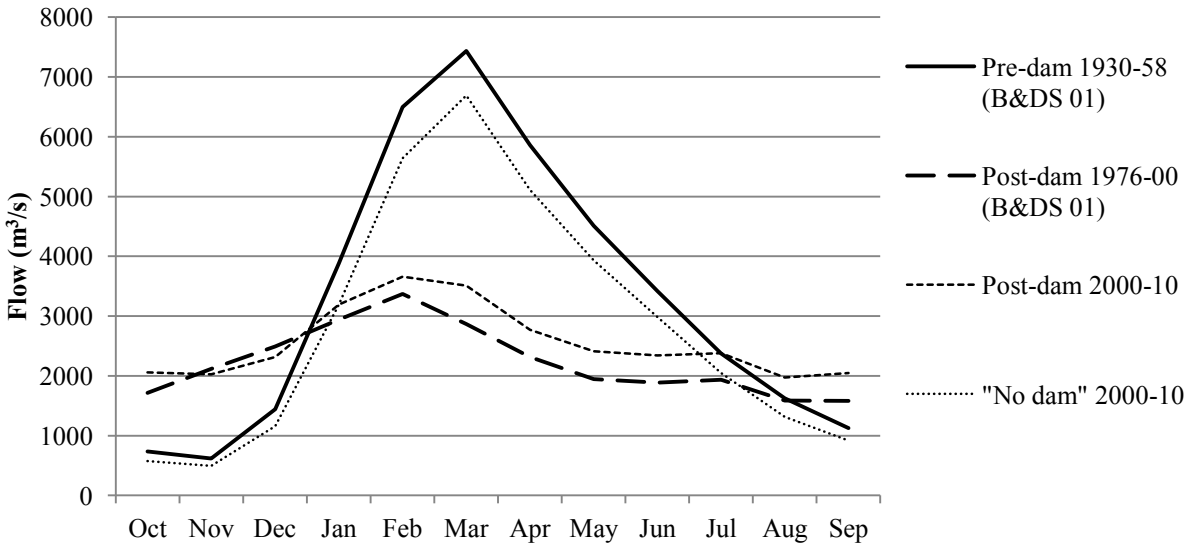

Figure 3-4 Mean monthly flows at Mutarara before and after the construction of dams

The last column of Table 3-4 shows the mean annual flow for each of the periods considered. The period from 1930 to 1958 is seen to be the wettest (3293m^3/s average flow); the period from 1976 to 2000 had much lower flows (2229 m^3/s average); and subsequently from 2000

to 2010 the mean flows increased slightly to 2557 m^3/s. The lower flows post-dams are largely due to climatic variations: 1976 to 2000 was a particularly dry period, 2000 to 2010 was slightly wetter, but not as wet as the period from 1930 to 1958[a]. Evaporation from the dams (and possibly also increasing upstream water abstractions) would also contribute to the lower post-dam flows.

Table 3-4 Average monthly flow (m^3/s) at Mutarara before and after the construction of dams

	Oct	Nov	Dec	Jan	Feb	Mar	Apr	May	Jun	Jul	Aug	Sep	Mean
Pre-dams 1930-58	736	617	1440	3886	6496	7436	5859	4509	3418	2372	1623	1125	3293
Post-dams 1976-00	1717	2115	2490	2940	3369	2868	2314	1945	1886	1937	1586	1582	2229
Post-dams 2000-10	2056	2026	2313	3193	3658	3508	2772	2412	2343	2379	1974	2046	2557
Scaled "pre-dams" 2000-10	*575*	*494*	*1159*	*3192*	*5641*	*6688*	*5111*	*3932*	*2983*	*2046*	*1314*	*920*	*2838*

Table 3-5 Average monthly distribution (%) of annual flow volume at Mutarara before and after the construction of dams

	Oct	Nov	Dec	Jan	Feb	Mar	Apr	May	Jun	Jul	Aug	Sep	Mean
Pre-dams 1930-58	1.9	1.6	3.6	9.8	16.4	18.8	14.8	11.4	8.6	6.0	4.1	2.8	8.3
Post-dams 1976-00	6.4	7.9	9.3	11.0	12.6	10.7	8.7	7.3	7.1	7.2	5.9	5.9	8.3
Post-dams 2000-10	6.7	6.6	7.5	10.4	11.9	11.4	9.0	7.9	7.6	7.8	6.4	6.7	8.3
Scaled "pre-dams" 2000-10	*1.9*	*1.6*	*3.6*	*9.8*	*16.4*	*18.8*	*14.8*	*11.4*	*8.6*	*6.0*	*4.1*	*2.8*	*8.3*

[a] After the addition of evaporative losses the mean flow for the period 2000 to 2010 is 2832 m^3/s, significantly lower than the 1930 to 1958 mean of 3293 m^3/s. While river abstractions have not been considered it is unlikely that consumptive use would make up a significant part of this difference, and therefore climatic factors are probably dominant.

3.2.2.3. Flows at Caia

Information on the historical annual distribution of flow was only available for Mutarara gauging station about 100 km upstream of Caia (and upstream of the Shire River confluence). Scaled flows were therefore first obtained for the Mutarara gauging station after which the flows at Caia were obtained by adding the difference between the Mutarara and Caia flows in the original post-dam record (on the assumption that the pre-dam and post-dam flows travel at the same speed so the lag between the stations is the same, and that the inflows from the Shire River tributary are the same for both scenarios[a]). Figure 3-5 shows the post-dam and "pre-dam" flows at Mutarara and Caia for a selected year of record.

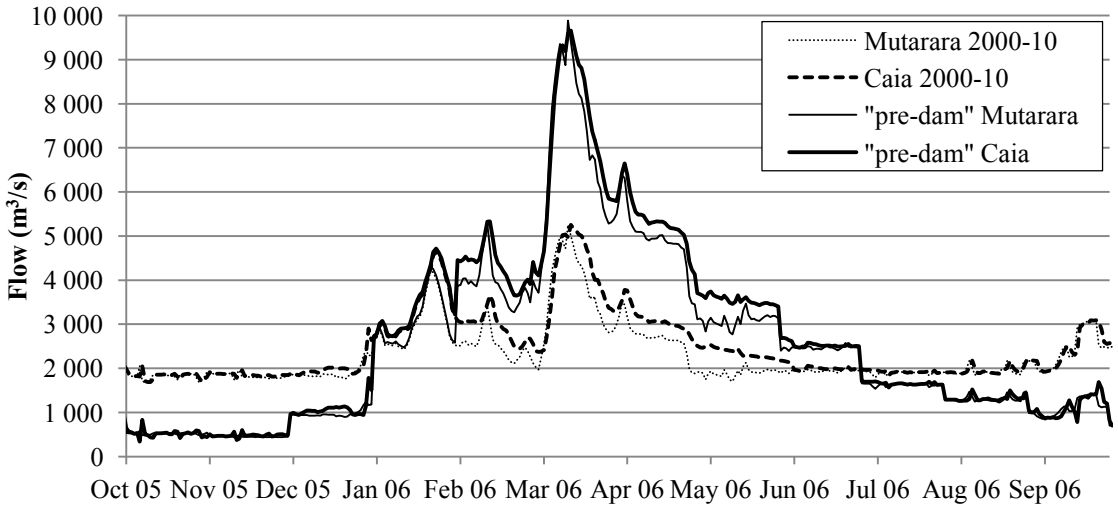

Figure 3-5 Observed post-dam flows and scaled "pre-dam" flows at Mutarara and Caia (2005-06)

3.3 Tidal water level

A generated tidal water level was provided from the Rio Tinto (2012) study for this research project, for which the AutoTide© software code (Geomatix Ltd, 2013)[b] was used. The tidal

[a] There are two hydropower stations on the Shire River but they are both run-of-the-river type instalments which do not have a large effect on the downstream flows.
[b] A comparison of generated tides with observed tidal levels for a 3 month period at Chinde showed AutoTide© to give the most accurate results (Rio Tinto, 2011)

water level is specified in 15 minute time steps. Figure 3-6 shows a section of the tidal water levels applied at the boundary.

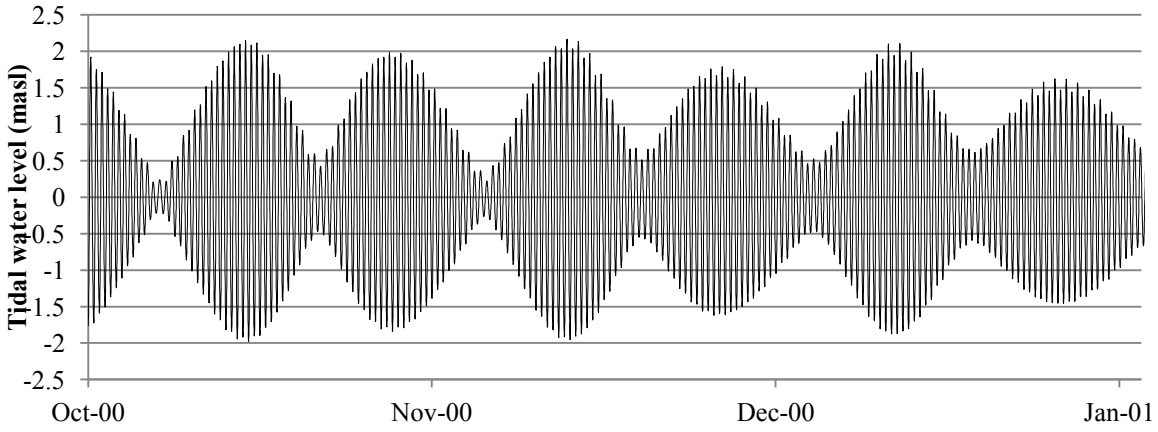

Figure 3-6 **Selected section of the tidal water level series used for the model downstream boundary**

3.4 Sediment fluxes

For the morphological modelling employed in this study bed loads and suspended loads are treated separately.

The majority of the Lower Zambezi bed is comprised of sand particles which are transported predominantly as a bed load. The bed load is simulated using an equilibrium equation calibrated with field data. Boundary conditions of zero bed level change were specified at both the upstream and downstream ends of the model (i.e. the in/out flowing sediment load equals the sediment carrying capacity of the flow for the first and last rows of cells in the model and therefore no erosion or deposition occurs on the boundary). The assumption implied is that there is no shortage of sediment available at the model boundary and the load is only a function of the flow characteristics and the sediment size.

The majority of the suspended particles in the Lower Zambezi, on the other hand, are of clay or silt size ($d<0.065$ mm) and are therefore affected by inter-particle forces and exhibit non-

equilibrium behaviour (i.e. the suspended load cannot simply be assumed to be equal to the sediment carry capacity of the flow as is done for course sediment) which is modelled using advection/dispersion theory. The suspended sediment behaviour within the model is highly dependent on the inflowing sediment flux which depends on the rates of erosion and deposition in the upstream catchment. Commonly, suspended sediment loads are specified from a sediment load versus water discharge rating curve, based on several years of local measurements, of the form:

$$Q_s = a Q_w^b \qquad \textbf{3-3}$$

Where Q_s = sediment load [m^3/s]

Q_w = water discharge [m^3/s]

a, b = constants

Insufficient suspended sediment load measurements have been performed on the Lower Zambezi for a direct load-discharge rating curve to be applied and therefore a two step process was adopted:

(a) A number of sources were considered to estimate the mean annual suspended sediment loads[t/year] for pre-dam and post-dam conditions; and

(b) A rating curve based on limited load and discharge measurements was adjusted to produce the desired mean annual sediment loads found in (1) for the 2000 to 2010 flow series.

The sediment load sources and calculations are described in detail in section 3.4.1. For the model study 45 Mt and 22.5 Mt were selected as the mean annual suspended sediment loads. These loads were distributed through the 10 year time series using a sediment load – discharge rating curve as discussed in section 3.4.2.

3.4.1 Estimation of mean annual suspended sediment loads to the Zambezi Delta

In order to make a reasonable estimate for the average annual suspended loads to the Zambezi Delta before and after dams, five different sources were considered as discussed in the sections which follow:

- The global sediment yields database (FAO, 2000);
- Global sediment yield distribution maps (from Walling & Webb, 1996) together with the Brune (1953) curve for sediment entrapment;
- A paper on the reservoir sedimentation of Kariba and Cahora Bassa (Bolton, 1984);
- Recorded suspended sediment loads at Marromeu from 1961-63 (COBA, 2011); and
- Recent once-off sediment load measurements from four field trips (ASP, 2012b; ASP, 2011; Vale, 2010; ASP, 2006)

Table 3-6 summarises the estimated suspended sediment loads to the Zambezi Delta from each of the methods considered. Both the load magnitudes and the ratios between the pre-dam and the post-dam loads differ significantly for the various methods considered. None of the methods can be considered highly accurate and thus a choice of loads was made to fall within the ranges predicted by most methods. The final pre-dam load to the delta was chosen to be 45 Mt/yr [a] and the post-dam load was chosen as 22.5 Mt/yr [b] (being a 50% reduction due to dams).

[a] Equivalent to an average sediment yield of 37 t/km·yr over the whole catchment area of 1.2 x10^6 km^2
[b] Equivalent to an average sediment yield of 70 t/km·yr over the 0.3 x10^6 km^2 downstream of Cahora Bassa Dam

Table 3-6 Mean annual suspended sediment loads to the Zambezi Delta estimated from various sources

Method	Pre-dam average annual load (Mt/yr)	Post-dam average annual load (Mt/yr)	Reduction due to dams
Rooseboom (1980)	38	20	47%
Walling&Webb(1983) map	32 to 73	13 to 29	40%
Lvovich,et al(1991) map	3 to 18	1 to 4	70%
Extended from Bolton (1984)	41 to 410	14 to 140	66%
MFPZ recorded 1960's	*51.5 and 125.4*	-	-
Chosen for model study	45	22.5	50%

3.4.1.1. Global river sediment yields database

A database of river sediment yields for about 800 of the world's largest rivers was compiled by HR Wallingford as part of the Food and Agricultural Organization of the United Nations' AQUASTAT program and is available online (FAO, 2000). This database gives a value of $38x10^6$ t/year for the total sediment load to the ocean before dams and $20x10^6$ t/year post-dams, and an average sediment yield for the catchment of 35 t/km^2·year with the reference being to Milliman and Syvitski (1992). However in the referenced article (Milliman & Syvitski, 1992), the authors refer to Milliman and Meade (1983), who in turn cite written communication with A. Rooseboom (1980) for the Zambezi load figure estimates. No further information is given on the basis of the estimate.

3.4.1.2. Global sediment yield maps with Brune curve for reservoir entrapment

Walling and Webb (1996) give two examples of global suspended sediment yield maps derived by Walling and Webb (1983) and Lvovich et al. (1991) and shown in Figure 3-7.

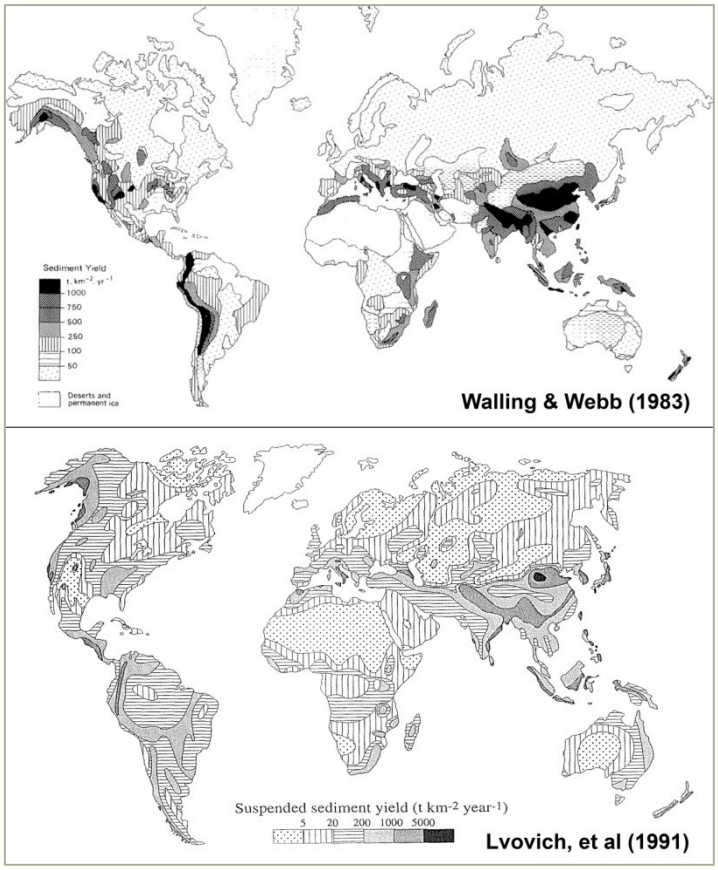

Figure 3-7 Global suspended sediment yield maps from Walling & Webb (1996)

The maps were derived from observed data from about 2000 rivers around the world, very few of which are in Africa, and are valid for catchment areas of about 1000 to 10 000 km^2 (Walling & Webb, 1996). Walling (personal communication, 2013) emphasized that the maps are highly generalised so cautioned that they may not provide accurate results for any specific area, particularly in Africa. Walling (2013) also suggested that the maps may be extended to larger areas except where there are reservoirs or vast wetlands where significant deposition is expected (the plotted values already take into account more standard conveyance losses). The sediment entrapment in reservoirs had been shown to be a function of the capacity to inflow ratio and can be predicted by the Brune's (1953) curve. If it is assumed that the sediment deposition in a wetland follows the same trend then the sediment loads to the Zambezi delta can be estimated by using the above-mentioned global sediment yield maps together with the Brune curve.

Figure 3-8 shows the Brune curve and Table 3-7 shows the calculation of the sediment trap efficiency of the major reservoirs and wetlands of the Zambezi catchment. Figure 3-10 shows the suspended sediment yields from the global maps on the Zambezi catchment, Figure 3-9 shows a demarcation of the Zambezi catchment into zones, and Table 3-8 and Table 3-9 show the calculations of the suspended sediment yields to the delta from the Walling & Webb and Lvovich et al. maps respectively. From the Walling & Webb map the predicted suspended sediment load to the delta is 32 to 73 Mt per year pre-dams and 13 to 29 Mt per year post-dams, while the Lvovich map predicts much lower loads of 3.5 to 18 Mt per year pre-dams and 1 to 4 Mt per year post-dams.

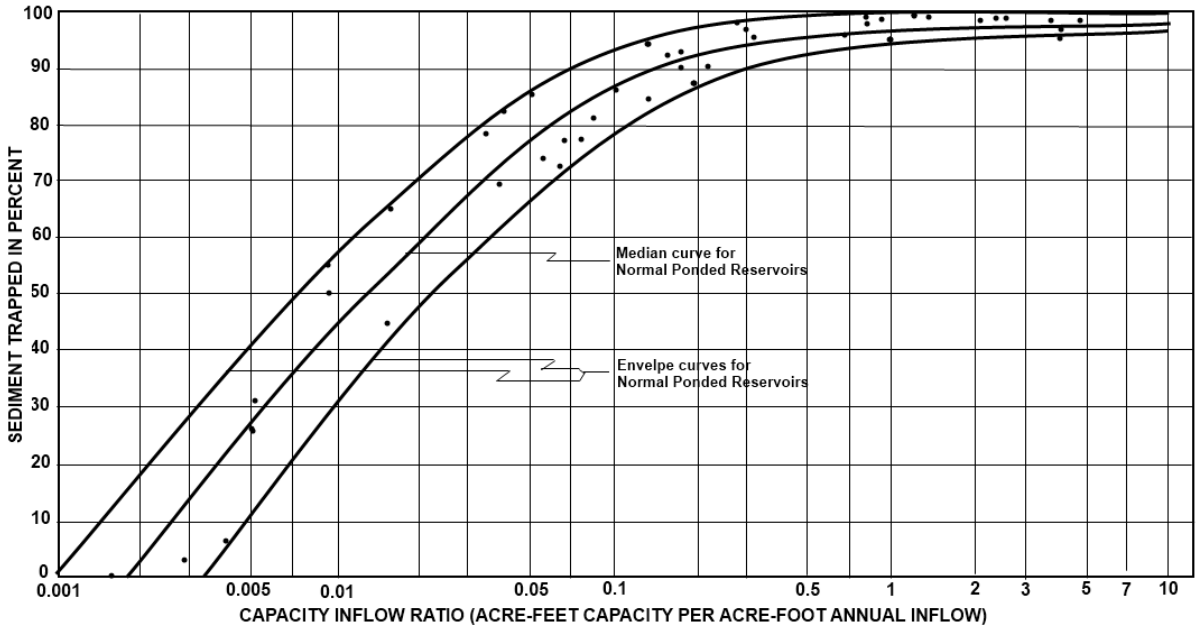

Figure 3-8 Brune (1953) curve for sediment entrapment in reservoirs

Table 3-7 Calculated sediment trap efficiency of major reservoirs and wetlands in the Zambezi River catchment

Reservoir		**Kariba**	**Itezhitezhi**	**Kafue Gorge**	**Cahora Bassa**
Year of Completion		1958	1977	1972	1974
Total Storage Volume (Capacity)	(10^6 m^3)	180 600	5 624	785	65 000
Average Annual Runoff (Inflow)	(10^6 m^3/yr)	40 240	8 780	9 300	75 120
Capacity/Inflow Ratio		4.5	0.6	0.1	0.9
Trap Efficiency (from Brune 1953)		98%	96%	87%	97%
Wetland		**Barotse Plains**	**Chobe Swamp**	**Kafue Flats**	**Elephant Marsh**
Flooded Area (km^2)		5500	3000	5000	400
Storage Volume (Capacity)	(10^6 m^3)	8 500	4636*	7727*	618*
Average Annual Runoff (Inflow)	(10^6 m^3/yr)	30200	33000	8800	15000
Capacity/Inflow Ratio		0.28	0.14	0.88	0.04
Trap Efficiency (from Brune 1953)		88%	84%	97%	75%

* Only the storage volume (mean annual) of the Barotse Plains could be found in the literature. The storage capacity of the other wetlands was estimated by assuming the same flooded area to storage volume ratio.

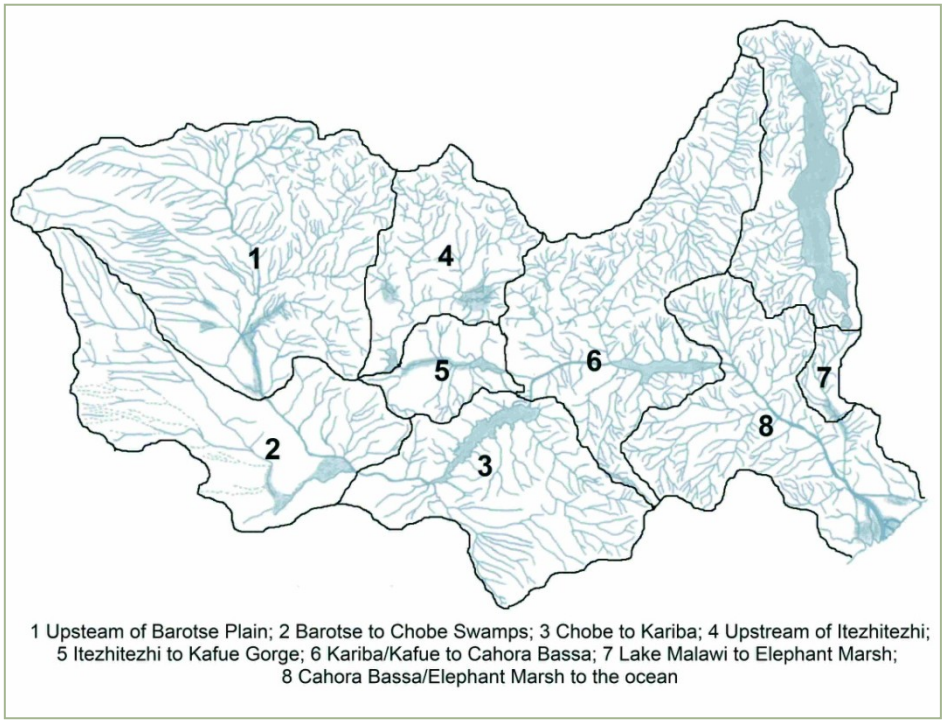

Figure 3-9 Sub-catchment zones within the Zambezi River basin

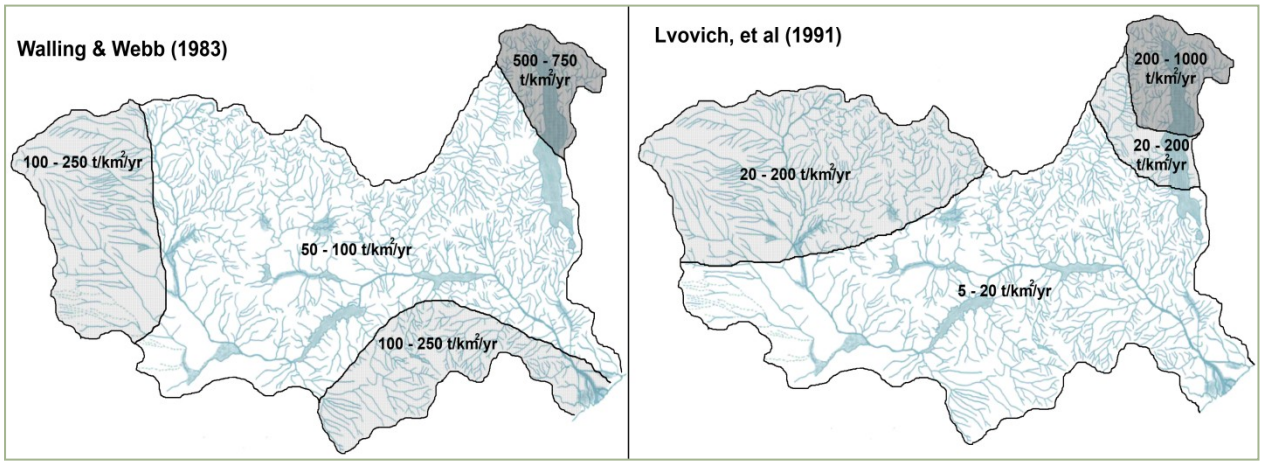

Figure 3-10 Suspended sediment yield of the Zambezi catchment from global sediment yield maps

Table 3-8 Calculation of sediment loads to the Zambezi Delta from Walling & Webb (1983) sediment yield map

Average sediment load production per sub-catchment zone from Walling & Webb (1983) map				
Zone	Area (km^2)	%	Sediment Yield ($t/km^2 \cdot yr$)	Sediment Load Produced in Zone (t/yr)
(1) Upstream of Barotse Plains	335 000	55% 45%	50 to 100 100 to 250	24 287 500 to 56 112 500
(2) Barotse Plains to Chobe Swamp	172 200	50% 50%	50 to 100 100 to 250	12 880 088 to 30 030 265
(3) Chobe Swamp to Kariba	156 600	51% 49%	50 to 100 100 to 250	11 666 700 to 27 170 100
(4) Upsteam of Itezhitezhi	105 600	100%	50 to 100	5 280 000 to 10 560 000
(5) Itezhitezhi to Kafue Gorge	45 400	100%	50 to 100	2 270 000 to 4 540 000
(6) Kariba/Kafue to Cahora Bassa	85 200	90% 8% 2%	50 to 100 100 to 250 500 to 750	5 367 600 to 10 650 000
(7) Lake Malawi to Elephant Marsh	22 500	100%	50 to 100	1 125 000 to 2 250 000
(8) Cahora Bassa/Elephant Marsh to Caia	178 200	62% 38%	50 to 100 100 to 250	12 295 800 to 27 977 400

Estimated pre-dam sediment trapping in major wetlands				
	Inflow sediment load (t/yr)	Trap Efficiency	Outflow sediment load (t/yr)	
Barotse Plain	24 287 500 to 56 112 500	88%	2 914 500 to	6 733 500
Chobe Swamp (a)	15 794 588 to 36 763 765	84%	2 527 134 to	5 882 202
Kafue Flats (b)	7 550 000 to 15 100 000	97%	226 500 to	453 000
Elephant Marsh (c)	1 125 000 to 2 250 000	75%	281 250 to	562 500
=> Total load to Caia = (a)+(3)+(b)+(6)+(c)+(8)			**32 364 984 to**	**72 695 202**

Estimated post-dam sediment trapping in major wetlands and reservoirs				
	Inflow sediment load (t/yr)	Trap Efficiency	Outflow sediment load (t/yr)	
Barotse Plain	24 287 500 to 56 112 500	88%	2 914 500 to	6 733 500
Chobe Swamp	15 794 588 to 36 763 765	84%	2 527 134 to	5 882 202
Kariba (A)	14 193 834 to 33 052 302	98%	283 877 to	661 046
Itezhitezhi	5 280 000 to 10 560 000	96%	211 200 to	422 400
Kafue Gorge	2 481 200 to 4 962 400	87%	322 556 to	645 112
Cahora Bassa (A)	5 974 033 to 11 956 158	97%	179 221 to	358 685
Elephant Marsh (B)	1 125 000 to 2 250 000	75%	281 250 to	562 500
=>Total load to Caia = (A)+(B)+(8)			**12 756 271 to**	**28 898 585**

Table 3-9 Calculation of sediment loads to the Zambezi Delta from Lvovich et al. (1991) sediment yield map

Average sediment load production per sub-catchment zone from Lvovich, et al. (1991) map				
Zone	Area (km^2)	%	Sediment Yield ($t/km^2 \cdot yr$)	Sediment Load Produced in Zone (t/yr)
(1) Upstream of Barotse Plains	335 000	8% 92%	5 to 20 20 to 200	6 273 290 to 61 879 482
(2) Barotse Plains to Chobe Swamp	172 200	79% 21%	5 to 20 20 to 200	1 393 242 to 9 830 903
(3) Chobe Swamp to Kariba	156 600	100%	5 to 20	783 000 to 3 132 000
(4) Upsteam of Itezhitezhi	105 600	33% 67%	5 to 20 20 to 200	1 588 447 to 14 837 364
(5) Itezhitezhi to Kafue Gorge	45 400	100%	5 to 20	227 000 to 908 000
(6) Kariba/Kafue to Cahora Bassa	85 200	83% 12% 5%	5 to 20 20 to 200 200 to 1000	1 368 311 to 7 540 649
(7) Lake Malawi to Elephant Marsh	22 500	100%	5 to 20	112 500 to 450 000
(8) Cahora Bassa/Elephant Marsh to Caia	178 200	100%	5 to 20	891 000 to 3 564 000

Estimated pre-dam sediment trapping in major wetlands			
	Inflow sediment load (t/yr)	Trap Efficiency	Outflow sediment load (t/yr)
Barotse Plain	6 273 290 to 61 879 482	88%	752 795 to 7 425 538
Chobe Swamp (a)	2 146 037 to 17 256 441	84%	343 366 to 2 761 031
Kafue Flats (b)	1 815 447 to 15 745 364	97%	54 463 to 472 361
Elephant Marsh (c)	112 500 to 450 000	75%	28 125 to 112 500
=> Total load to Caia = (a)+(3)+(b)+(6)+(c)+(8)			**3 468 266 to 17 582 540**

Estimated post-dam sediment trapping in major wetlands and reservoirs			
	Inflow sediment load (t/yr)	Trap Efficiency	Outflow sediment load (t/yr)
Barotse Plain	6 273 290 to 61 879 482	88%	752 795 to 7 425 538
Chobe Swamp	2 146 037 to 17 256 441	84%	343 366 to 2 761 031
Kariba	1 126 366 to 5 893 031	98%	22 527 to 117 861
Itezhitezhi	1 588 447 to 14 837 364	96%	63 538 to 593 495
Kafue Gorge	290 538 to 1 501 495	87%	37 770 to 195 194
Cahora Bassa (A)	1 428 609 to 7 853 704	97%	42 858 to 235 611
Elephant Marsh (B)	112 500 to 450 000	75%	28 125 to 112 500
=>Total load to Caia = (A)+(B)+(8)			**961 983 to 3 912 111**

3.4.1.3. Reservoir sedimentation estimate (Bolton, 1984)

Bolton (1984) estimated the sediment deposition in Kariba and Cahora Bassa Reservoirs. In his estimates he refers to sediment studies by Ward (1980) and Chikwanha (1980) on two of the Zambezi tributaries in Zimbabwe, the Gwaai and Umsweswe Rivers (sediment yield 40 t/km^2/year for both catchments), and to a study on the erosion potential of the whole of Zimbabwe (Stocking & Elwell, 1973). The sediment yields from other areas of the Zambezi basin were roughly estimated based on their hydrological and physical characteristics compared to the studied basins, and it was assumed that the large wetlands and dams trap all incoming sediment. The final estimated annual loads to the Kariba and Cahora Bassa reservoirs were 7 to 70 x 10^6 t/year and 20 to 200 x 10^6 t/year respectively. Table 3-10 shows a summary of Bolton's sediment yield and load estimates for various areas within the Zambezi catchment.

Table 3-10 Summary of suspended sediment yields and sediment loads in the Zambezi River as estimated by Bolton (1984)

Region	Sediment Yield (t/km^2/year)	Area (km^2)	Total Load (10^6 t/year)	References and/or Reasoning
Upstream of Victoria Falls		480 000	0	No yield estimated. Almost all sediment will be deposited in Barotse Plain/ Chobe Swamp.
Kariba tributaries in Zimbabwe	40 to 400	140 000	7 to 70	Ward(1980), Chikwanha(1980), Stocking&Erwell(1973)
Kariba tributaries in Zambia	40 to 400	30 000		Assumed same yield as in Zimbabwe
Kafue Basin		150 000	0	No yield estimated. Almost all sediment trapped in Itezhi Tezhi and Kafue Gorge Reservoirs.
CB tributaries in Zimbabwe	> 40 to 400	42 000	2 to 20	Stocking&Erwell(1973) suggests higher yield than Kariba tributaries.
Luangwa basin	100 to 1000	148 000	15 to 150	Physical & hydrological characteristics suggest higher yield than for upstream tributaries
CB tributaries in Zambia & Mozambique	< 100 to 1000	35 000	3 to 30	Yield probably slightly less than Luangwa

Following Bolton's method, the pre-dam sediment load to the Zambezi Delta could be estimated by adding the contribution from the area downstream of Cahora Bassa (170 000 km^2 with mean sediment yield similar to the Cahora Bassa Tributaries in Zambia and Mozambique of 80 to 800 t/km^2/year results in approximately 14 to 140 t/year) excluding the Shire basin because most of the sediment eroded in this region will be trapped in Lake Malawi or the Elephant Marsh. Similarly, the contribution of the Kafue River would be ignored for the pre-dam estimate because of the Kafue Flats wetland. The total pre-dam sediment load to the delta would then be 41 to 410 Mt/year, and the post-dam sediment load (only originating downstream of Cahora Bassa) would be 14 to 140 Mt/year (approximately a third of the pre-dam load).

3.4.1.4. Pre-Cahora Bassa sediment load measurements

In the 1960's several sediment load measurements were performed on the lower Zambezi by the Hydraulic Engineering Brigade's Mission for Development and Settlement of the Zambezi (*Brigada de Engenharia Hidráulica da Missão de Fomento e Povoamento do Zambeze* or MFPZ) in order to study the navigability of the river (COBA, 2011). These included daily measurements of bed and suspended sediment load at Marromeu for the 2 year period from November 1961 to October 1963 as well as some other scattered measurements from 1961 to 1970 (obtained for this study from an environmental impact assessment report for the proposed Mpanda Nkuwa Dam (COBA, 2011)). No details of the measurement procedures are given and a number of inconsistencies were evident in the records. Some (but relatively few) of the sediment load measurements are given with corresponding discharge or water level recordings (see more details in section 3.4.2). Figure 3-11 shows the recorded suspended sediment load at Marromeu and Table 3-11 gives the total annual loads for the two years of continuous measurement.

While only the sediment load information is required for the model boundaries, some aside mention is also required of the measured bed loads. The daily bed load measurements from MZFP (given in Appendix 1 of COBA, 2011) are given in units of m^3/day and the annual total is in the order of 20 000 m^3/year (±30 000 tons/year), or approximately 0.04% of the total load. This is (much) less than 1% as quoted by a number of authors who refer to the same MFPZ measurements (eg. Bolton, 1984; Ronco, et al., 2006). However, elsewhere in the COBA (2011) report Table 1.1.6 indicates that the bed loads should be a factor of one thousand larger, which would put the bed loads at a more similar magnitude to the post-dam measurements and would imply that the bed load contributes about 30 % of the total load. It should therefore definitely not be ignored.

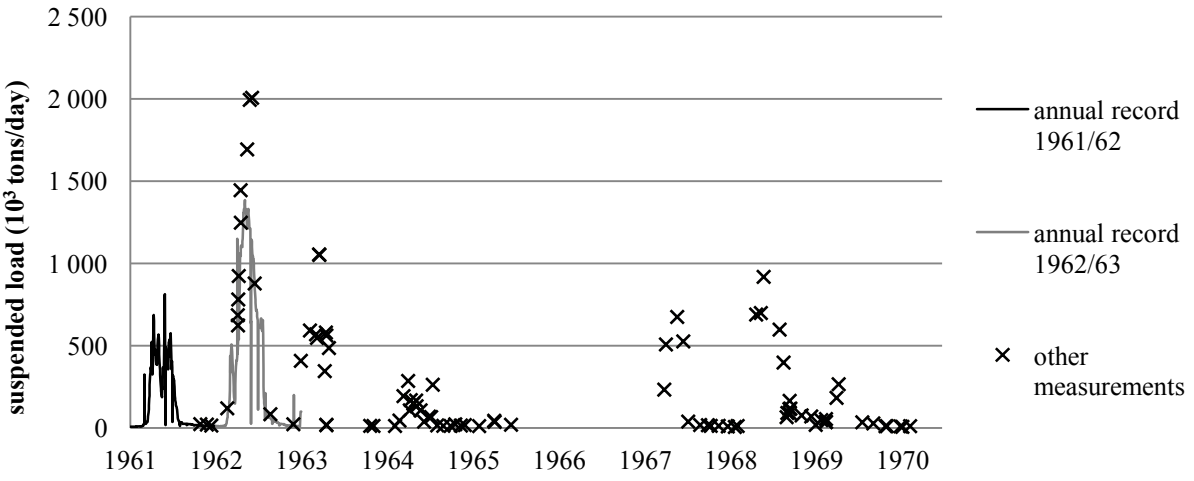

Figure 3-11 Measured suspended sediment loads at Marromeu from 1961 to 1970

Table 3-11 Total annual sediment loads at Marromeu for 1961 to 1963

Year	Mean water discharge (m^3/s)	Suspended sediment load (t/yr)	*Bed sediment load (t/yr)*	*Total sediment load (t/yr)*	*% Total load contributed by bed load*
1961/62	2800	51 415 000	*21 726 or 21 726 000*	*51 436 726 or 73 141 000*	*0.04% or 29.7%*
1962/63	4250	125 360 000	*40 392 or 40 392 000*	*125 400 392 or 165 752 000*	*0.03% or 24.4%*

3.4.1.5. Post-dam sediment load measurements

The sediment loads at various points in the lower Zambezi have been measured as part of a number of recent studies (see Table 3-12). The field measurements of February 2012, February 2011 and October 2010 involved a survey of a number of cross-sections with an acoustic Doppler current profiler (ADCP), and bed load and suspended sediment concentration (depth integrated) measurements at 5 points on each cross-section. The total bed and suspended sediment loads through each cross section were estimated from the 5 point load measurements on the cross section (using a unit-discharge weighted average) and the average loads for each of measurement periods.[a] The 2006 study gave only the total suspended and bed loads measured at Tete (as 2.469 and 0.179 ton/s respectively).

Figure 3-12 shows the estimated bed and suspended sediment loads from the 2011 and 2012 field measurements as a function of distance from the ocean (as chainage along the river). Only the sampling in Feb 2012 continued downstream as far as the delta region. These 2012 results show no distinct trends but the suspended loads tend to be larger downstream of Caia, perhaps due to an influx of suspended sediment from the Shire River.

[a] It is noted that the original field measurements were performed for the purpose of calibration of numerical morphological models and not to give total loads through a cross section (hence only 5 samples per cross section). The extrapolation of the point sediment load measurements to an estimate for a whole cross section was only performed in this study.

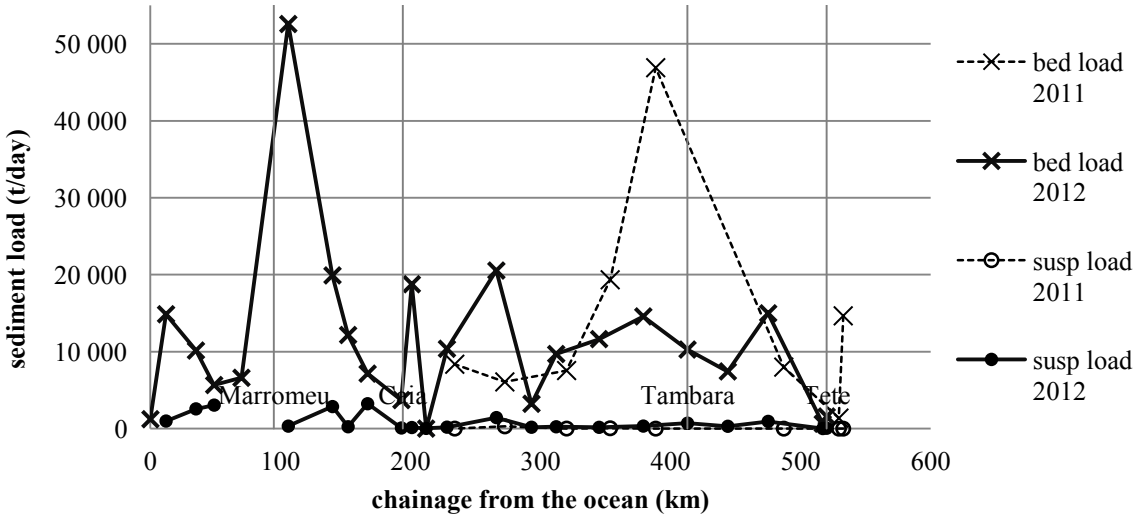

Figure 3-12 Estimated bed and suspended sediment loads at various cross sections on the Lower Zambezi from field measurements in February 2011 and February 2012

Table 3-12 Recent sediment load measurements in the lower Zambezi River

Field work date	Location	Number of cross-sections	Water discharge (m^3/s)	Average bed load (t/day)	Average suspended load (t/day)
Feb 2012	Tete to the Ocean	23	2900 - 3800	11 200	870
Feb 2011	Tete to Caia	8	2500 - 2900	14 000	48
Oct 2010	Tete	8	2800	11 500	900
May 2006	Tete	1	2600	15 500	213 000

The suspended load recorded in 2006 is of the expected order of magnitude, but the 2010, 2011 and 2012 measurements are much lower. The February 2011 field work report explained the extremely low sediment loads by the fact that the sampling was performed shortly after a period of high flow releases from Cahora Bassa which would have flushed the system, but that was not the case in October 2010 and February 2012. In the post-dam condition almost all the suspended sediment comes from the lower tributary catchments and therefore the loads can be expected to be related to the tributary flows rather than the total discharge. It is likely that the 2006 sampling coincided with high flows from the lower tributaries while the 2010, 2011 and 2012 did not. Unfortunately no detailed flow records for the tributaries were available.

3.4.2 Sediment – discharge rating

After estimating the average annual sediment loads to the Zambezi Delta by several methods, as discussed above, 45 Mt/year and 22.5 Mt/year were decided upon as the pre-dam and post-dam loads respectively (comparison was given in Table 3-6). The next step was to distribute these loads through the 10 year flow series. A sediment-discharge rating curve can be expected to fairly accurately represent the temporal load distribution for the pre-dam scenario. For the post-dam scenario the sediment loads would be better linked to tributary flows than to the total flow (as mentioned in section 3.4.1.5), but due to a lack of information the same sediment-discharge rating approach as for the pre-dam flows was applied.

A few of the MFPZ suspended sediment measurements from the 1960's (COBA, 2011) are given with corresponding water discharges and these were used to define a rating curve (see Figure 3-13 and Figure 3-14). For the 1960's data the best fit curve was found to be:

$$Q_s = 0.02\, Q_w^{2.2185} \qquad \textbf{3-4}$$

Where Q_s = suspended sediment load [g/s]

Q_w = water discharge [m^3/s]

This rating curve was applied to the pre-dam and post-dam flow series and then the coefficient of the rating curve was adjusted so that the average annual suspended loads over the 10 year period (2000 to 2010) were 45 and 22.5 Mt/year respectively. The resultant rating curves are given by Equations 3-5 and 3-6 and are included in Figure 3-14 along with the observed pre-dam and post-dam (see Table 3-12) data.

$$Q_{s(pre\text{–}dams)} = 0.011564\, Q_{w(pre\text{–}dams)}^{2.2185} \qquad \textbf{3-5}$$

$$Q_{s(post\text{–}dams)} = 0.011499\, Q_{w(post\text{–}dams)}^{2.2185} \qquad \textbf{3-6}$$

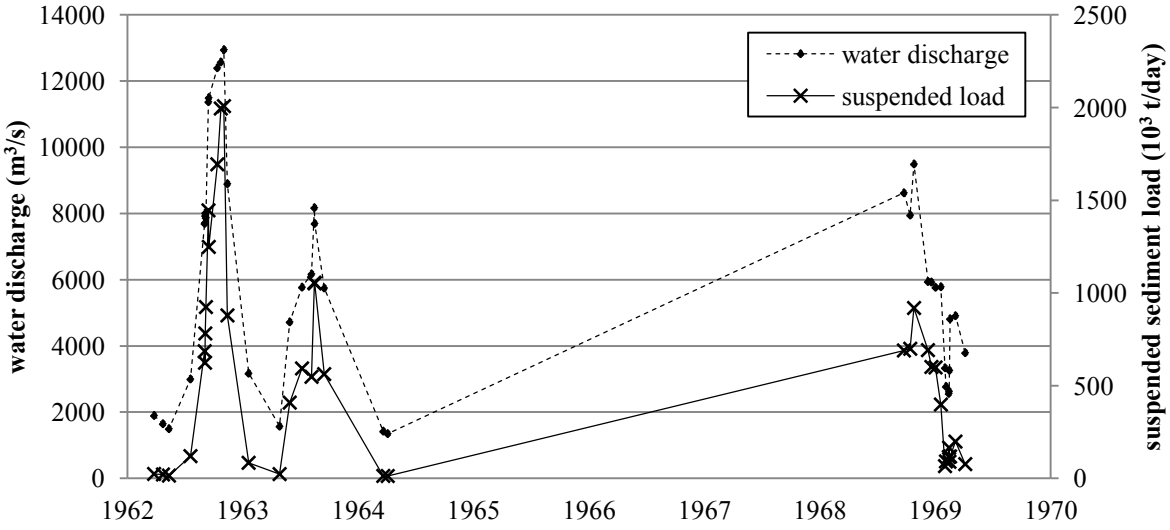

Figure 3-13 **Concurrent discharge and sediment load measurements from the 1960's**

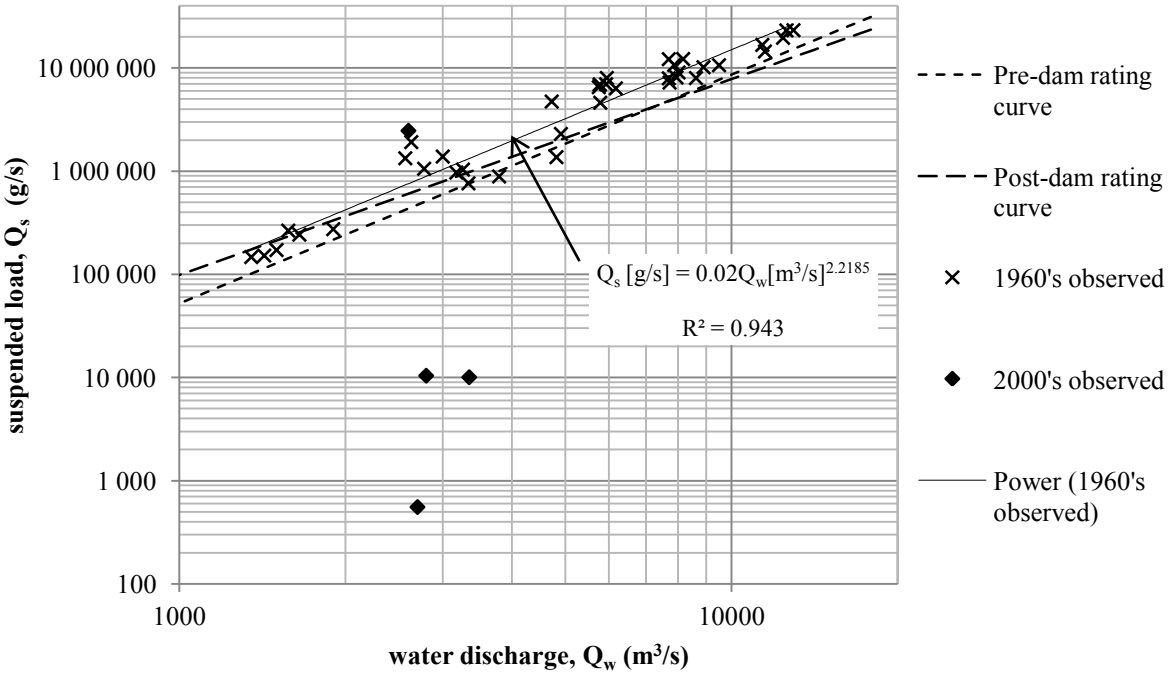

Figure 3-14 **Suspended load – discharge rating curve from MZFP measurements in the 1960's with altered ratings for pre-dam and post-dam simulations (2000-2010) shown**

Figure 3-15 and Figure 3-16 show the time-series for the inflowing suspended sediment loads (Q_s) and the cumulative inflowing suspended sediment loads (ΣQ_s) respectively. The largest difference between the pre-dam and post-dam sediment inflows occur during the large floods (particularly the major flood in 2001).

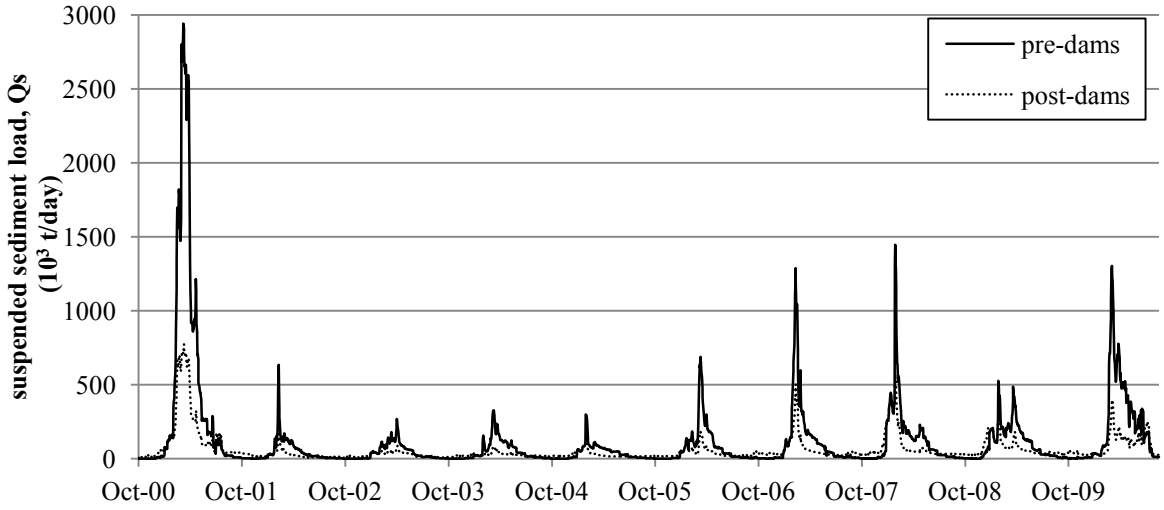

Figure 3-15 Inflowing suspended sediment loads

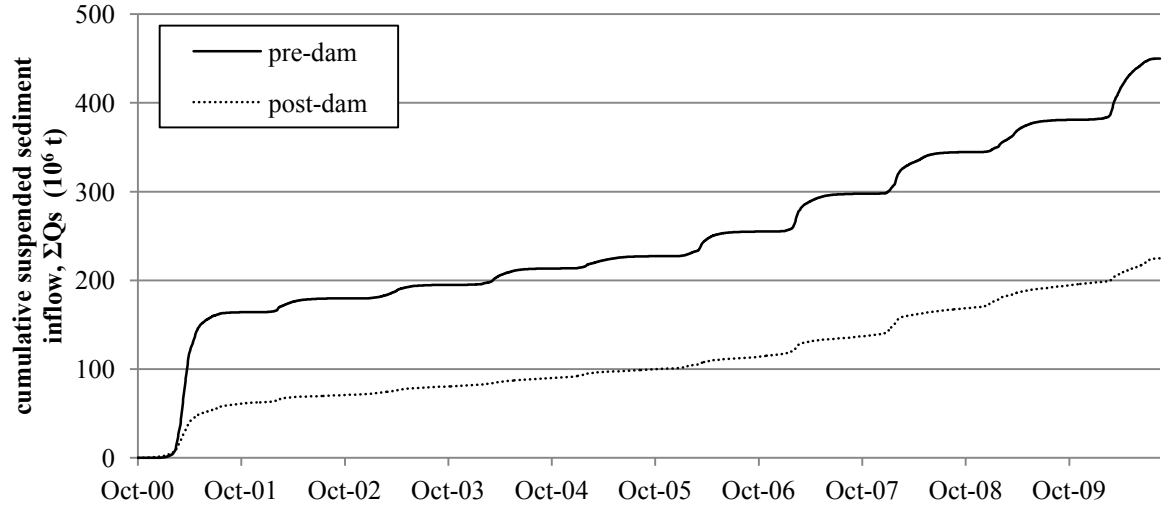

Figure 3-16 Cumulative suspended sediment inflow to the model

In the model the incoming suspended sediment load is specified as a concentration:

$$c_s\ [\mathrm{g/m^3}] = \frac{Q_s[\mathrm{g/s}]}{Q_w[\mathrm{m^3/s}]} \qquad \textbf{3-7}$$

The final input concentration time series are shown in Figure 3-17.

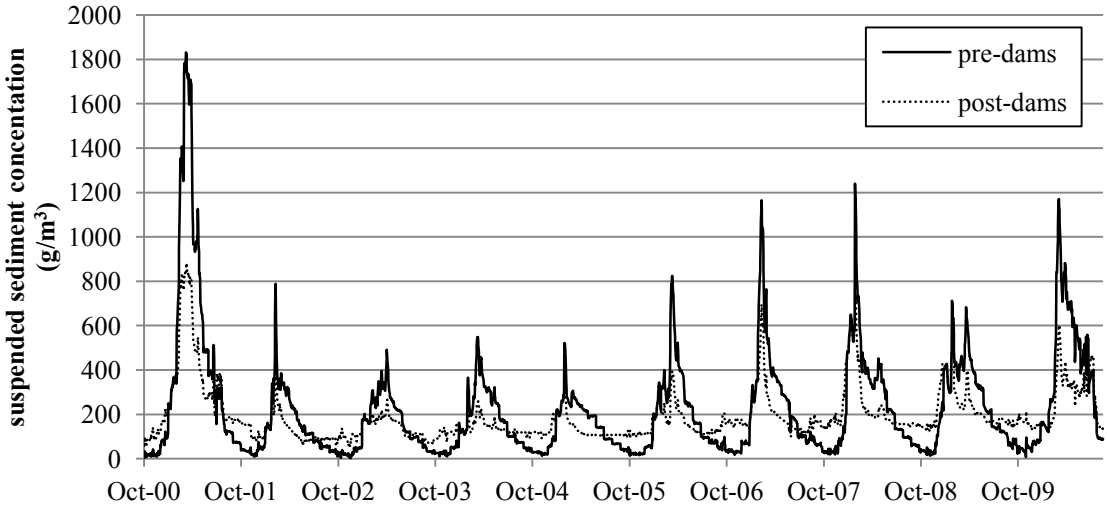

Figure 3-17 Time-series of suspended sediment concentration for model input

3.5 Bed sediment fractions

The sediment grading of 42 grab samples of the Zambezi River bed within the study reach, collected in February 2012 (ASP, 2012b), were analyzed to determine suitable sediment fraction sizes for the model. Figure 3-18 shows the grading curves for the 42 samples. No distinct spatial trends were evident so the average grading curve for the whole reach was used to derive a constant specification of the bed sediment for the model. The bed is sandy with very low proportions of cohesive material. The average component of fine sediment (d<0.065) is 0.2% (from the mean grading curve).

Four sediment fractions were specified for the model: three non-cohesive and one cohesive. The representative diameters for the three non-cohesive fractions were calculated from the mean grading curve of the 2012 bed samples (by calculating the mean settling velocity, v_{ss}, for each fraction and then calculating the corresponding sediment diameter, d_{rep}) as shown in Figure 3-19 and Table 3-13. The size of the fine (cohesive sediment fraction) is most important for the suspended sediment transport. The only suspended sediment size data for the study reach were found in COBA, 2011: two measurements (one near the right bank, the

other near the left) at Marromeu on 19 July 1964 of d_{50}'s of 0.0123 and 0.011 mm respectively. The diameter of the fine fraction was set to 0.012 mm. Table 3-14 summarizes the final bed grading specification for the model.

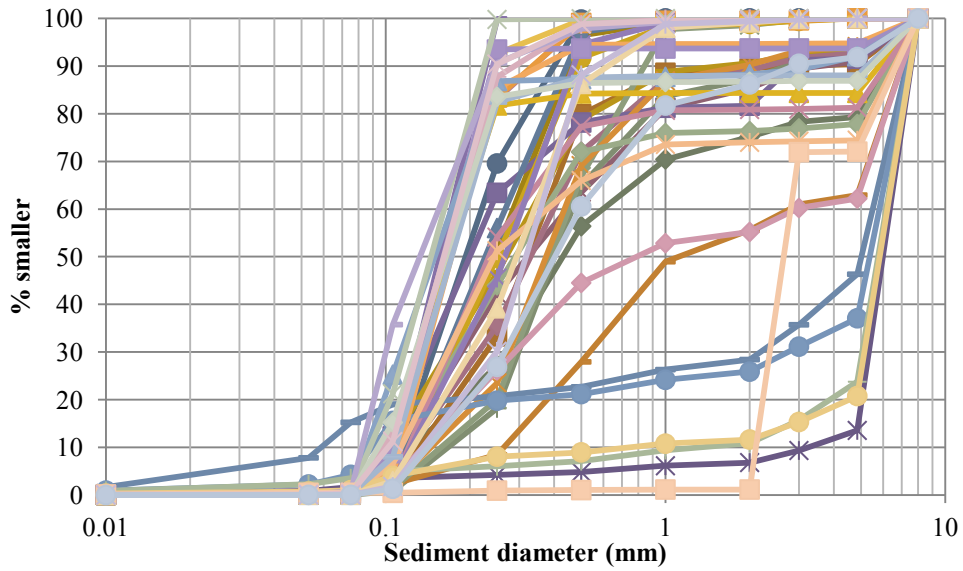

Figure 3-18 **Grading curves for 42 Zambezi River bed grab samples taken in February 2012 (ASP, 2012b)**

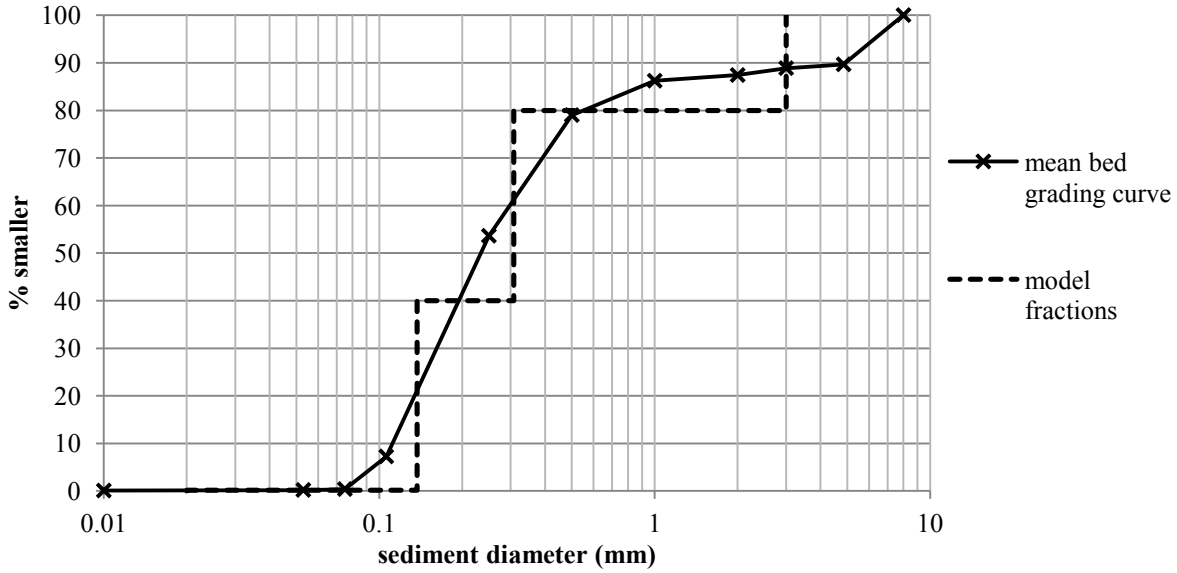

Figure 3-19 **Mean grading curve from Figure 3-18 with grading curve for model fractions**

Table 3-13 Calculation of representative sediment diameters (d_{rep}) for the non-cohesive sediment fractions

		% passing	d (mm)	V_{ss} (m/s)*	Average V_{ss} (m/s)	d_{rep} (mm)
Large Fraction (20%)	33.3%	96.67	6.808	0.606	0.402	3.000
	33.3%	90.00	4.931	0.515		
	33.3%	83.33	0.759	0.096		
Medium Fraction (40%)	33.3%	73.33	0.428	0.061	0.043	0.308
	33.3%	60.00	0.298	0.041		
	33.3%	46.67	0.220	0.027		
Small Fraction (38.8%)	33.3%	33.33	0.172	0.019	0.013	0.137
	33.3%	20.00	0.134	0.012		
	33.3%	6.67	0.103	0.007		

* for $d > 1\text{mm}: v_s = \sqrt{\frac{4}{3}\left(\frac{\rho_s - \rho}{\rho}\right)\frac{gd}{C_D}} = \sqrt{\frac{4}{3}(1.65)\frac{(9.81)}{0.4}d}$ for $0.1 < d < 1\text{mm}: v_s = \frac{10\nu}{d}\left[\sqrt{1 + \frac{1}{100}\left(\frac{\rho_s - \rho}{\rho}\right)\frac{gd^3}{\nu^2}} - 1\right]$;

Table 3-14 Sediment fractions specified for the model bed

	Large	Medium	Small	Fine (Cohesive)
Fraction	20.0%	40.0%	39.8%	0.2%
d_{rep} (mm)	3.000	0.308	0.137	0.012

3.6 Grid set-up

Creation of a suitable calculation grid or mesh is perhaps the most important part of the modelling process (DHI, 2003). Small grid cells which are well aligned with the flow direction give the most accurate solution. However, the required computation time for a simulation increases exponentially with the number of cells in the grid, and a more uniform grid generally leads to more rapid numerical convergence. The curvilinear grid required for a *Mike21C* simulation is created graphically and orthogonalised (by solving a set of elliptic partial differential equations as described in DHI, 2011) using the *Mike21C Grid Generator*. The accuracy of the model depends on the accuracy of the grid and is reduced when:

- Cells are not orthogonal;

- The difference in size between neighbouring cells is high;
- Cells are too course; or
- The aspect ratio of the cells is too high.

Recommended values for the grid orthogonality are between -0.05 and 0.05 everywhere but the achievable limits for the orthogonality will depend on the complexity of the grid. The optimal cell aspect ratio is 3 to 8 for channels where the flow is aligned with the grid and 1 to 3 for floodplains where the flow is expected to be less aligned with the grid. (DHI, 2011)

Before modelling the whole reach (160 km long) a number of different grid options were tested for a selected small reach (see Figure 3-20) at the upstream end of the domain as follows:

(a) Grids with cells that are accurately aligned with the low-flow banks as well as grids with more uniformly shaped cells following a more general flow direction, both with various cell sizes were created;

(b) hydrodynamic simulations were performed for the discharge measured in the February 2012 field work (Q_w=3700 m^3/s) for all grids;

(c) the velocities and depths of flow were compared to the field results at the 3 field cross-section locations within the short reach for each of the grids; and

(d) a decision was made on the most suitable grid for the full reach simulations considering the required simulation time as well as the model accuracy.

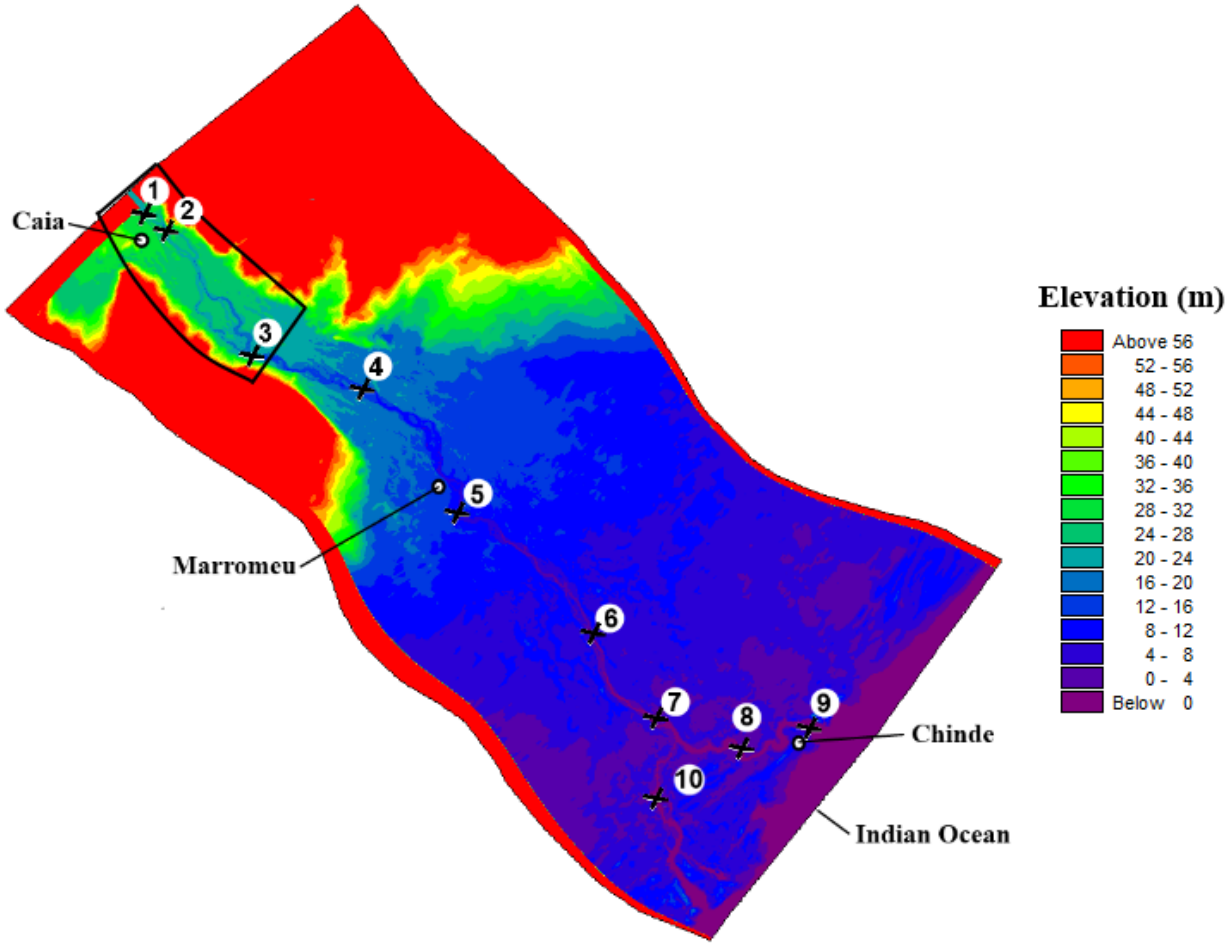

Figure 3-20 Model bathymetry with locations of field sampling cross sections and outline of short reach domain shown

It was found that the more uniformly shaped grid cells gave better numerical convergence and that increasing the grid size does not have much effect on the accuracy of the model compared to the field measurements (see Figure 3-21). Table 3-15 gives the details of the different sized grids tested and the resulting simulation times. Images showing the grid resolution and simulated velocity vectors are attached in Appendix A. The field recorded depths do not closely agree with the bathymetry of the model so model velocity and sediment transport results cannot be expected to match the field measurements at specific locations (see Figure 3-21). Larger cell sizes seem to only affect the model accuracy through a loss of resolution.

Table 3-15 Summary of short reach grids tested to determine

	Grid1	Grid2	Grid3	Grid4	Grid5	Grid6
Approx. cell length (m)	30	50	100	200	300	500
Approx. cell width (m)	10	17	33	67	100	167
# cells in s-direction	1004	720	361	181	121	71
# cells in n-direction	1152	690	351	171	116	67
Orth. check max	0.095	0.086	0.041	0.042	0.038	0.039
Orth. check min	-0.104	-0.099	-0.034	-0.034	-0.033	-0.033
Time step (s)	1	5	20	45	60	90
***CPU time for 48hr sim. (s)**	-	13554	805	61	22	5
Estimated run-time for full reach simulation (days)	-	*4401.0*	*248.6*	*19.4*	*7.6*	*2.2*

* Simulations may be performed using up to 4 parallel CPUs in which case the run-time is about a quarter of the CPU time

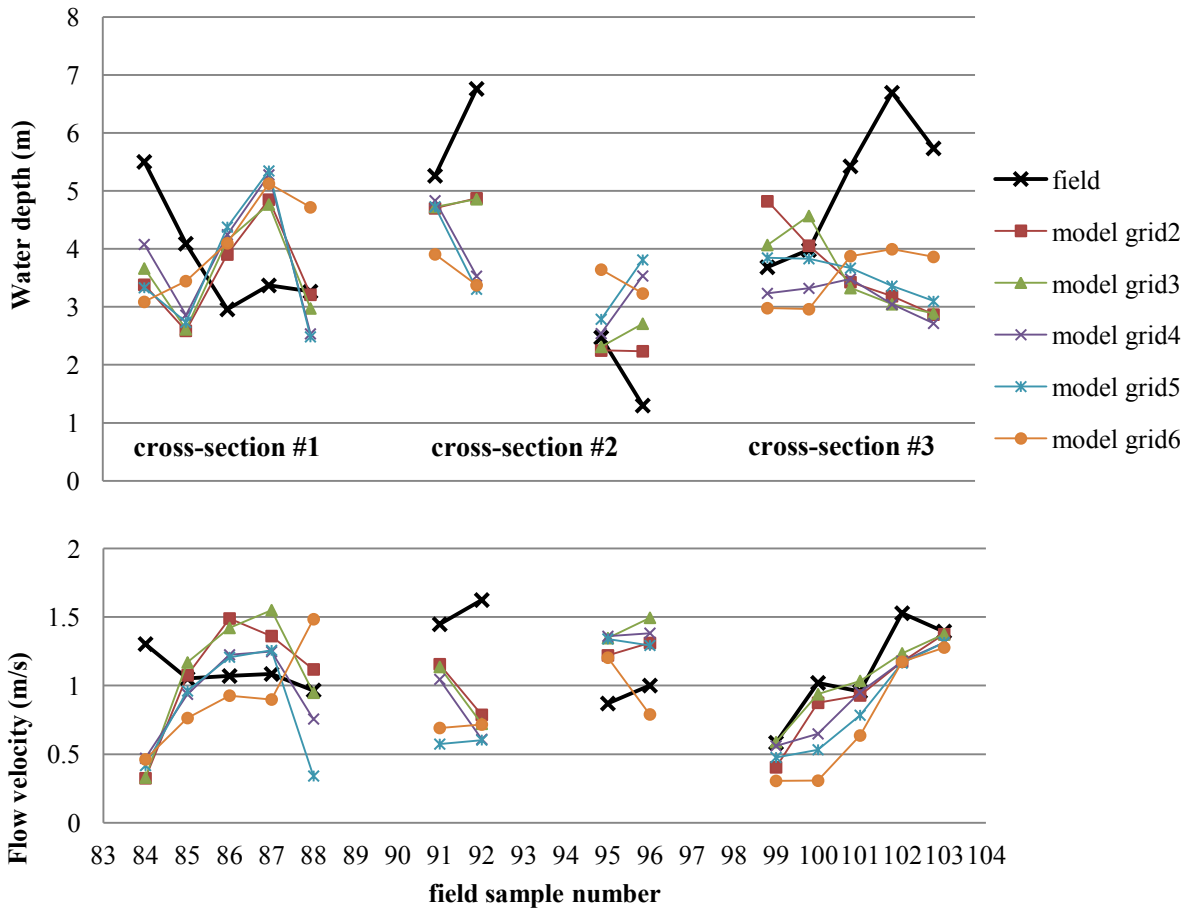

Figure 3-21 Comparison of model water depth and flow velocity with field measurement for grids with increasing cell sizes

The final grid for the full reach simulations contains 498 x 151 cells. Cells are approximately 330 m long by 150 m wide in the region of the main channel, with their width increasing gradually onto the floodplains. The bathymetry shown in Figure 3-20 was drawn with the cells of the final grid and gives an indication of the grid resolution.

3.7 Calibration of model roughness

The roughness for a *Mike21C* river model is best specified as a Manning value when bed levels differ significantly within the domain (DHI, 2011). The Manning roughness for the river channel was calibrated by comparing simulated water surface elevations to observed water levels at the Caia and Marromeu gauging stations for hydrodynamic simulations of approximately 1 year[a] in an iterative process. The final Manning M-value (inverse of Manning n) was 32.3 at Caia and 34.0 at Marromeu. Between Caia and Marromeu the roughness was varied linearly and downstream of Marromeu it was kept constant at 34.0. Figure 3-22 and Figure 3-23 show the comparison between simulated and observed water levels with the final calibrated roughness. The maximum error is about 0.5 m. The flow encounters more resistance on the floodplains than in the main channel so a reduced Manning M (higher roughness) of 25 – typical of tall grass or reeds with light scattered brush (Chow, 1959) – was applied to the flood plains.

[a] The last year hydrological year of record was used starting 1 October 2009 and ending 25 Aug 2010

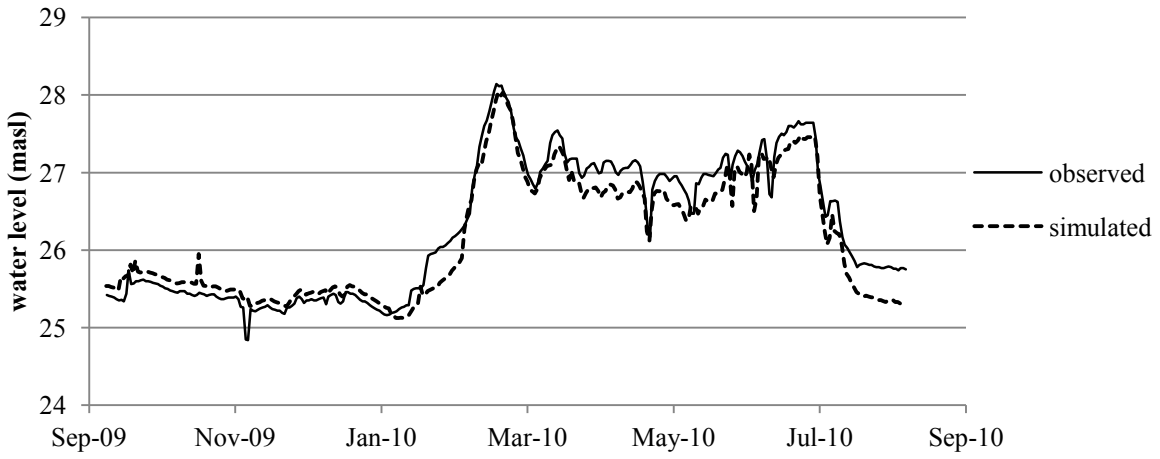

Figure 3-22 Comparison of observed and simulated water levels at Caia for calibrated model

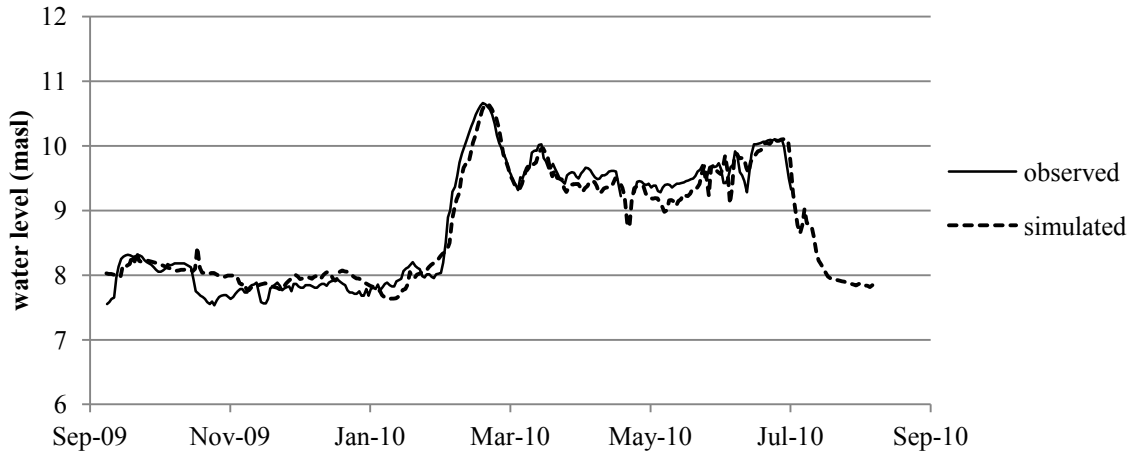

Figure 3-23 Comparison of observed and simulated water levels at Marromeu for calibrated model

3.8 Choice and calibration of bed load transport equation

Mike21C provides several options of sediment transport theories. As discussed in section 2.3.2, the van Rijn and the Engelund, Fredsoe & Zyserman (EFZ) models are the only ones applicable for this study because separate consideration is required for bed loads and suspended loads. Calibration of bed load transport is also possible in *Mike21C* through the application of a *bed load factor* which is a constant multiplier applied to the theoretical sediment carrying capacity of the flow calculated by the chosen theory. In order to choose the most suitable of the two transport models and to calibrate the bed load transport equation,

simulations were performed for a constant flow of 3700 m^3/s for 6 weeks (to allow the sediment transport to stabilize) and then the modelled bed loads were compared to the field measurements from February 2012 (ASP, 2012b).

Field measured bed loads were available for 4 or 5 points on each of the 10 cross sections over the model reach (cross section locations are indicated in Figure 3-20). The simulated bed loads for the whole river cross section at the field cross sections locations were extracted and compared to the corresponding field loads[a]. Figure 3-24 and Figure 3-25 show the model predicted bed loads with the field measured bed loads across each cross section and Table 3-16 compares the average bed loads for each cross section. The average loads for each cross section were compared and then the average error over the whole model was minimised, instead of comparing loads point-by-point, because the bathymetry of the model is not accurate to a site-specific level. Additionally, the mathematical formulation only allows a single blanket bed load calibration factor and therefore matching the model to field data at all locations would be impossible.

Before calibration both the EFZ and the van Rijn models severely under-predicted the bed loads but the EFZ predictions were much closer (differing by an average factor of about 3 as opposed to a factor of 50 relative to the field data). The EFZ bed load was then increased and the simulation repeated. An iterative procedure converged to a minimum average error of 2% for a bed load factor of 2.5.

[a] The extracted results were averaged over the few days of simulation so the simulated loads extracted for the tidal region are the mean loads for those locations.

Table 3-16 Comparison of average simulated bed loads at each cross section to field data

Cross section #	Average bed load (kg/s·m)				% Error compared to field data		
	Field	EFZ	vR	$EFZ_{BF=2.5}$	EFZ	vR	$EFZ_{BF=2.5}$
1	0.267	0.132	0.005	0.344	-50.3%	-98.0%	29.0%
2	0.104	0.066	0.006	0.149	-36.2%	-94.0%	43.1%
3	0.162	0.048	0.004	0.116	-70.2%	-97.6%	-28.5%
4	0.335	0.135	0.007	0.303	-59.6%	-97.8%	-9.6%
5	0.335	0.073	0.004	0.196	-78.3%	-98.8%	-41.6%
6	0.164	0.083	0.005	0.250	-49.7%	-96.9%	51.8%
7	0.191	0.071	0.007	0.155	-62.8%	-96.2%	-19.2%
8	0.211	0.007	0.000	0.044	-96.8%	-99.8%	-79.3%
9	0.112	0.006	0.001	0.015	-94.6%	-98.8%	-86.6%
10	0.043	0.003	0.000	0.010	-92.0%	-99.5%	-76.9%
All*	0.198	0.078	0.005	0.193	-60.5%	-97.6%	-2.1%

EFZ = Engelund, Fredsoe & Zyserman theory model; vR = van Rijn theory model;
* Note that the average loads over all cross-sections are the average of all the individual data points, not the average of the average loads for the each cross section.

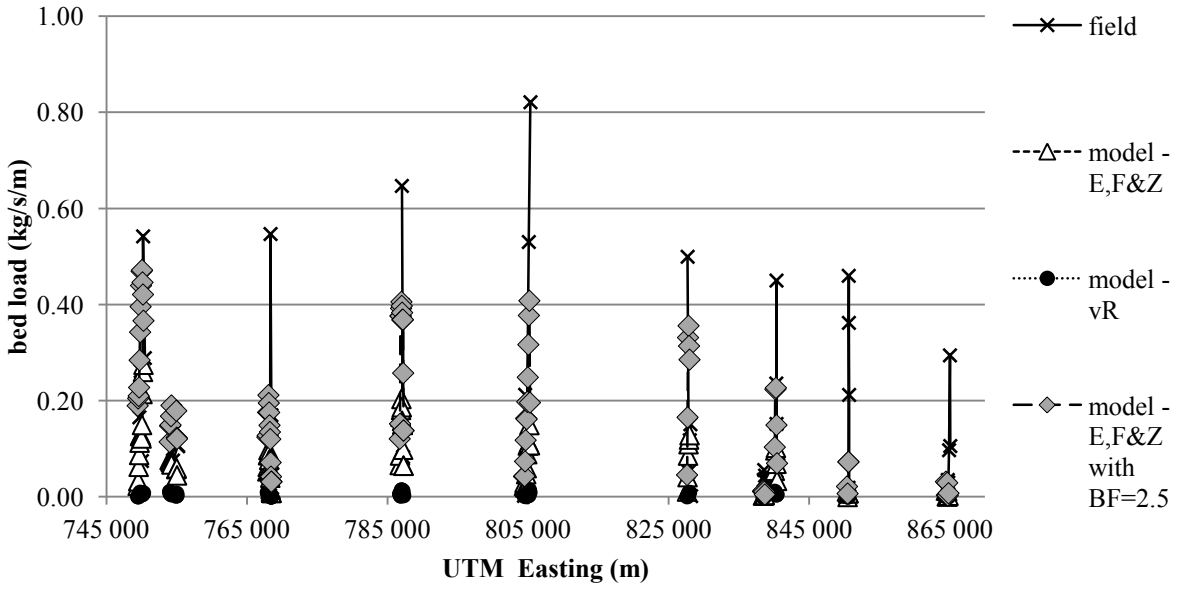

Figure 3-24 Simulated bed loads and field measured bed loads throughout the model reach

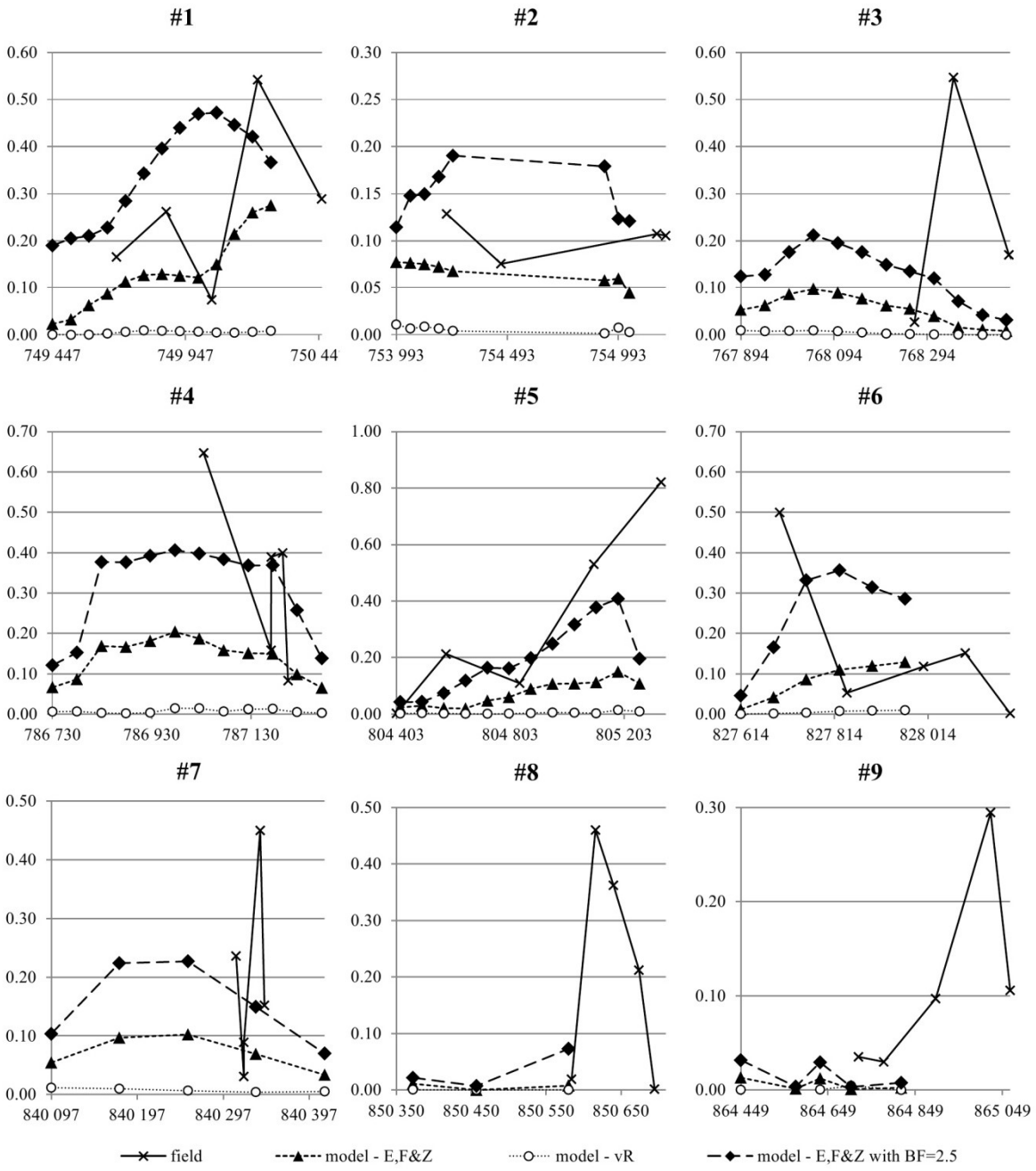

Figure 3-25 **Comparison of modeled bed loads to field measurements (kg/m/s) as a function of Easting (m) zoomed in at cross sections**

3.9 Final model inputs and settings

A summary of all the model inputs and settings are given in Table 3-17. Information on selection of the solver settings and minor parameters (not dealt with in this chapter) can be found in the literature review, section 2.3.3 or in DHI (2011).

Table 3-17 Summary of model inputs and settings

	Description	Section
Grid & bathymetry	498 x 151 curvilinear cells approximately 330x150 m in the main channel and larger on the flood plains	3.1
Simulation period	1 Oct 2000 - 25 Aug 2010	
Hydrodynamic boundaries	observed / adapted flow hydrographs at Caia	3.2
	tidal water level at Chinde	3.3
Sediment fractions	20% - 3.000 mm	
	40% - 0.308 mm	
	39.8% - 0.137 mm	
	0.12% - 0.012 mm (cohesive)	3.5
Bed layer thickness	12 m	
Sediment transport boundaries	zero bed level change upstream and downstream	
	estimated suspended sediment concentration for inflow	3.4
Time steps	30 s for hydrodynamics	
	300 s for sediment transport	
Flooding and drying depths	0.02 m for drying	
	0.03 m for flooding	
Resistance	Manning M = 32 to 34 for main channel	3.7
	Manning M = 25 for flood plains	
Sediment transport theory	EFZ bed load factor = 2.5 (calibrated)	3.8
	EFZ suspended load factor = 1.0 (default)	
Eddy viscosity	1.0 m^2/s	
Helical flow constant	1.0 (default)	
Slope effect constants	G = 1.25; a = 0.5 (default)	
AD dispersion coefficients	1.0 for both directions (default)	
HD integration	Fully dynamic specification	
AD scheme	"QUICKEST"	

4 RESULTS

4.1 Extent of flooding

Significantly higher high flows and lower low flows occur for the pre-dam scenario than for post-dam conditions. The effect of these altered flow rates on the flow depths and flow velocities for two selected flood peaks and one selected low flow period are shown in Figure 4-3, Figure 4-4 and Figure 4-5 on pages 80 and 81.

The total flooded area of the model varies from 3280 km^2 (28% of the model domain) at low flows (100 m^3/s) to 5384 km^2 (46 %) during the largest flood (18 500 m^3/s) for the pre-dam scenario. Figure 4-1 shows the flooded model area over the simulation period and Figure 4-2 shows the exceedance probability for flooded area for both scenarios. An area of 1094 km^2 within the model domain (9%) is inundated 5% of the time for the pre-dam scenario but remains dry throughout the post-dam simulation.

It is evident from the flow depth and velocity plots (Figure 4-3, Figure 4-4) that the model domain does not cover the full breadth of the delta, so the actual flooded area of the delta will be much greater than that shown by the model. Additionally, the flooded area during low flows may be smaller than that predicted by the model, as evaporation is not accounted for and even at the lowest flows the model shows significant areas of shallow stagnant water on the floodplains.

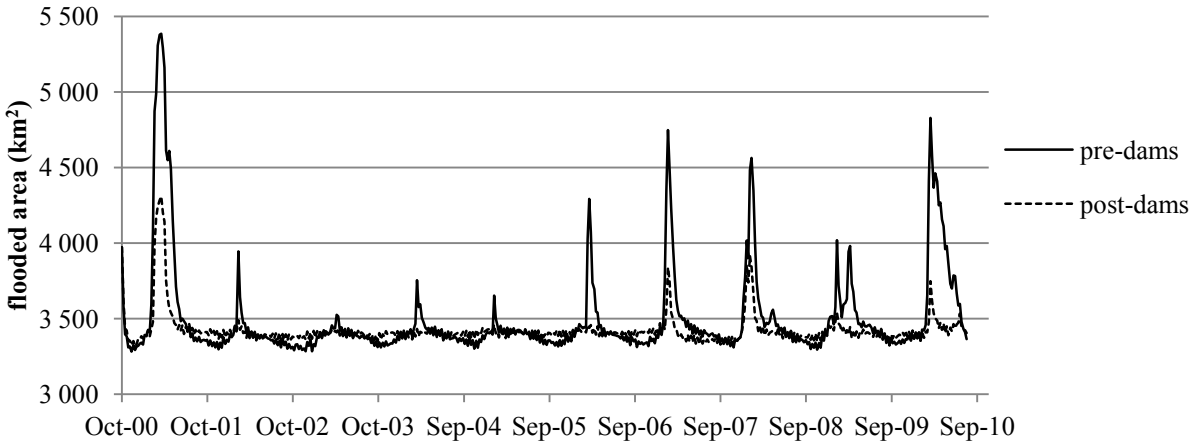

Figure 4-1 **Flooded model area over 10 year time series for pre-dam and post-dam simulations**

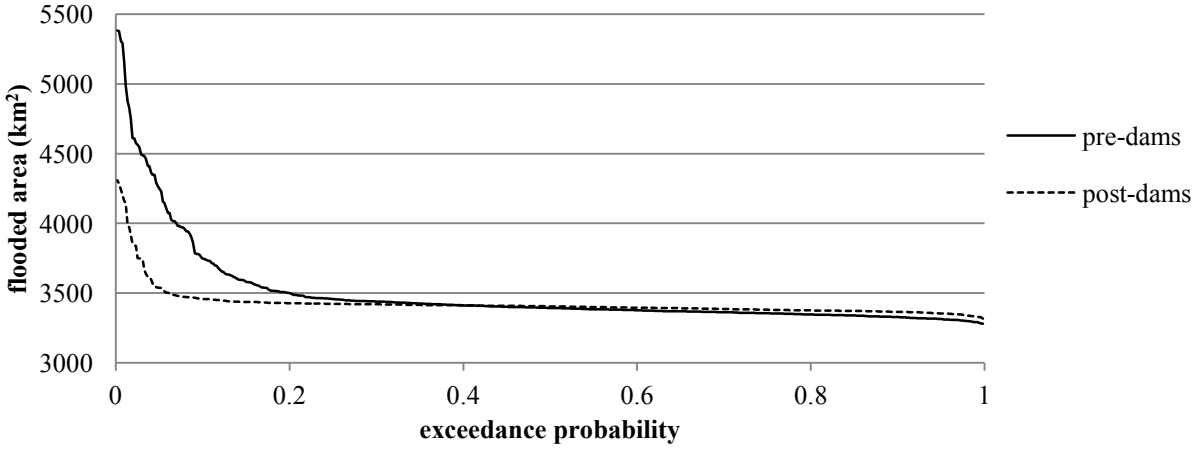

Figure 4-2 **Flooded model area versus exceedance probability for pre-dam and post-dam simulations**

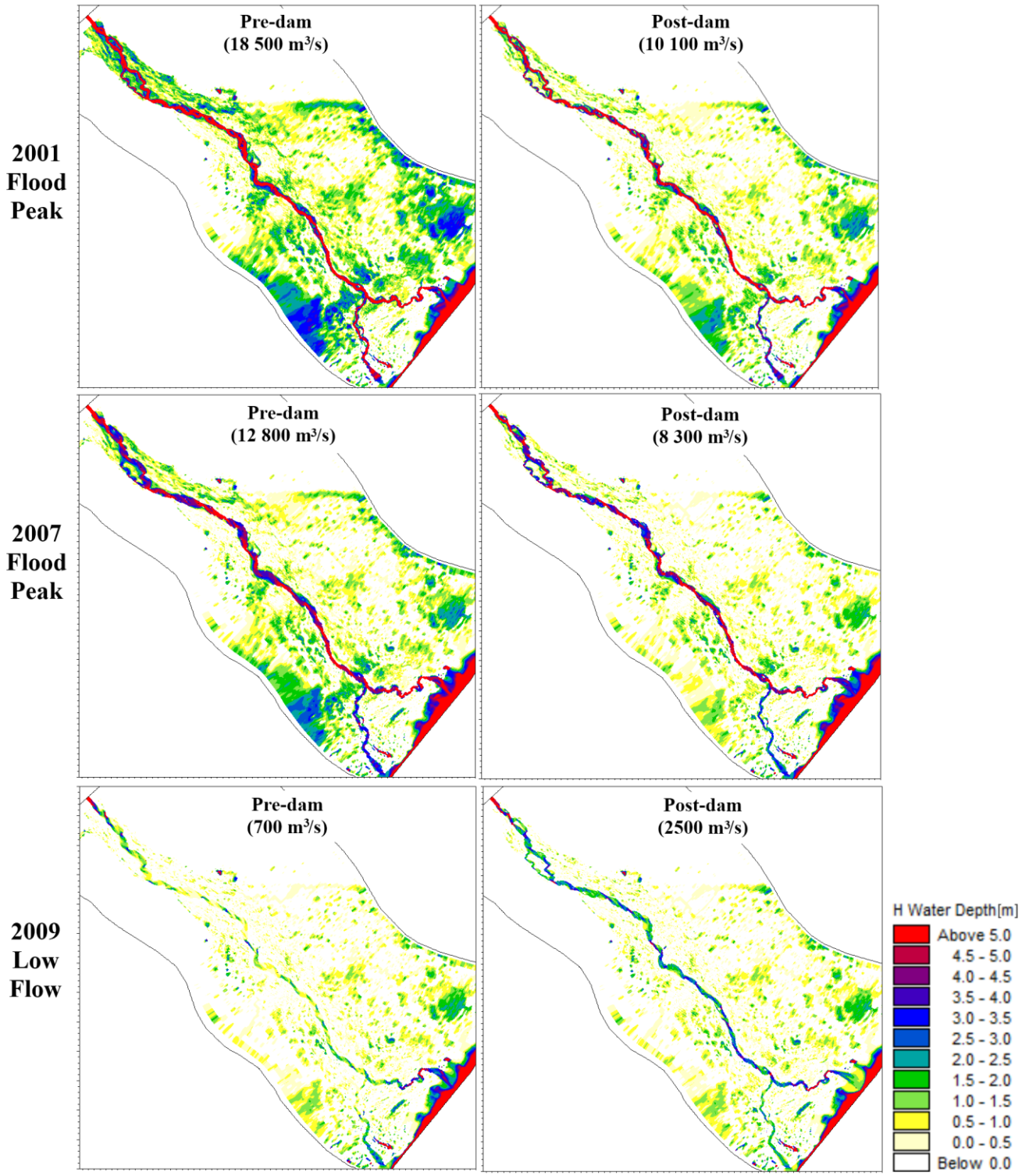

Figure 4-3 **Flow depth contours at selected flood peak and low flow periods for pre-dam and post-dam scenarios**

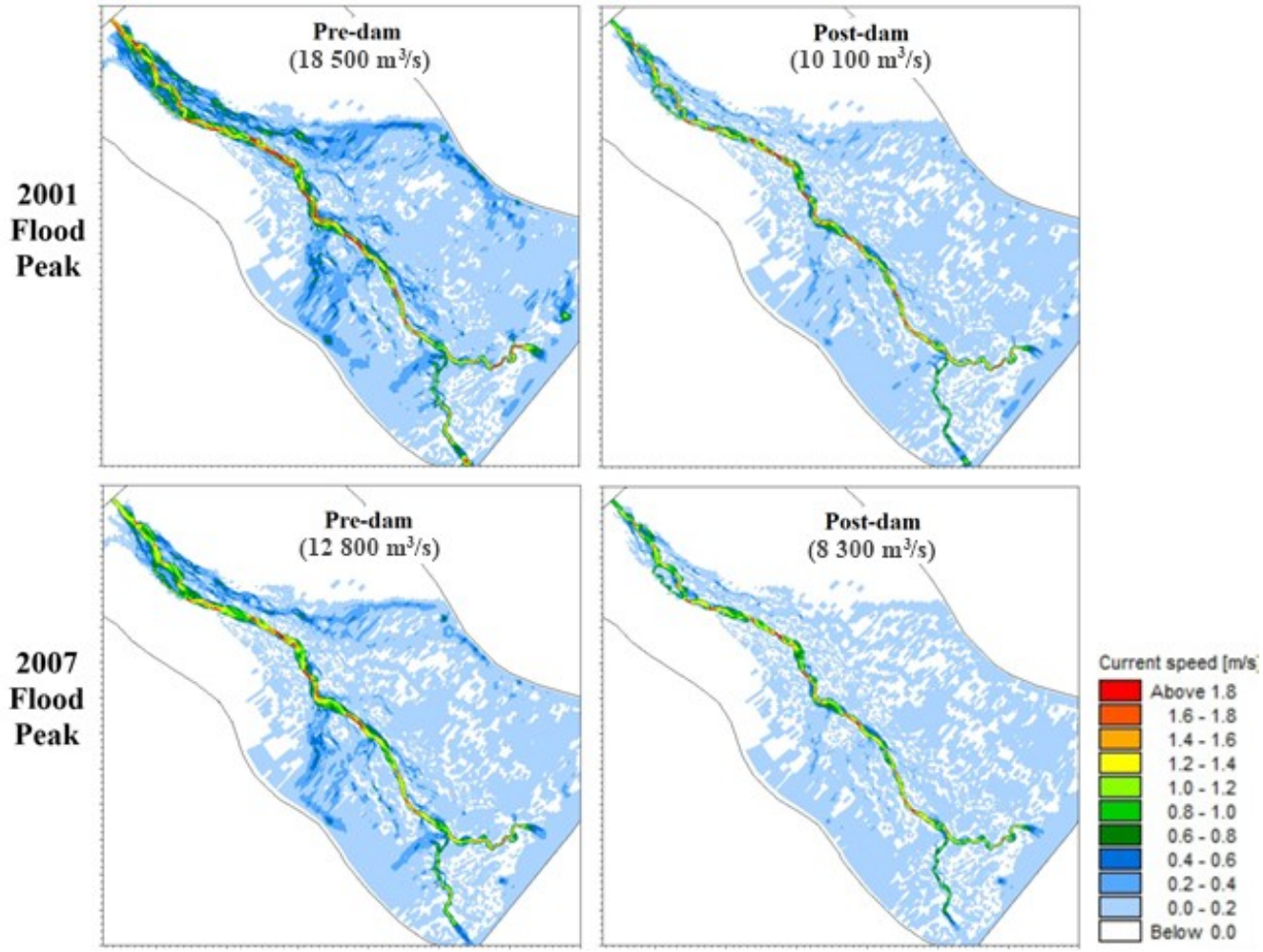

Figure 4-4 **Velocity contours at selected flood peaks for pre-dam and post-dam scenarios**

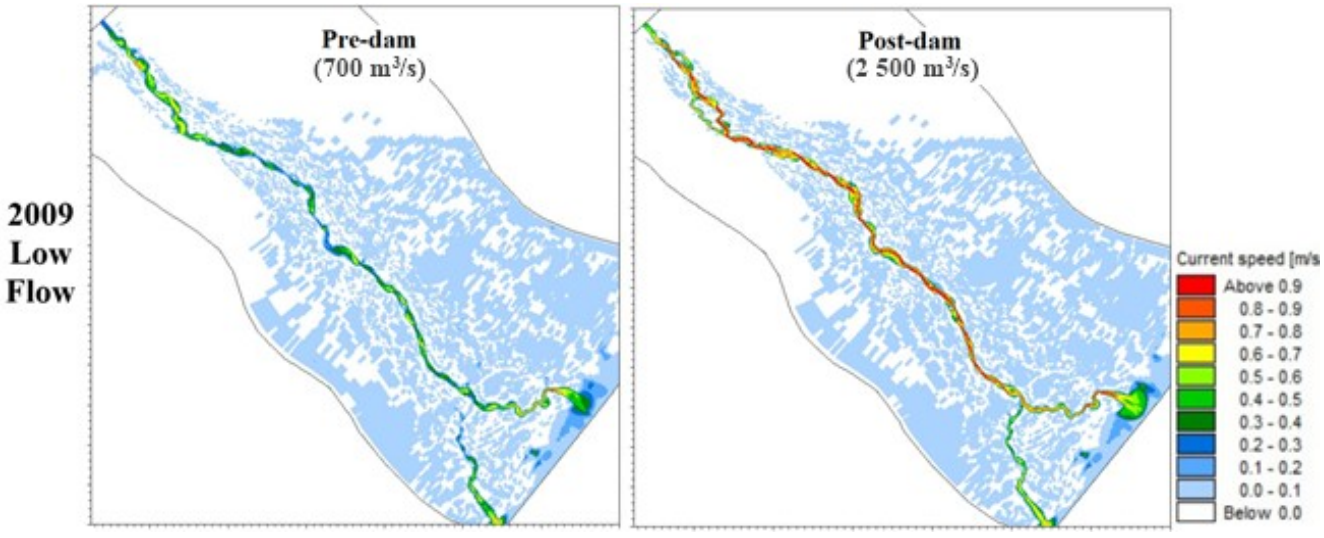

Figure 4-5 **Velocity contours for a selected low flow period for pre-dam and post-dam scenario (note the different palette scale to Figure 4-4)**

4.2 Morphological changes

Figure 4-6 and Figure 4-7 show the bed level changes over the 10 year simulations for pre-dam and post-dam conditions. Figure 4-5 uses a small step colour palette to illustrate the small bed level changes on the floodplains. It can be seen that for the pre-dam scenario there is some notable movement of sediments on the floodplains but for post-dam conditions there is virtually none. Figure 4-7 shows the same results with a different colour palette to more clearly show the sediment movement in the main river channel.

Figure 4-8 to Figure 4-11 on the following pages show the bed level changes with corresponding water levels (shown with thinner horizontal lines of the same colour) over time for the four selected cross sections labelled A to D in Figure 4-7. In these figures the dashed black lines show the levels at the start of the simulation, the coloured lines show the levels at the end of each year (purple for the end of the first year through to red for the end of the eighth) and the solid black lines show the final bed and water levels. For both pre-dam and post-dam scenarios the model bed changes rapidly in the first year of simulation from the bathymetry provided to a more stable configuration[a], and thereafter more gradual changes take place. A comparison of the final bed levels for the pre-dam and post-dam simulations for each cross section is given in Figure 4-12 (in this figure the starting bed is shown with a solid line, the pre-dam final bed is shown with small dashes and the post-dam bed is shown with longer dashes). The changes in the channel shape are similar for both simulations with more sediment movement generally leading to slightly wider channels with more gently sloping banks for the pre-dam scenario.

At section D, in the ocean at the northern river mouth, the model shows the build up of a very large sand bank right up to the minimum tidal level for the post-dam scenario, while for the

[a] The rapid bed changes during the first year of simulation are also partly due to the large flood which occurs in this year

pre-dam scenario deposition also occurs but a deep channel is maintained through the centre by frequent high flows. However, in the field this sand bank may be eroded by wave action and resultant long shore currents in the ocean which are not included in the numerical model and therefore this area of deposition and any related damming effects (see further discussion in section 4.5) may not be realistic.

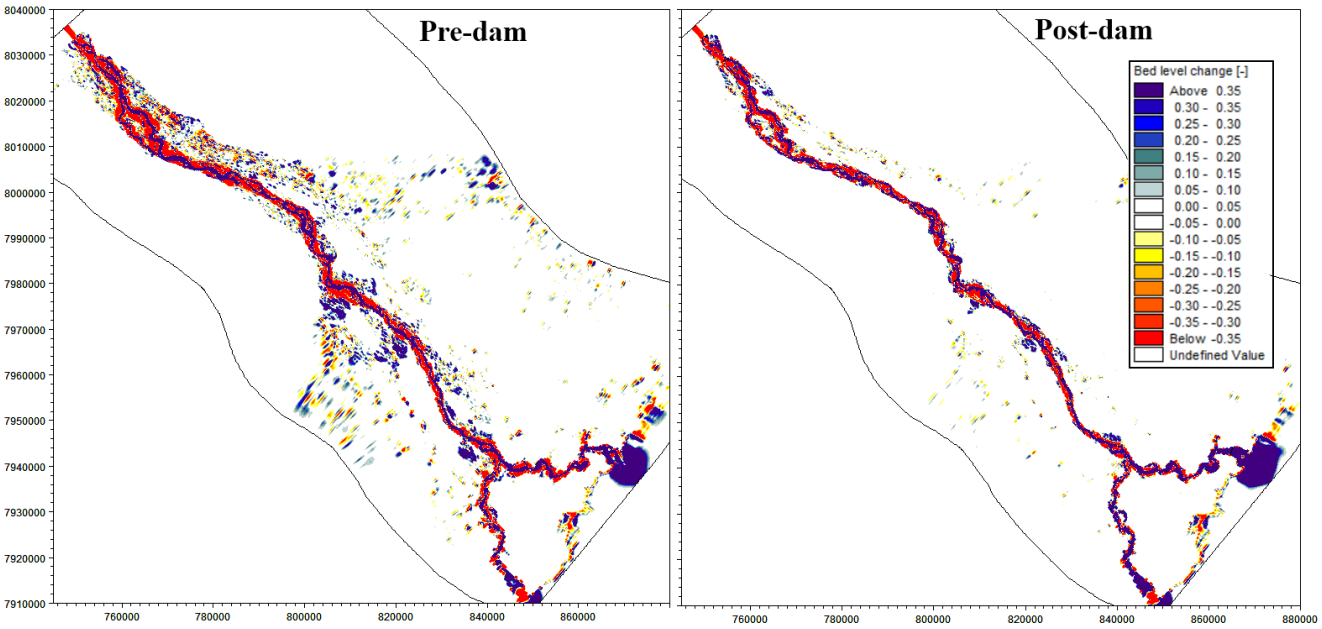

Figure 4-6 **Final bed level change contours for pre-dam and post-dam scenarios to show regions of sediment movement on the floodplains**

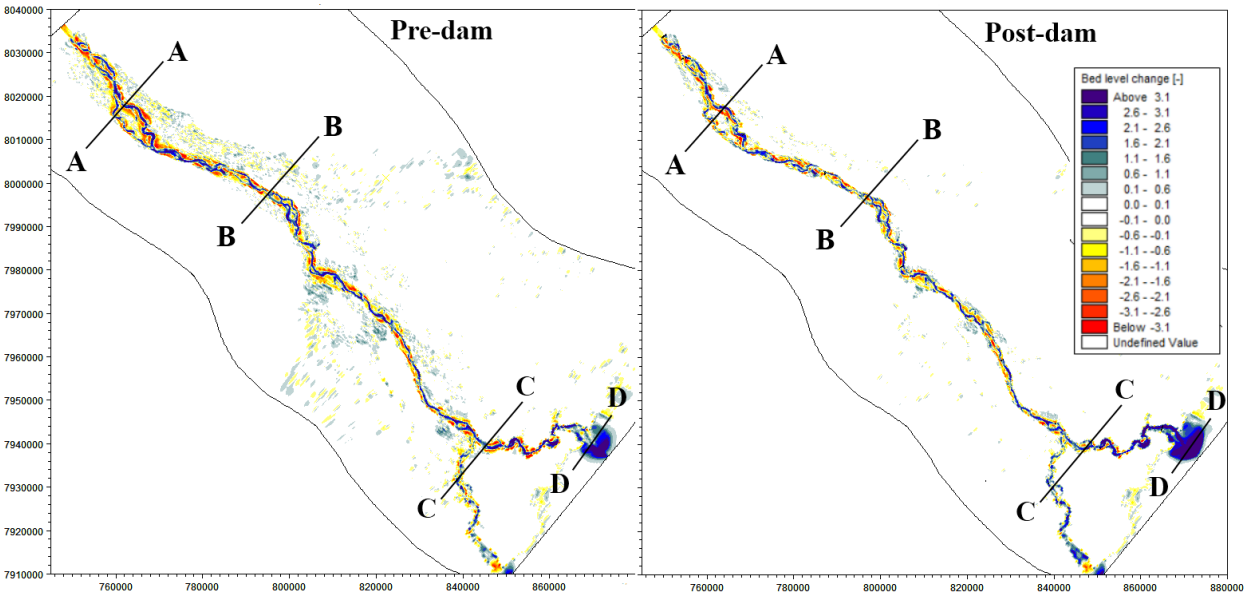

Figure 4-7 **Final bed level changes for pre-dam and post-dam simulations showing location of cross-sections examined**

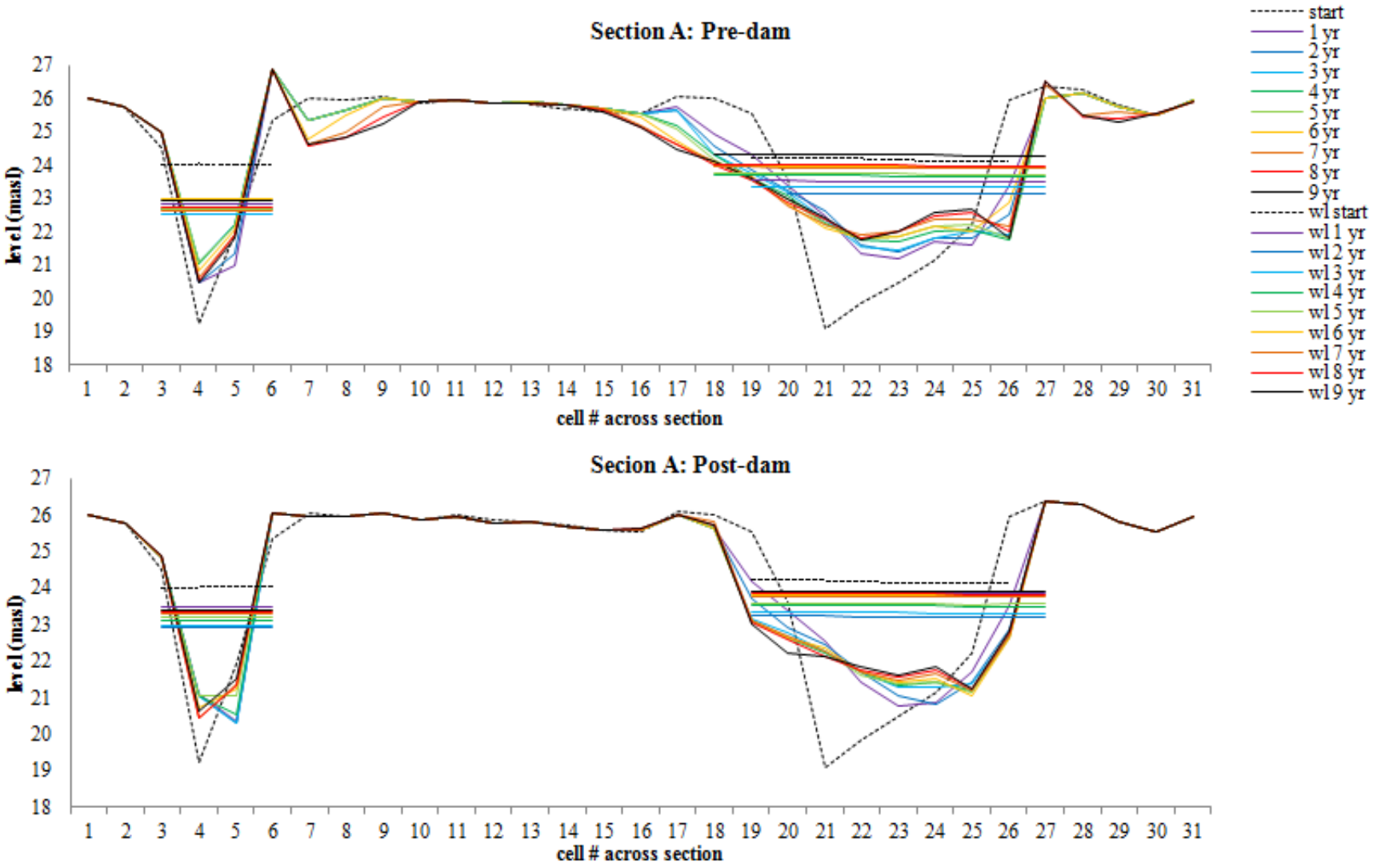

Figure 4-8 **Bed levels (with water levels) for the end of each year of simulation for cross section A (facing upstream)**

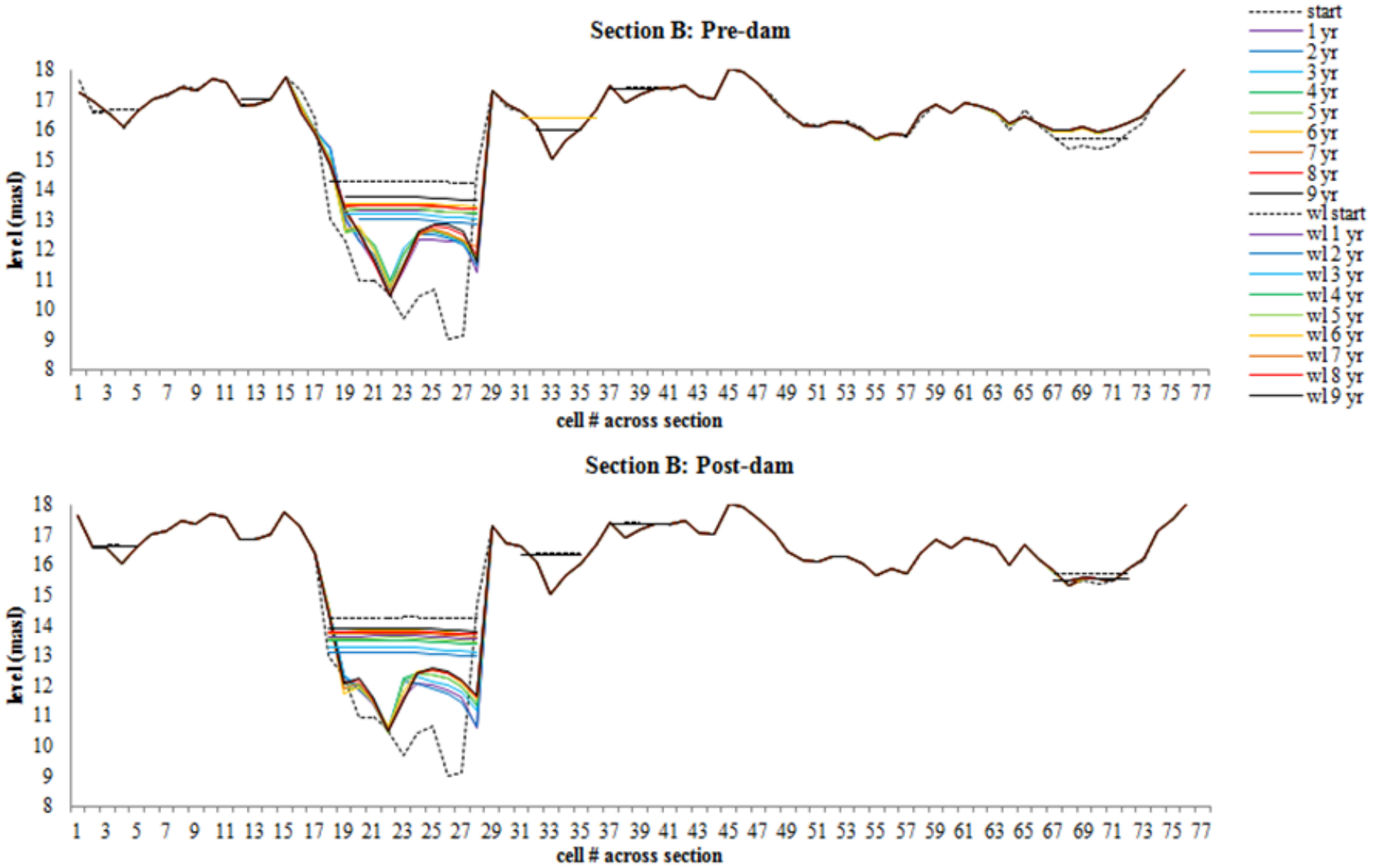

Figure 4-9 **Bed levels (with water levels) for the end of each year of simulation for cross section B (facing upstream)**

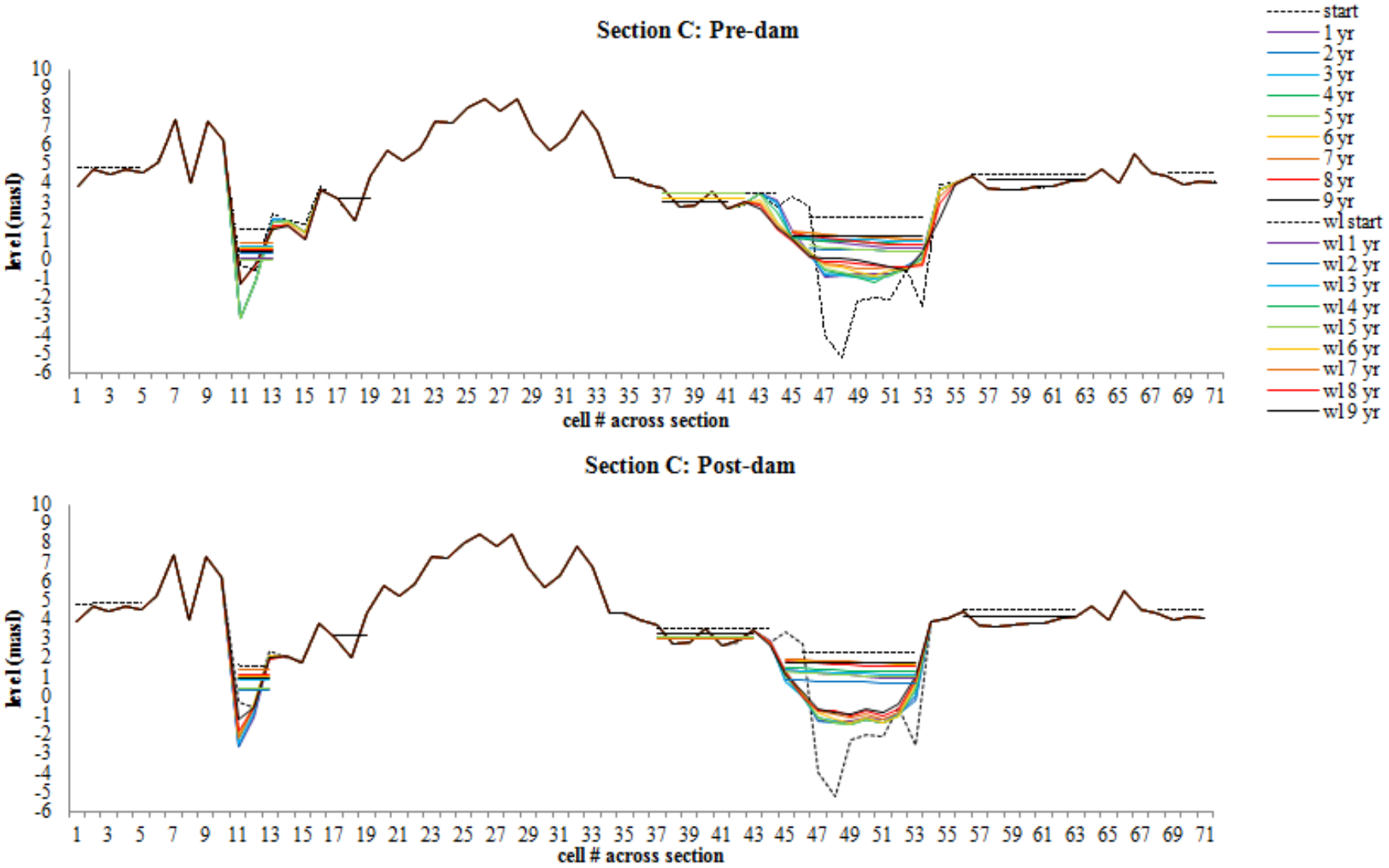

Figure 4-10 Bed levels (with water levels) for the end of each year of simulation for cross section C (facing upstream)

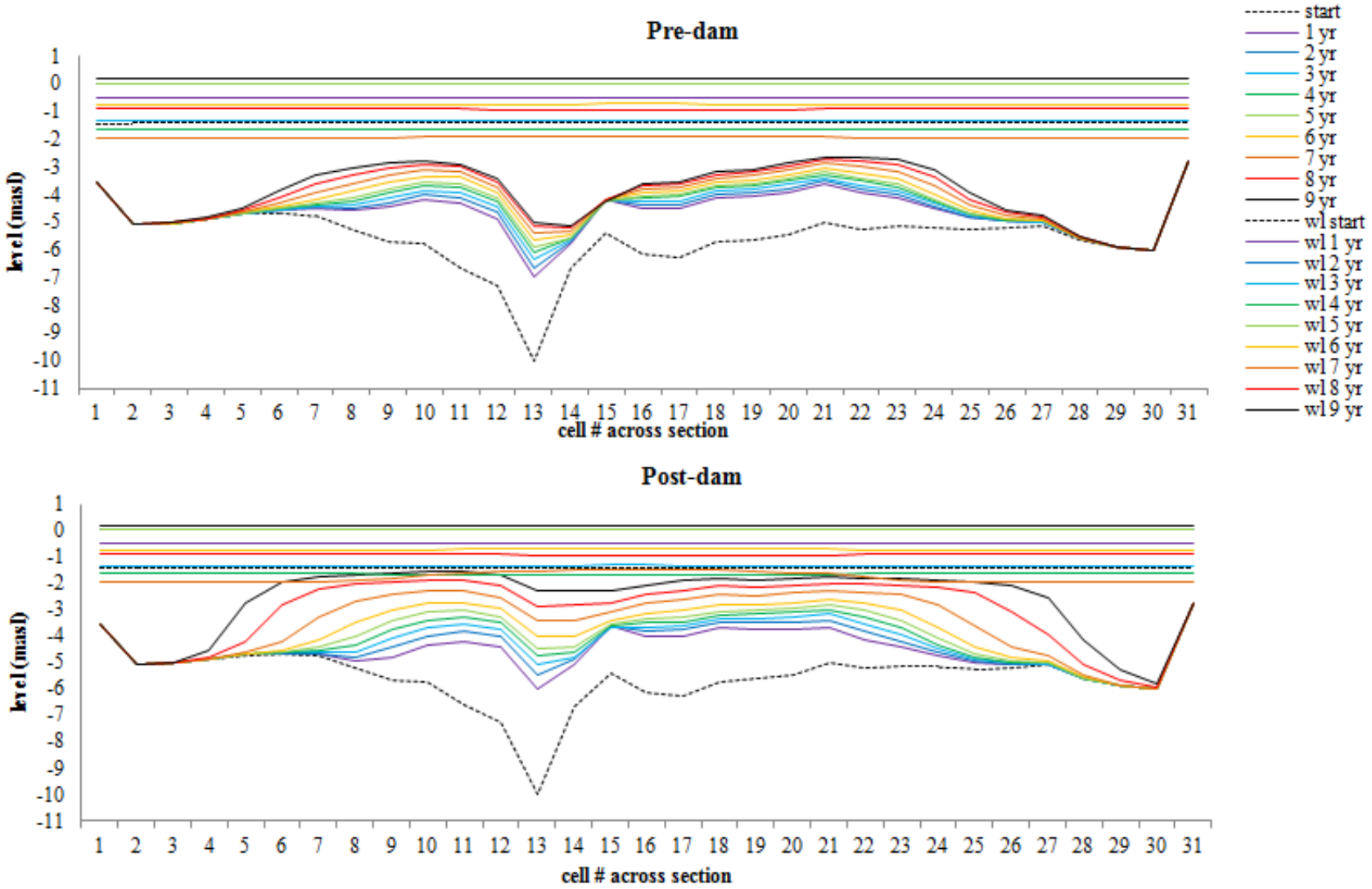

Figure 4-11 Bed levels (with water levels) for the end of each year of simulation for cross section D (facing upstream)

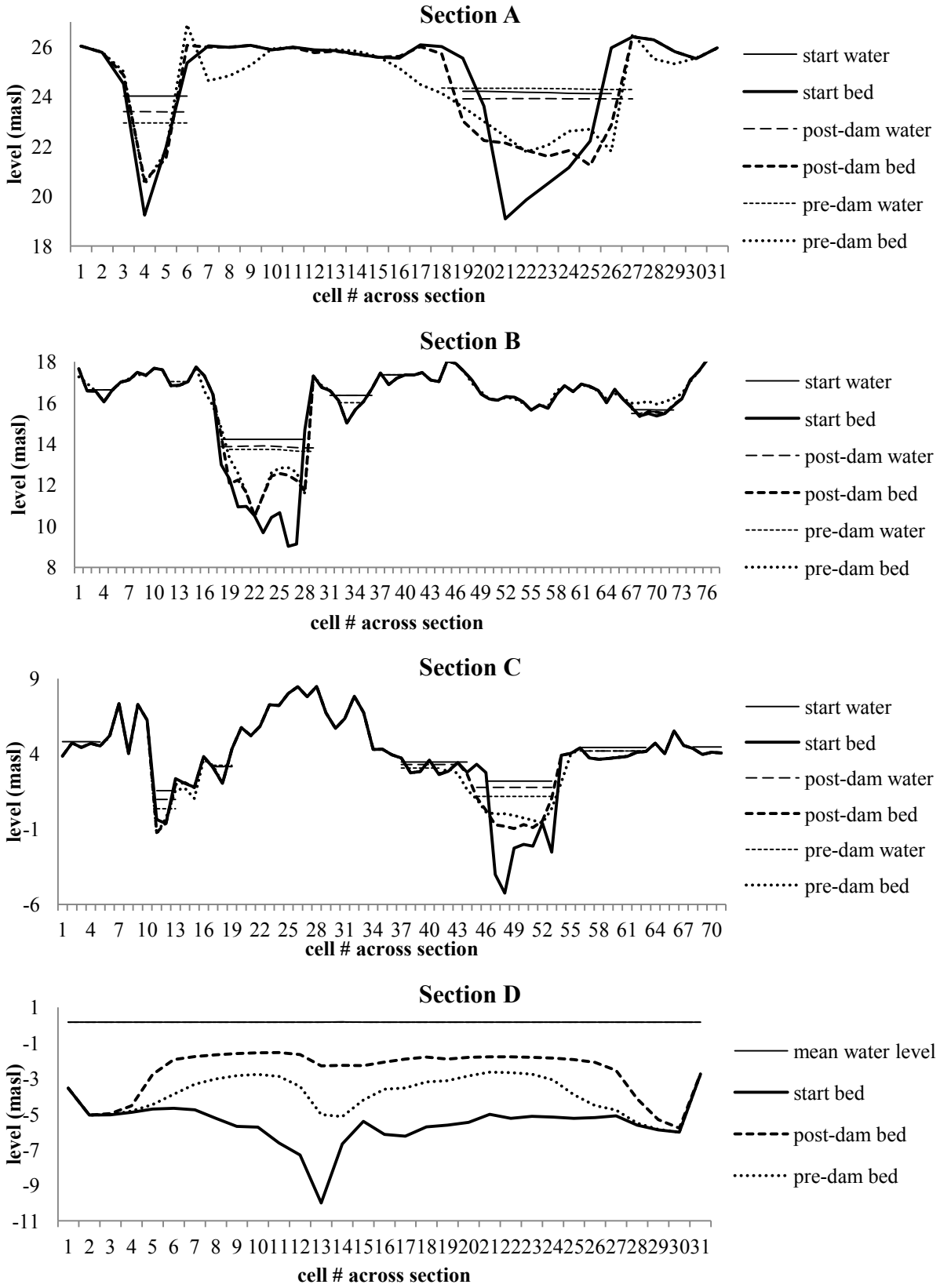

Figure 4-12 Comparison of starting bed and water levels with final levels for pre-dam and post-dam simulations

4.3 Bed grading changes

The grading of the model bed was specified using four sediment fractions: three non-cohesive fractions and one fine cohesive fraction (as discussed in section 3.5). *Mike21C* calculates the transport of each fraction separately (with reduction factors to account for armouring and other effects of there being multiple fractions present) and hence can give results on the grading evolution throughout a simulation.

Figure 4-13 shows contours of the mean grain size distributions in the river channel at the end of the 10 year simulations. In Figure 4-13 the starting mean grain size (0.778 mm) is shown in white, while yellow to red indicates bed coarsening and blue indicates a finer bed. The results show the mean grain size for the whole bed layer which was initially defined as 12 m thick. The mean grain sizes at the surface can therefore be expected to be significantly further from the starting condition than predicted by the values in Figure 4-13. The pre-dam and post-dam results show similar patterns but with greater changes for the pre-dam scenario. In both cases a two-dimensional pattern with patches of local coarsening and fining are evident throughout the model domain.

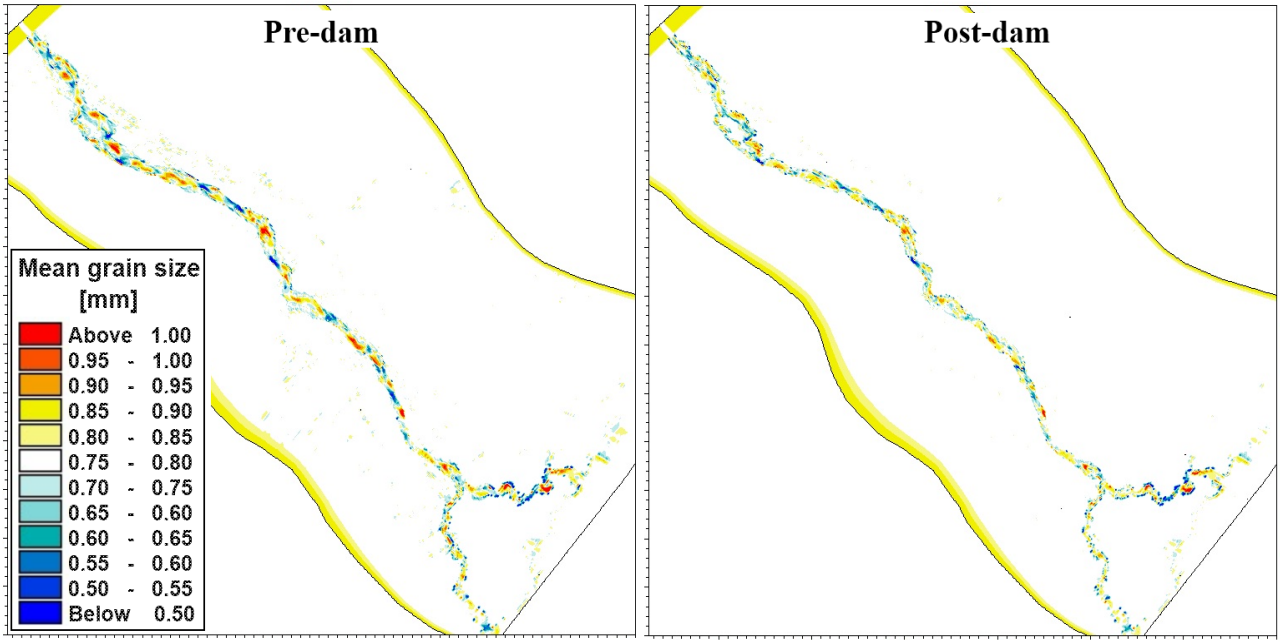

Figure 4-13 Mean grain size distributions at the end of the 10 year pre-dam and post-dam simulations

Fine clay/silt sized sediment particles are often accompanied by nutrients which are important for river and floodplain ecology and therefore the deposition patterns of these fractions are of particular interest to specialists investigating possible environmental effects of dams. Figure 4-14 shows the net deposition of the fine sediment fraction for the pre-dam and post-dam simulations. The initial deposition of the fine fraction within the model domain is 14.4 mm[a] (0.12% of the 12 m thick bed layer) and is indicated by the darkest green in Figure 4-14. Areas where additional fine sediment has been deposited at the end of the simulations are shown in yellow to red while areas of fine sediment erosion are shown in blue to purple.

For both pre-dam and post-dam simulations the fine fraction within the main river channel is completely washed out (during the first few months of simulation). It seems that the model may not sufficiently account for armouring (protection of small particles deep in the bed from erosion by the larger particles above) as it allows the fine fraction to be completely washed out from places where the overall layer is still very deep (see more discussion on this possible

[a] On land boundary cells there is zero deposition, and at the model inflow canal a very thick model layer is specified (see section 4.4 for more discussion)

model inaccuracy in section 4.4). On the floodplains much more deposition (as well as erosion) of fine sediment occurs for the pre-dam scenario. For the post-dam scenario most of the silt deposition occurs within the channel in the main distributaries close to the ocean. As mentioned in section 4.2, the sediment deposits in and very close to the ocean may be cleared by wave action (not included in the model) so the model may over-estimate deposition in this region of the model.

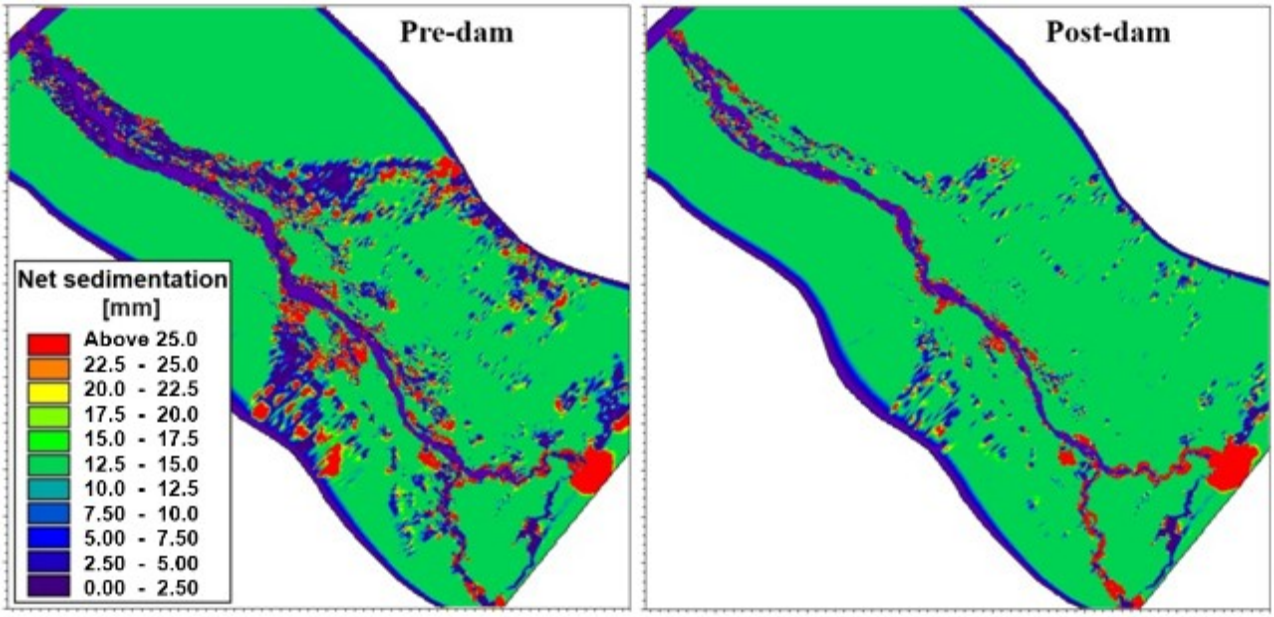

Figure 4-14 Net sedimentation of the fine sediment fraction at the end of the 10 year pre-dam and post-dam simulations

4.4 Suspended sediment concentrations

Figure 4-15 shows suspended sediment concentration contours at selected flood peaks for pre-dam and post-dam scenarios. Figure 4-16 shows time-series of sediment concentrations, suspended sediment loads and cumulative suspended sediment loads over the simulation period for two selected points in the river channel (point “a” near the upstream boundary and point “b” on the main northern distributary near the outlet as shown in Figure 4-15).

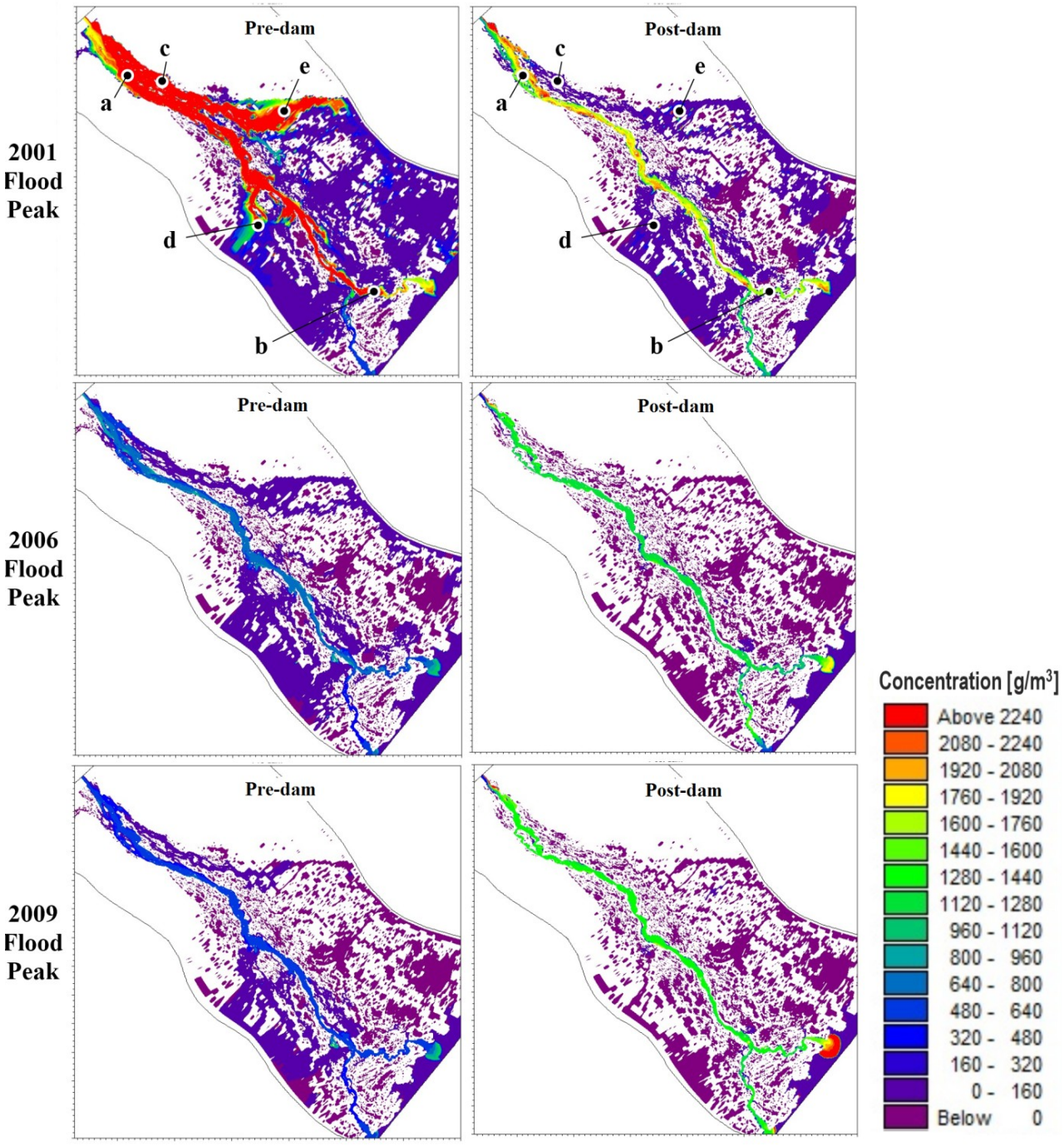

Figure 4-15 **Sediment concentration contours for selected flood peaks for pre-dam and post-dam conditions**

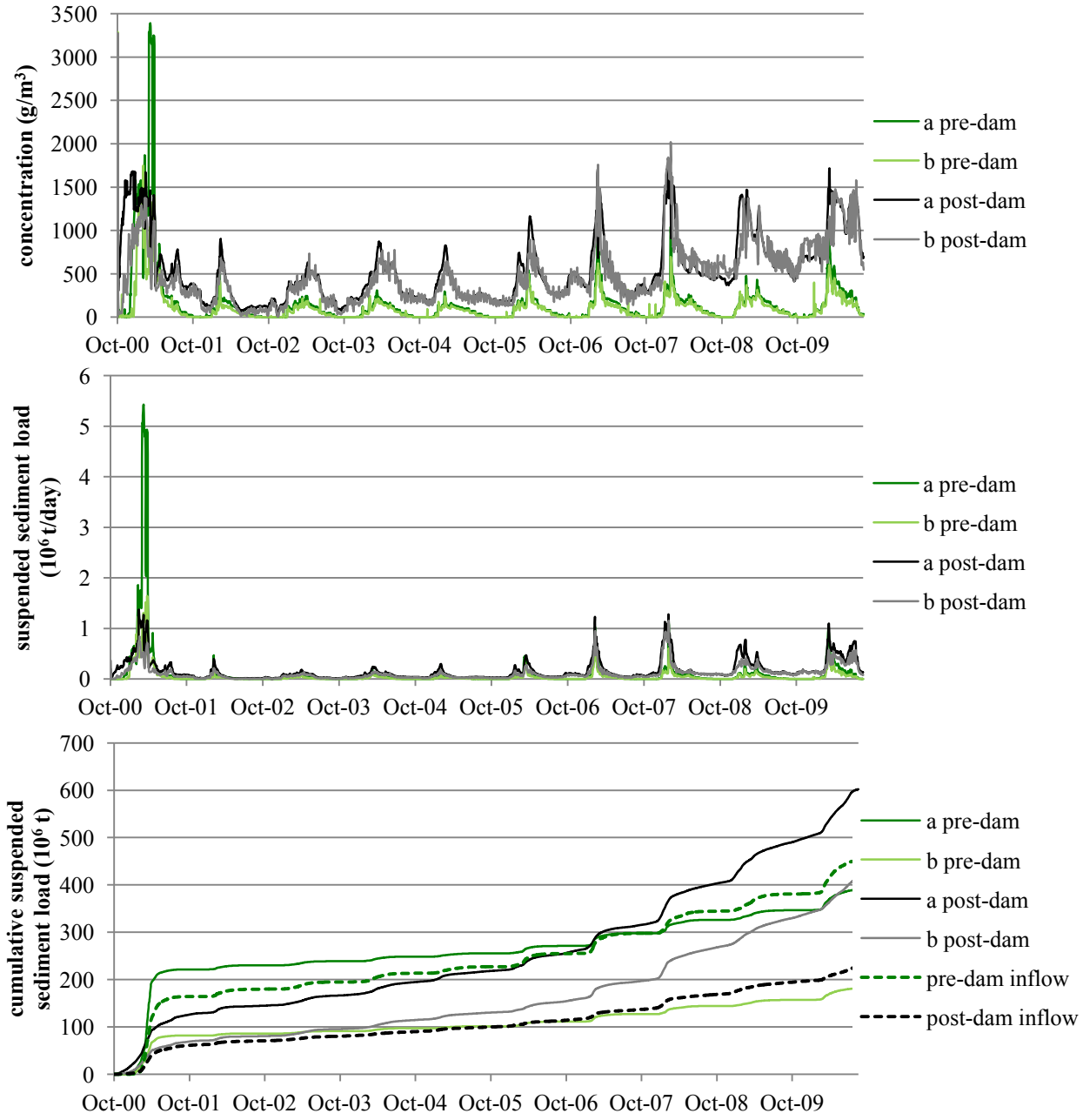

Figure 4-16 Suspended sediment concentration, load and cumulative load time-series over the model period for selected points within the river channel (a & b in Figure 4-15) for pre-dam and post-dam conditions

While the highest sediment concentrations and loads are observed during the major flood in 2001 for the pre-dam scenario, simulated sediment loads within the river channel are generally higher for the post-dam scenario. The graph at the bottom of Figure 4-16 shows the cumulative sediment loads passing points "a" and "b" together with the cumulative sediment inflow defined at the upstream boundary. For the pre-dam simulation (shown in green lines)

the total suspended load passing through the cross section at point "a" for the whole simulation is slightly less than the inflowing load (as expected) and the total load passing point "b" is considerably less (partly due to deposition within the model and partly because only part of the total flow (78%) exits through the northern distributary). However, for the post-dam simulation (and for the early parts of the pre-dam simulation) the simulated sediment loads are significantly greater than the inflowing loads.

The unexpectedly large simulated suspended sediment loads would appear to be due to an erroneous inflow specification, but the boundary was confirmed to be correct (as determined in section 3.4) and it appears that the additional suspended sediment is getting picked up predominantly in the inflow canal at the upstream boundary[a]. Closer analysis of the inflow canal region shows that no exceptionally large bed level changes occur (maximum erosion at the end of the simulation is 3 m) but that almost all of the fine fraction is "sucked" out of the (extremely deep) bed by the end of the post-dam simulation (see Figure 4-7 for bed level changes and Figure 4-14 for net sedimentation of the fine fraction). This points to an insufficient handling of armouring by the model. More realistic sediment load results could be obtained by specifying a thinner layer thickness at the boundary but throughout the model it appears that fine sediment is being removed from deep layers too readily. Perhaps more accurate results could be obtained by using more sediment fractions and specifying a number of separate layers or perhaps the general model handling of armouring needs improvement. Additionally, for accurate simulation of suspended sediments, the suspended sediment transport equation should be calibrated and this would be possible with additional field data.

[a] The boundary region of a model is most susceptible to numerical instability and so it is common practice to create a few model rows without rapidly changing geometries leading into the model region of interest. In this model an artificially straight inflow "canal" (500 m wide and 1500 m long) with a flat floor and a very thick bed layer (300 m deep) was created at the upstream boundary to aid numerical stability.

4.5 Tidal effects

Figure 4-18 shows water surface elevations for the 2001 flood and for a selected low flow period in the estuary section of the model (point locations indicated in Figure 4-17) together with the inflowing discharge (Q shown with the dotted black line on the secondary axis). Model results were saved every 24 hours during the simulations (as saving more often for the full 10 year simulations would require excessive storage space) so the water levels for each high and low tide are not captured, but over several weeks the variations in water level due to the tides are visible. With this resolution, variations in water level due to the tides are visible almost up to the main delta split (about 45 km from the coast along the river centre-line) during low flows.[a] (The water levels are influenced by both the tidal boundary and the incoming flow. The variations at the furthest upstream point shown, p6, are similar to those at all points further upstream and are not visibly affected by the tide).

For the pre-dam scenario the tidal effect is less dominant during floods and more dominant during low flows than for the post-dam scenario (as would be expected due to the greater variability in flows). The difference in levels is most significant during low flows when the water levels near the coastal boundary are up to 1 m lower for the pre-dam scenario.

In the post-dam simulation a large sand bank formed at the Zambezi River mouth (see section D in Figure 4-12). As discussed in section 4.2, this sand bank may be removed in reality by wave action and/or long shore currents which are not included in the model. Figure 4-19 shows the water levels near the end of the post-dam simulation with water levels for a similar flow rate (about 2500 m^3/s) observed earlier in the same simulation when the sand bank was much smaller. It can be seen that the sand bank causes a slight degree of damming upstream and dampens the tidal effect in the estuary which may not be realistic.

[a] If the model results were saved more frequently (say hourly) it is possible that tidal effects further upstream may be visible.

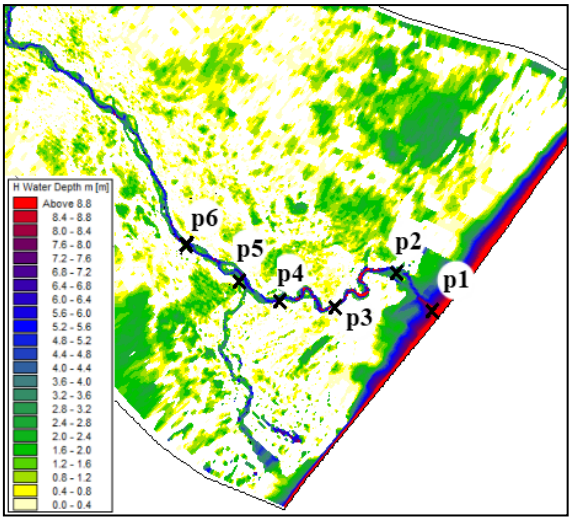

Figure 4-17 **Locations of points for which water level time-series are shown in Figure 4-18 and Figure 4-19**

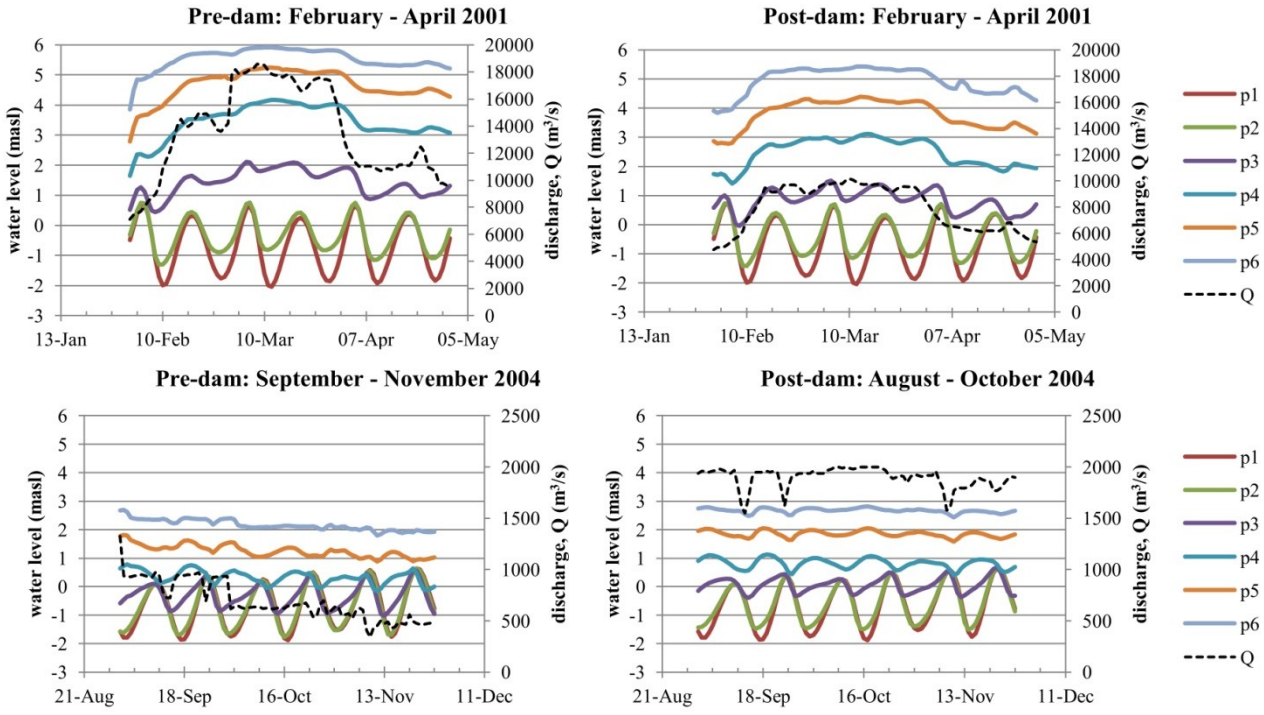

Figure 4-18 **Water levels at various model points for pre-dam and post-dam simulations over the peak 2001 flood and for a selected low flow period (September to November 2004)**

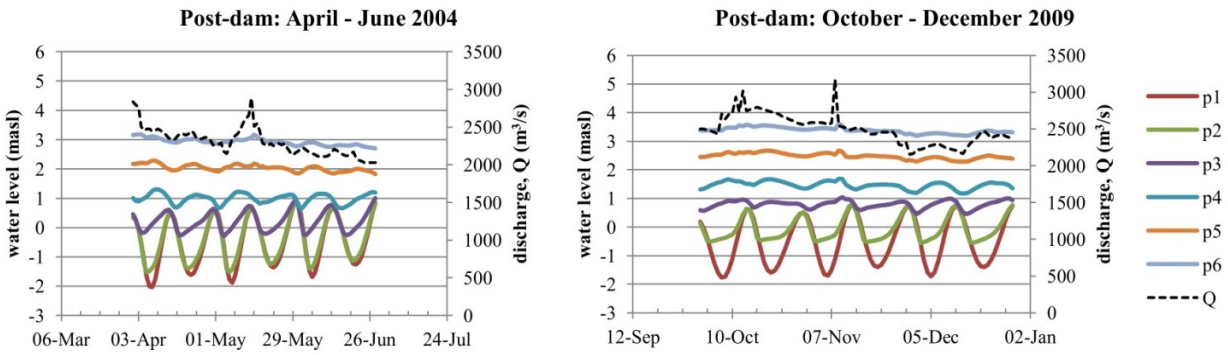

Figure 4-19 **Water levels at various model points for two periods with similar discharge for the post-dam simulation**

4.6 Summary and discussion of effects of dams predicted by model

The model results show a drastic decrease in the extent of flooding in the Zambezi Delta as a result of dams. The model domain does not cover the entire width of flooding but within the model domain an area of about 1100 km^2 (9%) would be inundated approximately 5% [a] of the time in pre-dam conditions but is now virtually never flooded.

From the model it appears that dams do not have a drastic effect on the channel morphology of the Lower Zambezi. The more frequent high flows that occur in the pre-dam condition cause slightly more sediment movement leading to a somewhat wider channel in most areas but the general channel patterns appear similar to those for post-dam conditions. However, the starting model bathymetry was based on recent surveys and therefore the starting point is a post-dam condition. The correct interpretation of the results is therefore not that dams do not have a major effect on the river morphology, but rather that dam removal would not result in drastically altered channel patterns (within 10 years). On the floodplains, significantly less sediment movement occurs as a result of dams and this may have implications for the floodplain ecology.

The higher low-flows caused by dams result in constantly higher water levels and less tidal variations (during periods of low flow) in the estuary region of the model than for pre-dam conditions[b]. Conversely, during periods of flooding, the smaller post-dam floods cause the tidal effect to be "washed-out" to a lesser degree than for the larger pre-dam floods. These alterations caused by dams to the natural tidal zone flow patterns may have many ecological implications. In addition to water levels and flow velocities, the salinity of the estuary zone

[a] The area is inundated for 5% of all days, generally in the form of flooding for a few weeks at a time approximately once every 3 years

[b] Towards the end of the post-dam simulation this effect is possibly unrealistically increased by the growth of a large sand bank in the ocean at the river mouth, which would probably be removed in reality by wave action and long shore currents that are not included in the model.

will be affected by these flow pattern changes and this would also have ecological implications. The addition of a salinity module to the current hydrodynamic and sediment transport model would provide additional important information for assessing the environmental effects of dams

The model over-predicts the suspended sediment loads because considerable volumes of fine sediment particles are “sucked” out of the very deep bed layer specified at the inflow boundary. These elevated suspended sediment loads are particularly severe for the post-dam scenario as additional sediment is drawn into the flow (from deep within the bed) even during low-flow periods. The much lower low flows in the pre-dam scenario have lower transport capacities and therefore do not entrain as much sediment. A thinner bed layer at the boundary (and perhaps throughout the model domain) would lead to more realistic results but, for an accurate model, more attention needs to be given to the source of the problem. Perhaps more sediment fractions, specified using a number of layers, could be found to give more realistic results. Additionally, calibration of the suspended sediment transport equation (with additional field data) would be desirable, as would a more accurate specification of the inflowing sediment concentration for the post-dam scenario using a tributary flow based rating curve.

5 SIMULATION OF AN ENVIRONMENTAL FLOOD RELEASE SCENARIO

The numerical hydrodynamic and sediment transport model developed for the Zambezi Delta provides a useful tool for comparing and assessing environmental flood release scenarios (described in section 2.2.3). A simulation of a single example flood release scenario was performed as part of this study and the results were compared to the pre-dam and post-dam conditions.

5.1 Model boundaries

In Figure 5-1 the inflow for the environmental flood release (EFR) scenario is shown with the pre-dam and post-dam model inflow. The EFR scenario is defined by the post-dam flow scenario with annual flood freshets with peaks of approximately 8500 m^3/s at the delta (requiring a 6750 m^3/s release from Cahora Bassa Dam) in February. The additional flow was assumed to be released as a triangular hydrograph over four weeks (equivalent in volume to a constant two week flood release). This release scenario would result in a 4 % reduction in average annual hydropower production, and would decrease the firm power reliability from 98.4% to 94% (Beilfuss & Brown, 2010) [a]. The EFR peak of 8500 m^3/s is lower than the pre-dam mean annual flood peak of 10 000 m^3/s (Beilfuss & Brown, 2006) but approximately equal to that of the post-dam 3 year flood (see Table 5-1 for the post-dam recurrence interval flood peaks).

A clear-water release from Cahora Bassa Dam was assumed for extra releases for the environmental flood so the sediment inflow loads to the delta for the EFR simulation were kept the same as for the post-dam scenario.

[a] This flood release scenario has a medium-high flood peak and a short duration compared to other flood release scenarios typically considered. For example Beilfuss & Brown (2010) investigated flood releases from 4000 m^3/s to 10 000 m^3/s for periods of 2 to 8 weeks.

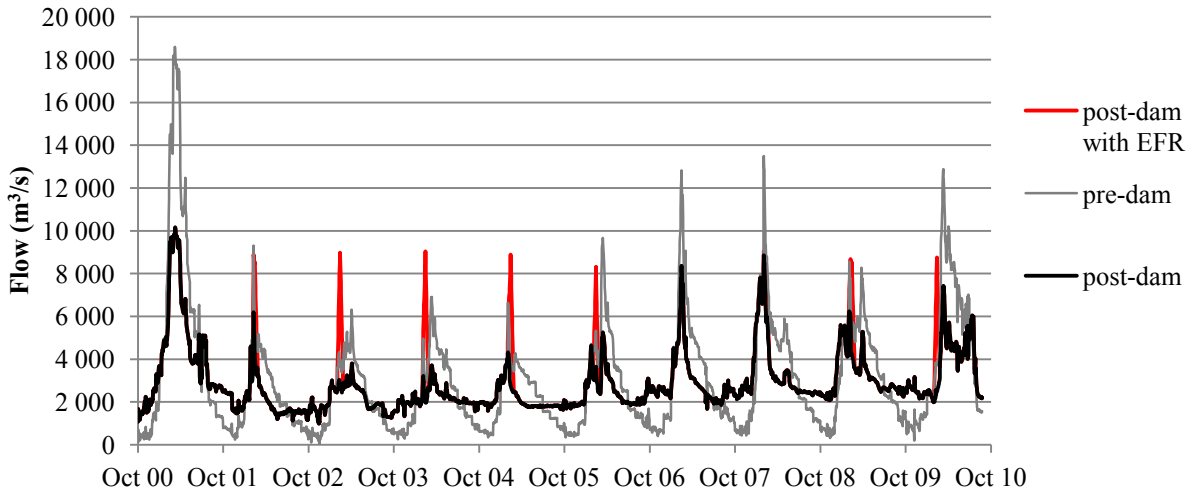

Figure 5-1 **Model inflow for simulation of an environmental flood release scenario (red) shown with the pre-dam and post-dam scenario inflows**

Table 5-1 **Post-dam recurrence interval flood peaks at Caia (ASP, 2012a)**

Return Period (years)	**2**	**5**	**10**	**20**	**50**
Flood Peak (m^3/s)	6 600	10 200	12 450	14 600	17 200

5.2 Results

Figure 5-2 shows the depth and velocity contour plots for the peak of a typical EFR.

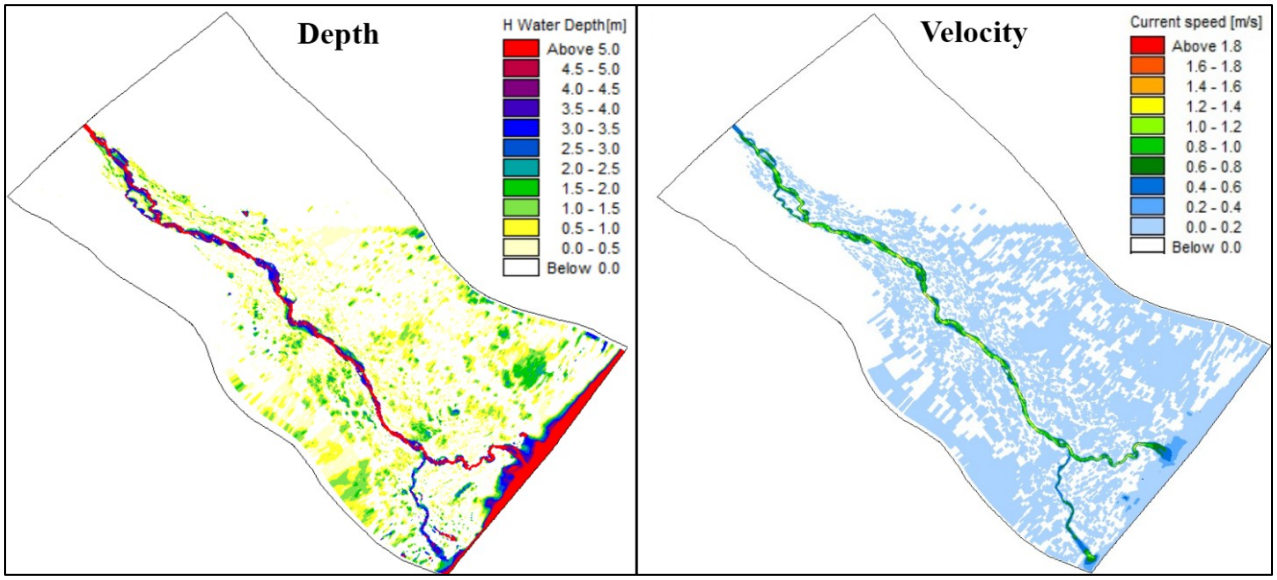

Figure 5-2 Depth and velocity contours at a typical EFR peak (Feb 2004)

Figure 5-3 and Figure 5-4 show the model flooded areas, on a time-series and as an exceedance probability respectively, for the EFR scenario compared to pre-dam and post-dam conditions. The EFRs considered in this scenario do not flood very large areas compared to the pre-dam floods. However, relative to current post-dam conditions the EFR scenario considered causes inundation of an additional 200 km^2 (2% of the model domain) at the 5% exceedance level (see Figure 5-4).

Figure 5-5 compares the net sedimentation of fine sediment for the EFR and the post-dam simulations. And finally Figure 5-6 compares the channel morphological changes of the three scenarios for a selected cross section (cross section A in Figure 4-7).

As discussed in section 4.4 and 4.6, the current model does not predict the suspended transport of fine sediments correctly so the effect of the EFR on sediment concentrations and the general transport of the fine fraction is not known.

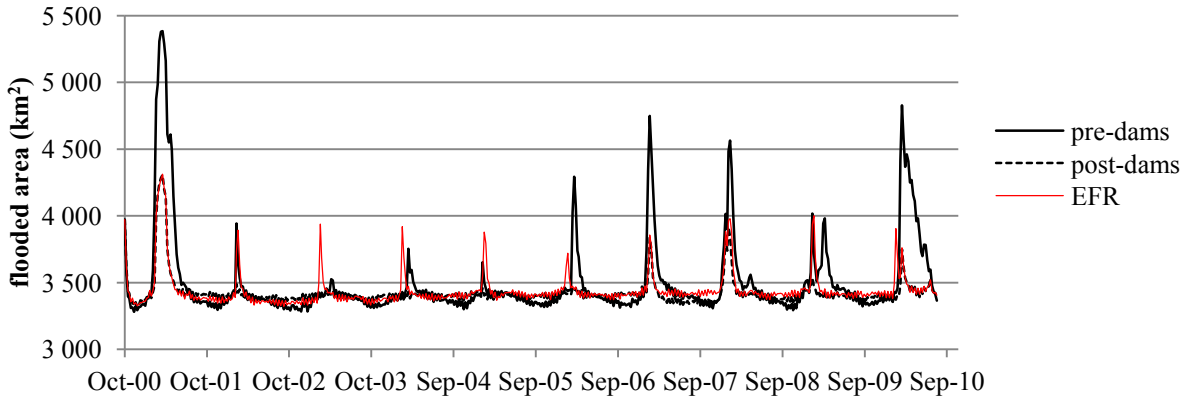

Figure 5-3 **Flooded areas over the 10 year simulation for the pre-dam, post-dam and EFR scenarios**

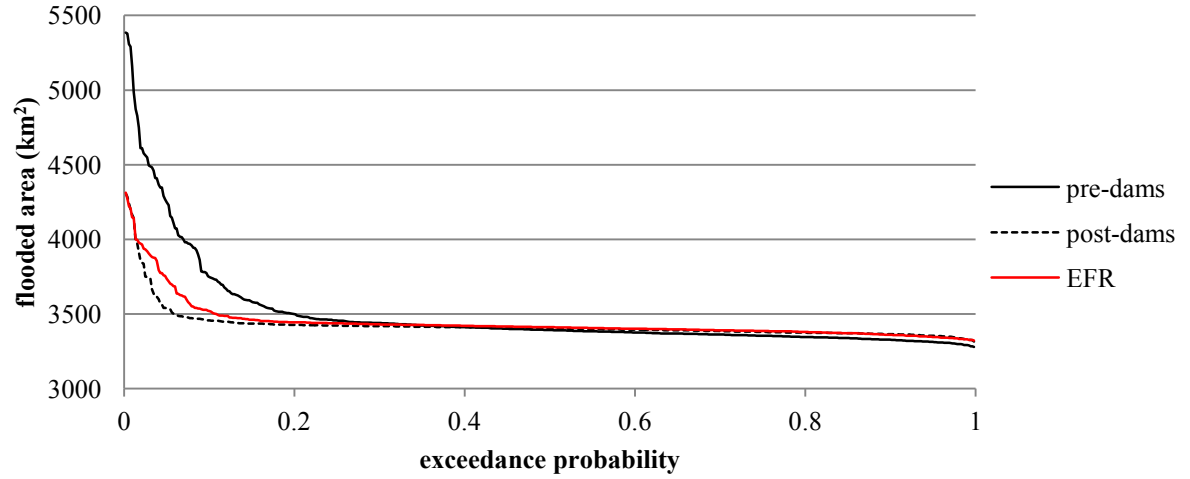

Figure 5-4 **Flooded model area versus exceedance probability for pre-dam, post-dam and EFR simulations**

Figure 5-5 shows the net deposition of fine sediment predicted by the model for the EFR simulation compared to the post-dam simulation and they appear virtually identical (as should be expected because the environmental peak flows do not flood very far onto the floodplains).

The channel bed configurations are visibly affected by the environmental flood releases at some sections. For example the wider channel at section A (Figure 5-6) shows a bed shape almost half-way between that for the pre-dam and post-dam simulations.

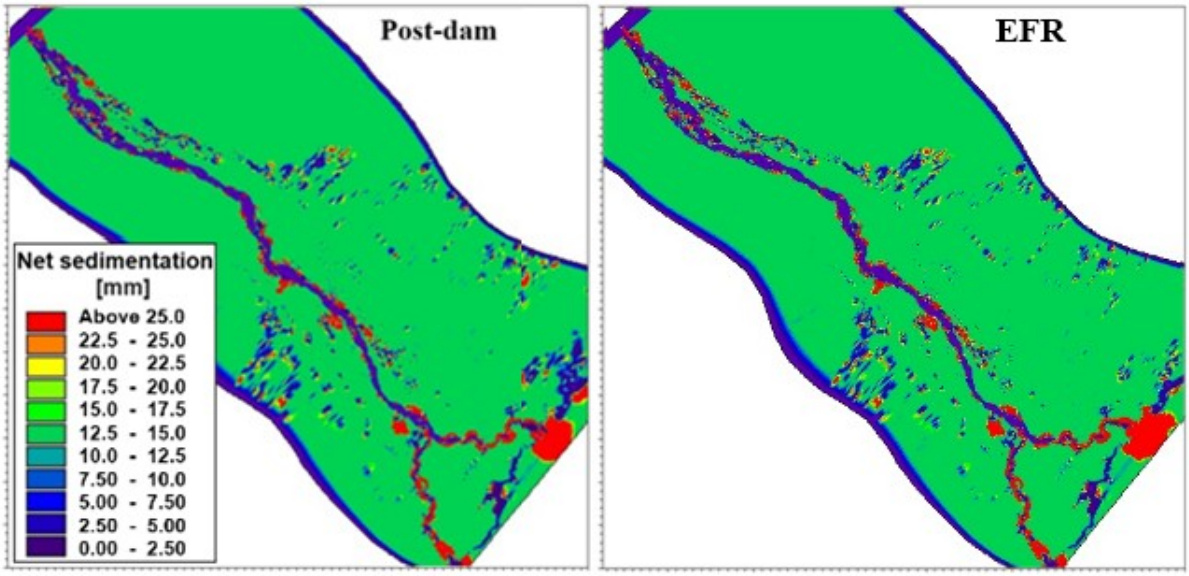

Figure 5-5 **Net sedimentation of the fine sediment fraction for the EFR simulation compared to the post-dam simulation**

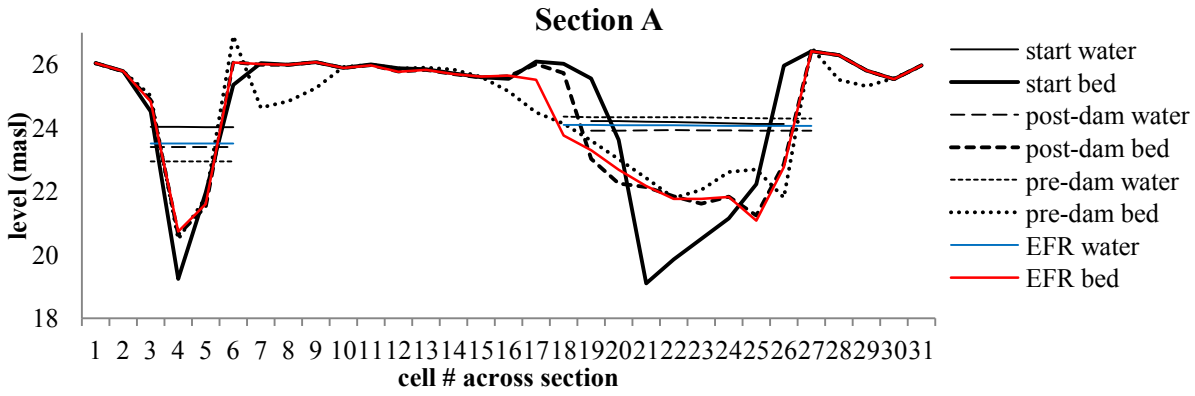

Figure 5-6 **Comparison of starting bed and water levels with final levels for environmental EFR, pre-dam and post-dam scenarios at cross section A (shown facing upstream)**

The results from this EFR simulation show that freshet releases do have some effects on the downstream river. The model could be used further to compare the river effects for different flood release scenarios.

6 CONCLUSIONS AND RECOMMENDATIONS

A two-dimensional numerical flow and sediment transport model for the Zambezi Delta was successfully developed, and the hydraulic roughness and bed sediment transport calibrated, using available field data and by making carefully considered assumptions based on supplementary information where necessary. The model was used to simulate pre- and post-dam 10 year flow scenarios. The predicted effects of the dams include:

- a significant decrease in the extent of flooding;
- small impacts on the width and shape of the river channel (the channel is generally slightly narrower with steeper banks than it would be if "pre-dam" conditions were to be re-introduced);
- a drastic reduction in rates of erosion and deposition on the flood plains;
- slightly less variation in the grading of the bed; and
- higher water levels and less water level variations in the estuary due to the tide and mouth conditions during low flow periods.

Despite the promising overall reliability of the model the suspended sediment transport of fine sediments was not accurately predicted because fine sediment was allowed to be "sucked" up into the flow from very deep in the model bed, particularly at the inflow boundary where an effectively infinitely deep bed layer was specified. The simulation of the transport of fine sediments is an area requiring further research. If the model created in this study is to be further developed to accurately predict suspended transport of fine sediments the following starting points are recommended:

- Specify a thinner bed layer, most importantly at the inflow boundary but perhaps through the whole model domain. This would give more realistic results but is a

"quick-fix" which won't actually make the simulation of the suspended sediment transport behaviour more accurate.

- Investigate the effects of specifying more sediment fractions, and multiple sediment layers.
- Calibrate the suspended sediment transport equation using additional field data (if/when available).
- Improve the inflow boundary suspended sediment total loads as well as rating relationships using information from additional field load measurements and flow records of the major Lower Zambezi tributaries (if/when available).

If additional computational or time resources are available the model may be further improved by a refinement of the numerical grid to give greater resolution. Extension of the model width to include the whole breadth of the delta and inclusion of more accurate survey information in the bathymetry would further improve the ability of the model to accurately predict the river behaviour at specific locations of interest as well as for the delta as a whole.

The numerical model created in this study provides a useful tool for evaluating the effects of environmental flood releases and possible future dams from a hydrodynamic/morphological perspective. One such environmental flood release was simulated in this study and it was shown to have small but notable effects on the extent of flooding and the on river channel morphology when compared to the current post dam condition. The detailed flow, sediment and river morphological information produced by such a model can enable specialists in other fields to make more informed predictions of the environmental effects of dams.

REFERENCES

Acreman, M. C., 1996. Environmental effects of hydro-electric power generation in Africa and the potential for artificial floods. *J. CIWEM,* Issue 10.

ASP, 2006. *Zambezi River fluvial mophological investigation for the proposed pumpstation at Tete,* Stellenbosch: ASP Technology.

ASP, 2011. *Zambezi River navigation channel sedimentation study - Report on first field work carried out during February 2011,* Stellenbosch: ASP Technology.

ASP, 2012a. *Zambezi River navigation channel sedimentation study - Flood hydrology report,* Stellenbosch: ASP Technology.

ASP, 2012b. *Zambezi River navigation channel sedimentation study - Report on second field work carried out during February 2012,* Stellenbosch: ASP Technology.

Basson, G. R., 2004. *Hydropower dams and fluvial morphological impacts - an African perspective.* Paper from United Nations Symposium on Hydropower and Sustainable Development, pp. 27-29.

Basson, G. R., 2013. *Reservoir sedimentation in Africa: historical trends and possible future impacts of land use and climate change.* Seattle, USA, ICOLD Symposium.

Beck, J. S. & Basson, G. R., 2003. *The hydraulics of the impacts of dam development on the river morphology,* Stellenbosch: Water Research Commission Report No. 1102/1/03.

Beilfuss, R., 2010. Modelling trade-offs between hydropower generation and environmental flow scenarios: a case study of the Lower Zambezi River Basin, Mozambique. *International Journal of River Basin Management,* Volume 8:3-4, pp. 331-347.

Beilfuss, R., 2001. *Prescribed flooding and restoration potential in the Zambezi Delta, Mozambique: Working Paper #4,* International Crane Foundation, USA: Program for the sustainable management of Cahora Bassa Dam and the Lower Zambezi Valley.

Beilfuss, R. & Brown, C., 2006. *Assessing environmental flow requirements for the Marromeu Complex of the Zambezi Delta,* Maputo, Mozambique: Museum of Natural History.

Beilfuss, R. & Brown, C., 2010. Assessing environmental flow requirements and trade-offs for the Lower Zambezi River and Delta, Mozambique. *International Journal of River Basin Management,* 8(2), pp. 127-138.

Beilfuss, R. & dos Santos, D., 2001. *Patterns of hydrological change in the Zambezi Delta, Mozambique,* Program for the Sustainable Management of Cahora Bassa Dam and the Lower Zambezi Valley.

Bolton, P., 1984. Sediment deposition in major reservoirs in the Zambezi basin. *Challenges in African Hydroloy and Water Resources (Proceedings of the Harare Symposium, July 1984),* Volume IAHS Publ. no. 144.

Brandt, S. A., 2000. Classification of geomorphological effects downstream of dams. *Catena,* Volume 40, pp. 375-401.

Brandt, S. A., 2000. Prediction of downstream geomorphological changes after dam construction: A stream power approach. *International Journal of Water Resources Development,* 16(3), pp. 343-367.

Brown, C. & King, J., 2012. Modifying dam operating rules to deliver environmental flows: experiences from southern Africa. *International Journal of River Basin Management,* Volume 10:1, pp. 13-28.

Brune, G. M., 1953. Trap efficiency of reservoirs. *American Geophysical Union,* 34(3).

Cheng, N. S. & Chiew, Y. M., 1998. Pick-up probability for sediment entrainment. *Journal of Hydraulic Engineering, ASCE,* 124(2), pp. 232-235.

Chow, 1959. *Manning's n for channels (Chow, 1959).* [Online] Available at: www.fsl.orst.edu/geowater/FX3/help/FX3_Help.html#8_Hydraulic_Reference?Mannings_n_Tables.htm [Accessed 15 Jan 2013].

COBA, 2011. *Aproveitamento hidorelectrico de Mphanda Nkuwa, Estudo de impacto ambiental estudo de sedimentos no Rio Zambeze e da evolucao da geometria do leito,* Unpublished report.

Davies, B. R., 1986. The Zambezi River system. In: *The Ecology of River Systems.* Dordrecht, The Netherlands: Dr W. Junk Publishers, pp. 225-261.

Davies, B. R., Beilfuss, R. D. & Thoms, M. C., 2000. Cahora Bassa retrospective, 1974-1997: Effects of flow regulation on the Lower Zambezi River. *Verh. Internat. Verein. Limnol.,* Volume 27, pp. 1-9.

DHI, 2003. *Mike 21 flow model - Hints and recommendations in applications with significant flooding and drying,* Horsholm, Denmark: Mike by DHI.

DHI, 2004. *Mike21C river morphology - a short desciption,* Horsholm, Denmark: Mike by DHI.

DHI, 2011. *MIKE 21 C curvilinear model for river morphology user guide,* Horsholm, Denmark: Mike by DHI.

DHI, 2011. *Mike21C curvilinear model scientific documentation,* Horsholm, Denmark: Mike by DHI.

Dorfmann, C. & Knoblauch, H., 2009. ADCP measurements in a reservoir of a run-of-river hydro power plant. *6th International Symposium on Ultrasonic Doppler Methods for Fluid Mechanics and Fluid Engineering,* pp. 45-48.

Engelund, F. & Fredsoe, J., 1976. A sediment transport model for straight alluvial channels. *Nordic Hydrology,* 7(5).

Engelund, F. & Hansen, E., 1967. *A monograph on sediment transport in alluvial streams,* Copenhagen, Denmark: Teknisk Forlag, Danish Technological University.

Erskine, W. D., 1985. Downstream geomorphic impacts of large dams: the case of Glenbawn Dam, NSW. *Applied Geography,* Volume 5, pp. 195-210.

FAO, 2000. *Aquastat - Global river sediment yields database.* [Online] Available at: http://www.fao.org/nr/water/aquastat/sediment/index.stm [Accessed 5 June 2013].

Geomatix Ltd, 2013. *AutoTide prediction.* [Online] Available at: http://www.geomatix.net/tides/autotide.htm

Grams, P. E., Schmidt, J. C. & Topping, D. J., 2007. The rate and pattern of bed incision and bank adjustment on the Colorado River in Glen Canyon downstream from Glen Canyon Dam, 1956-2000. *Geological Society of America Bulletin,* 119(5-6), pp. 556-575.

Gray, J. R. & Simoes, F., 2009. Estimating sediment discharge. In: M. Garcia, ed. *Sedimentation Engineering.* ASCE.

ICOLD, 2013. *Position paper: Dam development in Africa.* [Online] Available at: http://academic.sun.ac.za/icold-africa/documents/Position%20Paper%20Dam%20development%20in%20AFRICA.pdf [Accessed 19 July 2013].

Kovacs, Z., 1988. *Regional Maximum Flood Peaks in Southern Africa,* SA Department of Water Affairs.

Ludwig, W. & Probst, J., 1998. River sediment discharge to the oceans: present-day controls and global budgets. *American journal of science,* Volume 298, pp. 265-295.

Ma, Y. et al., 2012. Channel adjustments in response to the operation of large dams: The upper reach of the Lower Yellow River. *Geomorphology,* Volume 147-148, pp. 35-48.

Meyer-Peter, E. & Muller, R., 1948. *Formulas for bed load transport,* Stockholm: Proc, 2nd Congr. IAHR. Vol. 2, paper 2.

Mhlangwa, S. Z. & Sakala, W. K., 2013. *Hydropower potential and development opportunities on the Zambezi River.* Addis Ababa, International conference and exhibition on water storage and hydrpower development for Africa.

Milliman, J. D. & Syvitski, J. P., 1992. geomorphic / tectonic control of sediment discharge to the ocean: The importance of small mountainous rivers. *The Journal of Geology,* Volume 100, pp. 525-544.

NASA, 2009. *Shuttle Radar Topography Mission.* [Online] Available at: http://www2.jpl.nasa.gov/srtm/

NASA, 2013. *The Thematic Mapper*. [Online] Available at: http://landsat.gsfc.nasa.gov/about/tm.htm

Petts, G. E. & Gumell, A. M., 2005. Dams and geomorphology: Research Progress and future directions. *Geomorphology,* Volume 71, pp. 27-47.

Piest, R. F., Kramer, L. A. & Heinemann, H. G., 1975. Sediment movement from loessial watersheds. *Present and Prospective Technology for Predicting Sediment Yields and Sources.,* Volume ARS-S-40, pp. 130-141.

Pritchard, D., Bamba, A. & Rilla, F., 2009. *Marromeu Complex Ramsar site, Mozambique, Mission Report,* Ramsar Advisory Missions - No. 62.

Rio Tinto, 2011. *Navigation study of the lower Zambezi River.*

Ronco, P., Fasolato, G. & Di Silvio, G., 2006. The case of the Zambezi River in Mozambique: Some investigations on slid transport phenomena downstream Cahora Bassa Dam. In: Ferreire, Alves, Leal & Cardoso, eds. *River Flow 2006.* London: Taylor & Fancis Group, pp. 1345-1354.

Ronco, P., Giacomo, F., Nones, M. & Di Silvio, G., 2010. Geomorphological effects of damming on lower Zambezi River. *Geomorphology,* Volume 115, pp. 43-55.

Rooseboom, A., 1992. *Sediment transport in rivers and reservoirs - a South African perspective,* Water Research Commission Report No. 297/1/92.

Schleiss, A. et al., 2013. *Adapted reservir management in the Zambezi River Basin to meet environmental needs.* Addis Ababa, Africa 2013: International conference and exhibition on water storage and hydropower development for Africa.

Shields, A., 1936. *Anwendung der Aehnlichkeits-mechanic und der turbulenz for schung auf die Geschliebe beweging.,* Berlin: Mitteilungen der Preuss. Versuchsanstalt fur Wasserbau und Schiffsbau.

Smart, G. M. & Jaeggi, M. N. R., 1983. *Sediment transport on steep slopes,* Zurich: Mitteilung nr. 64 of the laboratory for hydraulics, hydrology and glaciology at the federal technical university.

Southern Waters, 2011. *Environmental flow assessment volume 2: Specialist reports (first report). ESHIA for the Riversdale Coal Barging Project Phase 2, Zambezi River, Mozambique,* Unpublished project report for ERM.

Southern Waters, February 2011. *Environmental Flow Assessment Volume 2: Specialist Reports (FIRST Report),* ESHIA for the Riversdale Coal Barging Project Phase 2, Zambezi River, Mozambique: Unpublished project report for ERM.

Stocking, M. & Elwell, H. A., 1973. Soil erosion hazard in Rhodesia. *Rhodesian Agric. J.,* 70(4), pp. 93-101.

Suschka, J. & Napica, P., 1986. *Ten years after the conclusion of Cahora Bassa Dam. The impacts of large water projects on the environment.*. Paris, France, UNEP/UNESCO.

Takeuchi, K., 2004. *Importance of sediment research in global water system science.* Yichang, China, Proceedings of the ninth international symposium on river sedimentation.

Thoms, M. C., 2003. Floodplain-river ecosystems: lateral connections and the implications of human interference. *Geomorphology,* Issue 56, pp. 335-349.

Tumbare, M. J., 1999. Equitable sharing of the water resources of the Zambezi River Basin. *Phys. Chem. Earth (B),* 24(6), pp. 571-578.

USBR, 2006. *Erosion and Sedimentation Manual.* Denver, Colorado: U.S. Department of the Interior Bureau of Reclamation.

Vale, 2010. *Technical draft report on Zambezi River Fluvial Morphology,* CTE Moatize Project.

van Rijn, L. C., 1984. Part I: Bed load transport & Part II: Suspended load transport. *Journal of hydraulic engineering,* Volume 110.

Walling, D. E., 1983. The sediment delivery problem. *Journal of Hydrology,* Volume 65, pp. 209-237.

Walling, D. E., 2006. Human impact on land–ocean sediment transfer by the world's rivers. *Geomorphology,* Volume 79, pp. 192-216.

Walling, D. E. & Webb, B. W., 1996. Erosion and sediment yiel: a global overview. *Erosion and Sediment Yield: Global and Regional Perspectives (Proceedings of the Exeter Symposium),* pp. 3-19.

WCD, 2000. *WCD case study: Kariba Dam, Zambia and Zimbabwe,* Lusaka, Zambia: World Commission on Dams.

Wischmeier, W. H. & Smith, D. D., 1958. Predicting rainfall erosion losses - a guide to conservation planning. *Agricultural Handbook - US Department of Agriculture,* Volume 537.

Yang, C. T., 1983. *Rate of energy dissipation and river sedimentation.* Nanjing, China, 2nd International symposium on river sedimentation.

Yang, C. T., 1984. Unit stream power equation for gravel. *Journal of Hydraulic Division, ASCE,* Volume 110 (HY12), pp. 1783-1798.

Yin, X. A., Yang, Z. F. & Petts, G. E., 2012. Optimizing environmental flows below dams. *River Research and Applications,* Volume 28, pp. 703-716.

Yuan, W., Yin, D., Finlayson, B. & Chen, Z., 2012. Assessing the potential for change in the middle Yangtse River channel following impoundment of the Three Gorges Dam. *Geomorphology,* Volume 147-148, pp. 27-34.

Zyserman, J. A. & Fredsoe, J., 1994. Data analysis of bed concentration of suspended sediment. *Journal of Hydraulic Engineering, ASCE,* 120(9), pp. 1021-1042.

APPENDIX A – GRID ANALYSIS IMAGES

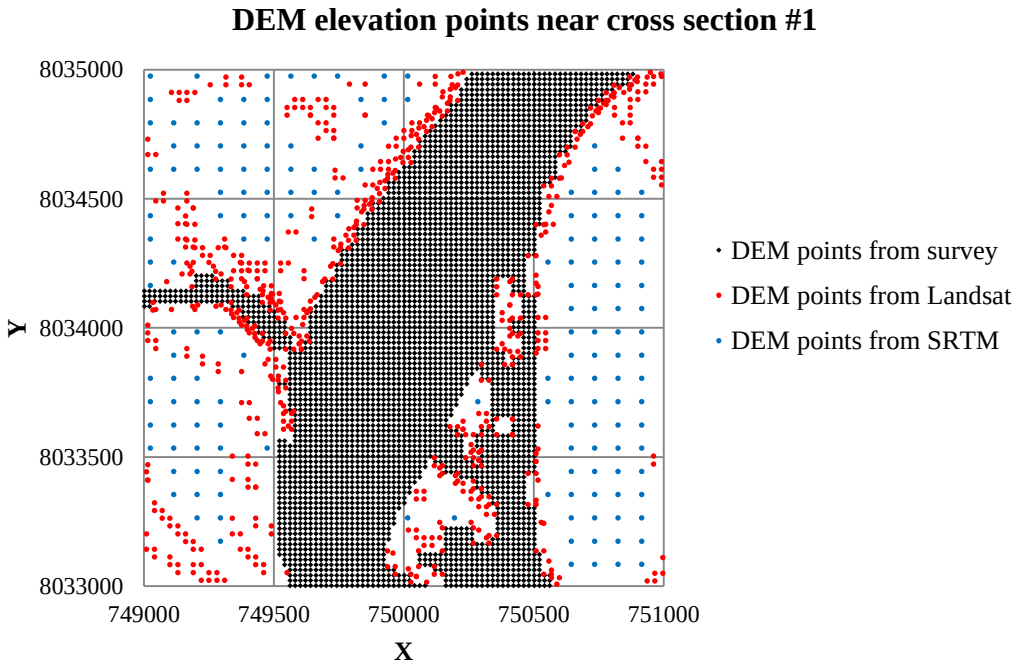

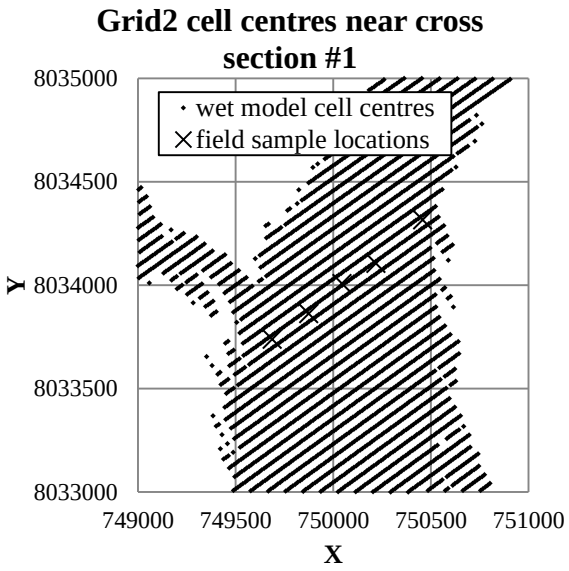

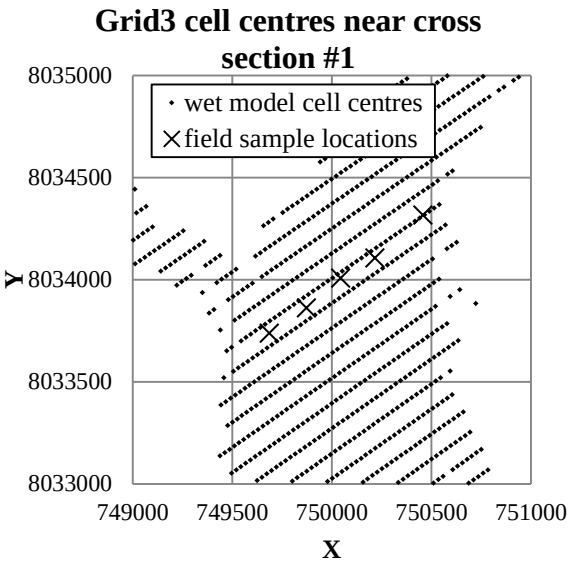

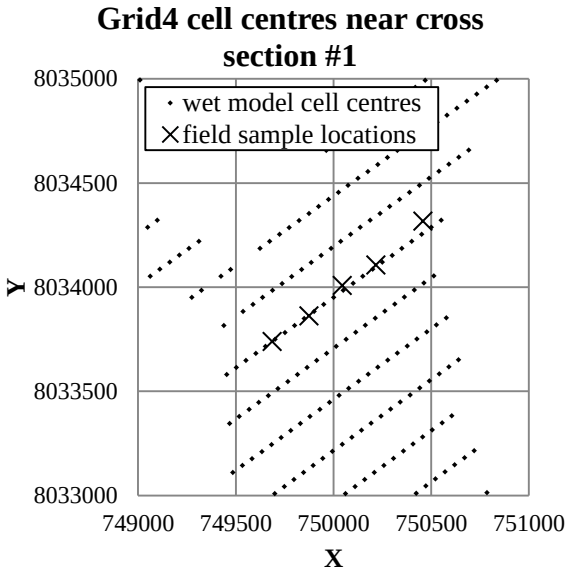

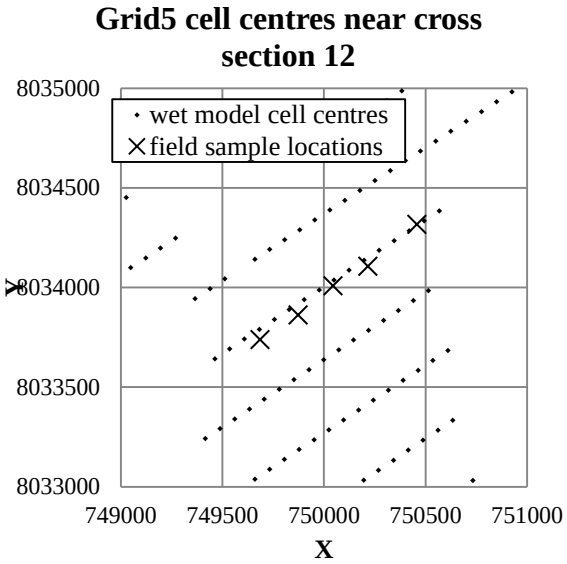

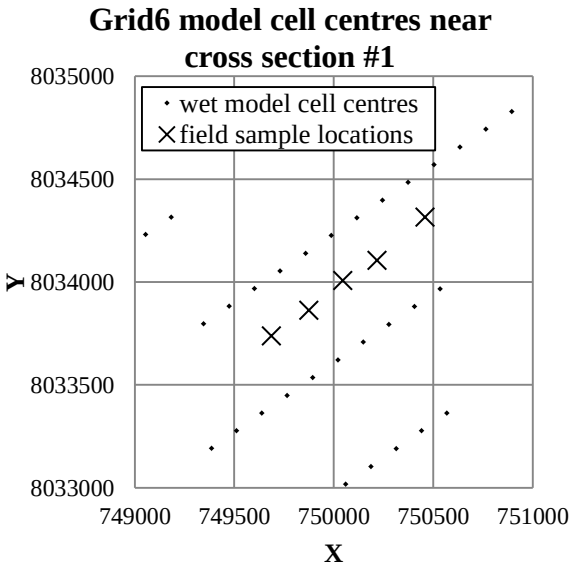

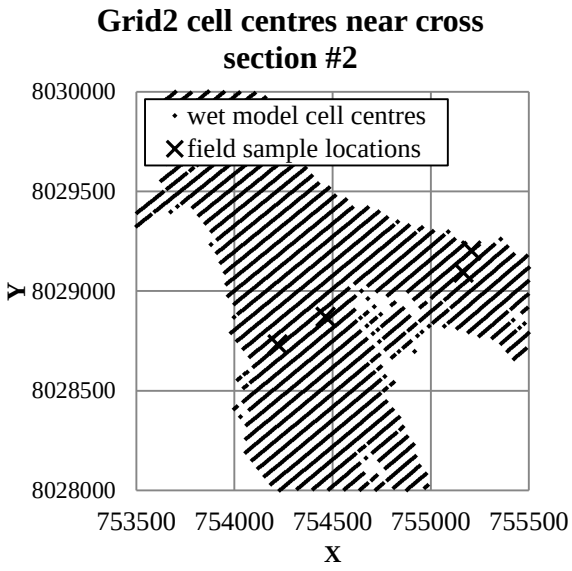

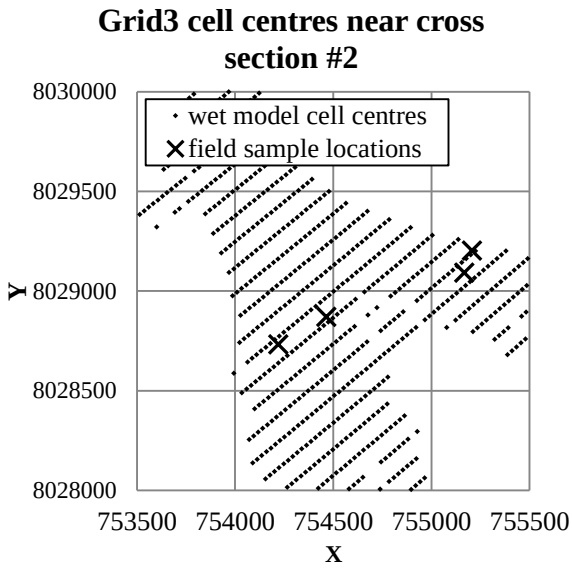

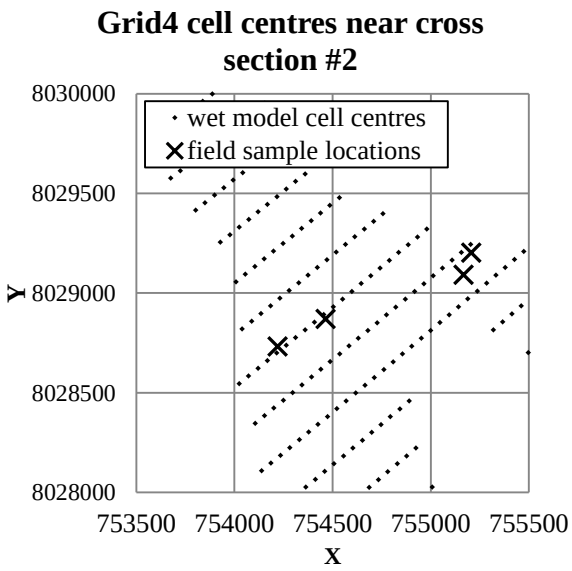

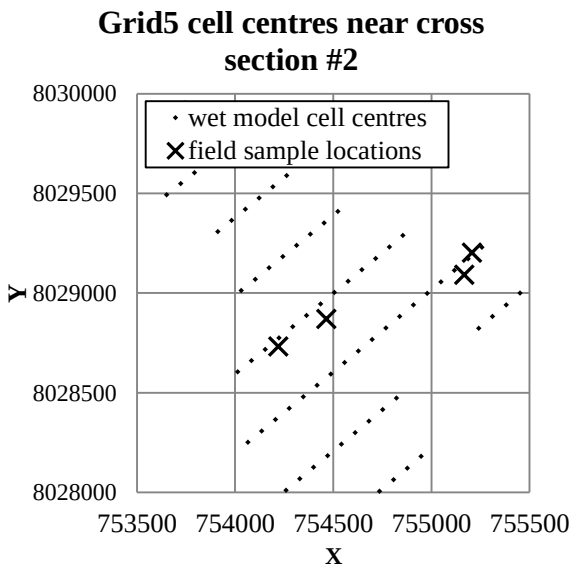

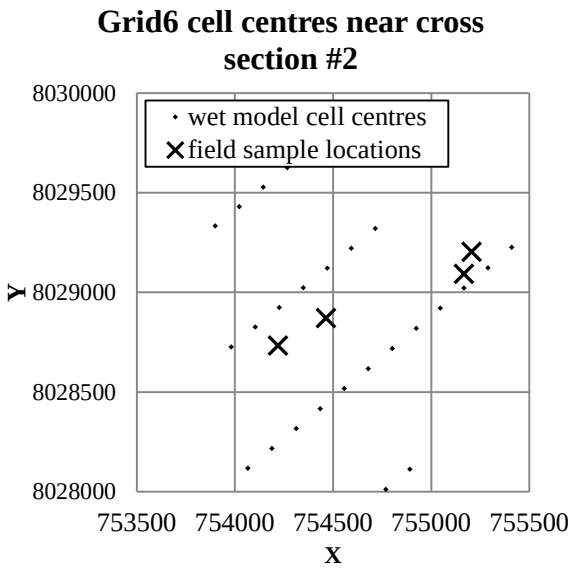

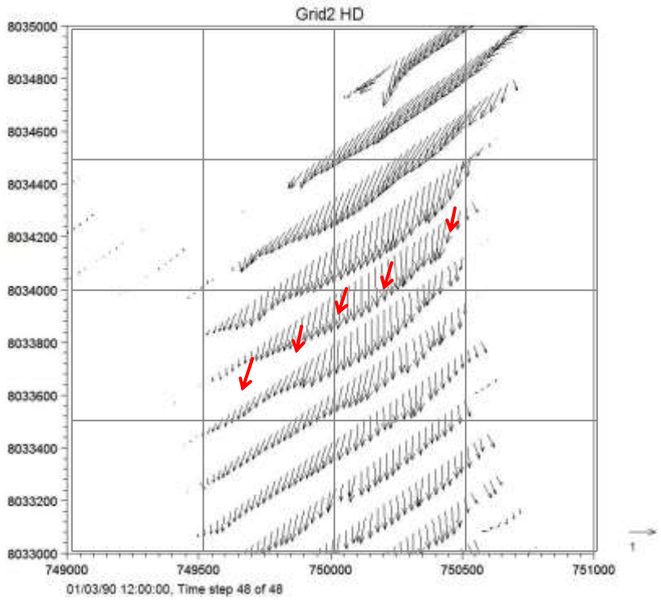

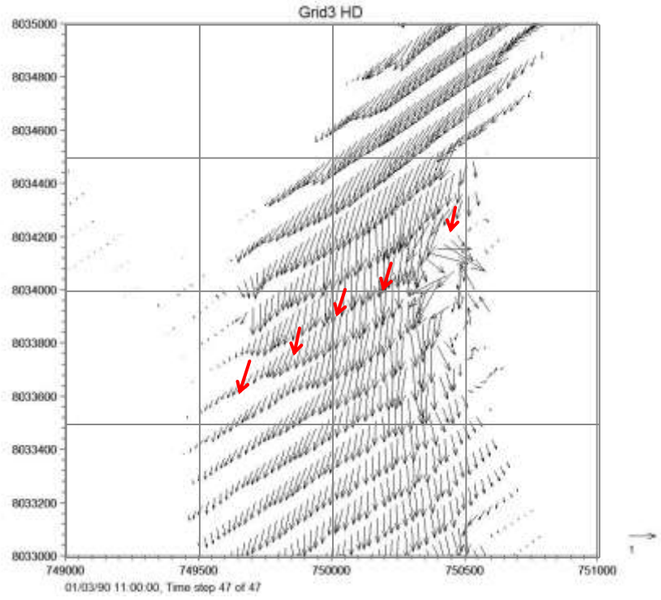

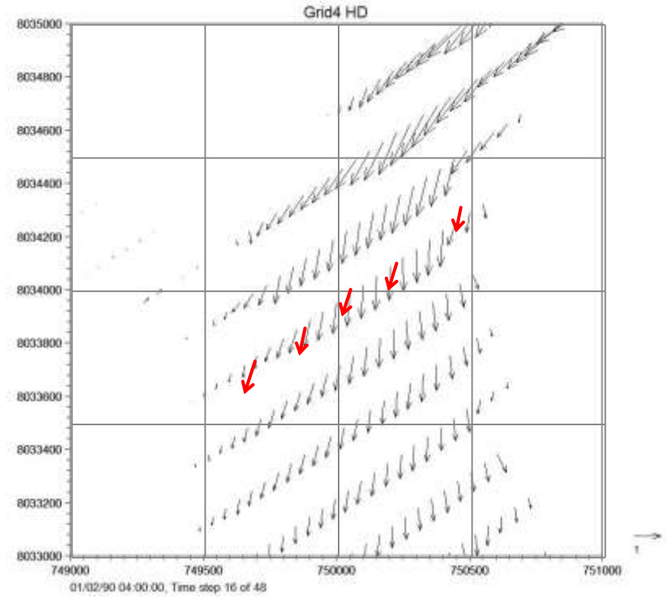

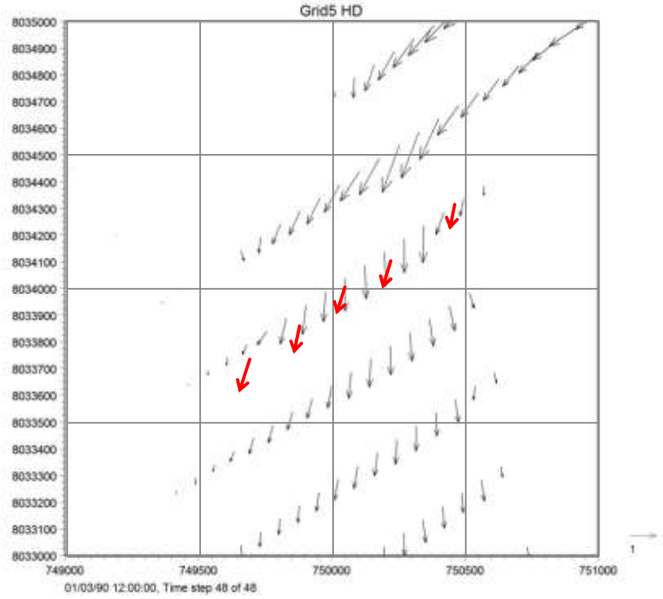

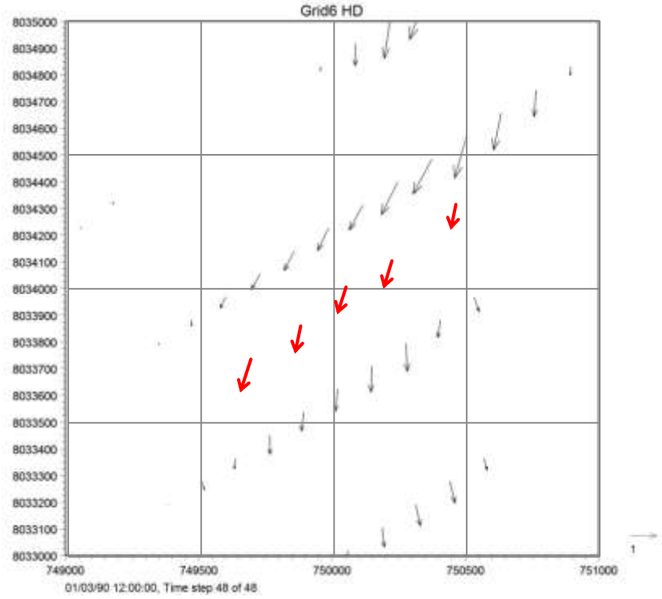

Measure field velocity vectors at cross section #1 (thick red arrows) shown with simulation velocity vector results (thin black arrows) for various grids

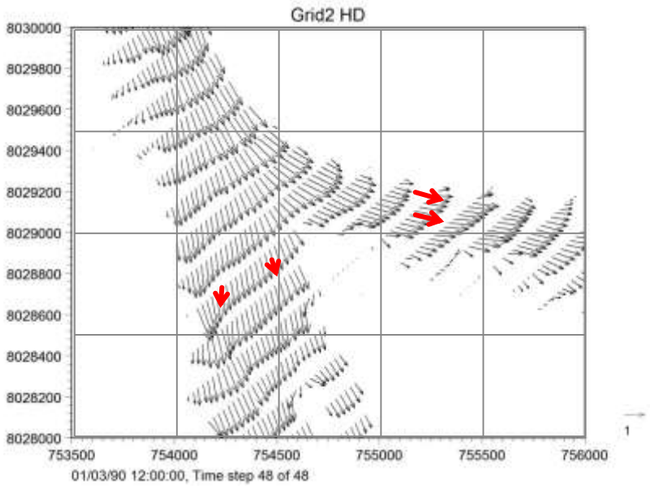

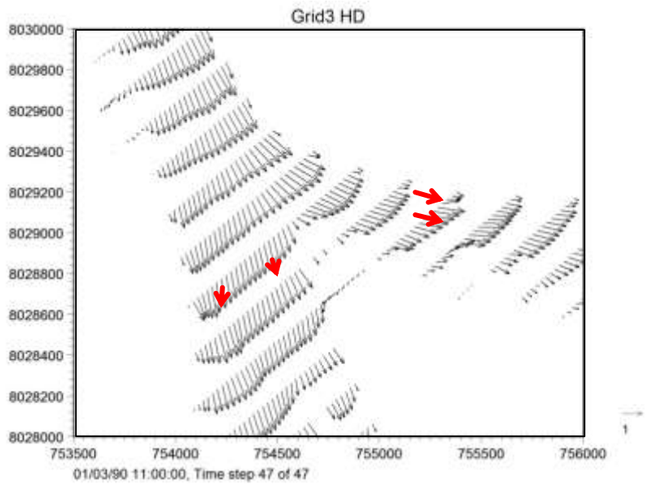

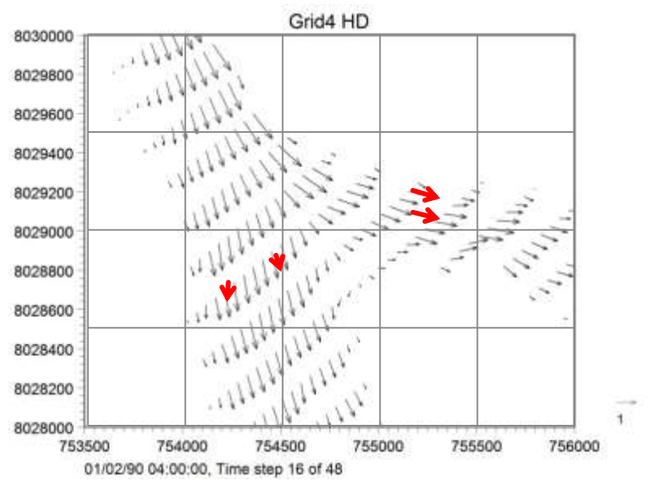

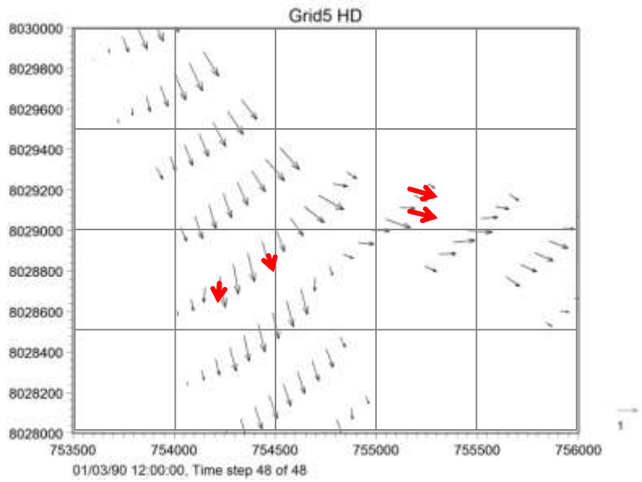

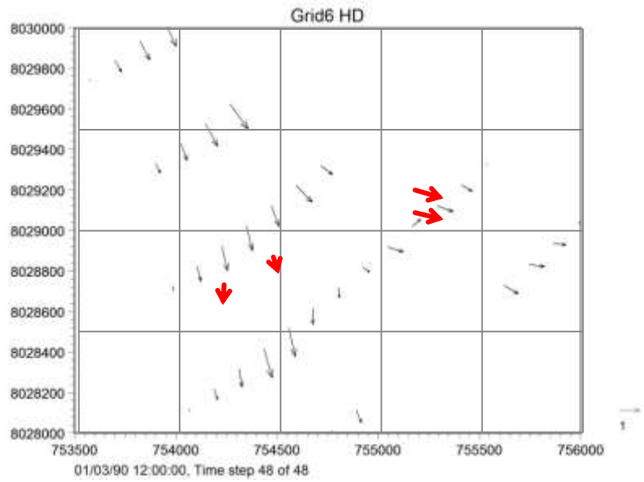

Measure field velocity vectors at cross section #2 (red arrows) shown with simulation velocity vector results for various grid sizes